



## Copyright Undertaking

This thesis is protected by copyright, with all rights reserved.

**By reading and using the thesis, the reader understands and agrees to the following terms:**

1. The reader will abide by the rules and legal ordinances governing copyright regarding the use of the thesis.
2. The reader will use the thesis for the purpose of research or private study only and not for distribution or further reproduction or any other purpose.
3. The reader agrees to indemnify and hold the University harmless from and against any loss, damage, cost, liability or expenses arising from copyright infringement or unauthorized usage.

### IMPORTANT

If you have reasons to believe that any materials in this thesis are deemed not suitable to be distributed in this form, or a copyright owner having difficulty with the material being included in our database, please contact [lbsys@polyu.edu.hk](mailto:lbsys@polyu.edu.hk) providing details. The Library will look into your claim and consider taking remedial action upon receipt of the written requests.

**The Hong Kong Polytechnic University**  
**Department of Building Services Engineering**

**Experimental and Numerical  
Investigation of Air Cross-  
Contamination around Typical High-  
Rise Residential Building in Hong Kong**

**Liu Xiaoping**

**A thesis submitted in partial fulfillment of the requirements for the  
Degree of Doctor of Philosophy**

**April, 2010**

## **Certificate of Originality**

I hereby declare that this thesis represents my own work and that, to the best of my knowledge and belief, it reproduces no material previously published or written, nor material that has been accepted for the award of any other degree or diploma, except where due acknowledgement has been made in the text.

---

Liu Xiaoping

Department of Building Services Engineering  
The Hong Kong Polytechnic University  
Hong Kong SAR, China  
April, 2010

## Abstract

Abstract of thesis entitled: Experimental and Numerical Investigation of Air  
Cross-Contamination around Typical High-Rise  
Residential Building in Hong Kong

Submitted by : Liu Xiaoping

For the degree of : Doctor of Philosophy

at The Hong Kong Polytechnic University in April, 2010.

The dispersion of air pollutant in complex building environment has become of great concern for the modern society as more and more people live in large and crowded cities in many parts of the world. For high-rise residential buildings, understanding the air flow and pollutant dispersion characteristics around buildings is essential to minimize the risk of outdoor pollution into buildings. The contaminant distribution and transmission route near a building can be extremely complicated due to the interaction between plumes of pollutants and building structure. Reliable prediction of the pollutant concentration field near a building is therefore of vital importance in providing comfortable and healthy indoor conditions free of outdoor air pollution. Air cross-contamination in high-density residential building environment can have a wide range of negative consequences for the residents' health and productivity, particularly during the period of a highly infectious disease outbreak. The primary aim of this work is to evaluate the risk of air cross-contamination around two typical forms of high-rise residential building in Hong Kong under two different naturally-ventilated conditions, i.e. buoyancy-dominated and wind-dominated conditions, respectively.

First a series of numerical studies were carried out to investigate the mechanism of contaminant transmission under the condition of single-sided natural ventilation, using Computational Fluid Dynamics (CFD) method. The focus is on one of the typical designs in HRR buildings with a rectangular plan layout and having a common-corridor separating the two sides, each of which has a flat-façade with openable windows. When the wind speed is low, with doors closed and windows opened, the flats become single-sided natural ventilation driven by buoyancy effects. It was found that under specific weather conditions, the presence of the pollutants originating from the lower floor is generally two orders of magnitude lower in the immediate upper floor. The results identified that the air pollutants can travel from a lower flat to an adjacent upper flat in the vertical direction through open windows caused by the indoor/outdoor temperature-difference induced buoyancy, revealing windows flush with the façade can be a major route of the air cross-contamination in high-rise residential buildings. Also, the study attempted to evaluate the effects of an architectural feature in minimizing such cross contamination. Moreover, with regards to ventilation design, the possible optimal strategies were preliminarily evaluated by CFD methods.

Subsequently, an experiment study was carried out to further investigate the dispersion characteristics around another typical building with more complex building shape under wind effect. The experiments were performed in a boundary layer wind tunnel using tracer gas technique. Two different model scales, 1:150 and 1:30, were designed for different purposes, representing a 33-story, and a 10-story residential building in prototype, respectively. The tracer gas concentrations on the envelop surfaces were measured using fast flame ionization detectors, while the pressure distributions along building facade were also examined. Through the

pressure and concentration distribution, the possible transport process of air pollutant induced by cross-contamination was thoroughly examined.

The first stage of the experiment was designed to be undertaken in the high speed section for model A, which was constructed as a block without any openings on the building envelope. The experimental results indicate that the flow pattern around the High-Rise Residential (HRR) building has the potential to transport gaseous pollutant within the re-entrance space under the wind effect. It was revealed that the pollutant can spread in both vertical directions, not only in the upward direction that was found under buoyancy effect, but also in the downward direction. Furthermore, dispersion can also occur in the horizontal direction, indicating a potential risk of cross-contamination in the horizontal adjacent flats. The experiment data were also used to evaluate the CFD methods, illustrating that CFD method with three kinds of  $k-\varepsilon$  turbulence models is not recommended in predicting the near building pollutant dispersion.

The second stage of the experiment was performed in the low speed section for model B, with openable windows, which was designed in a larger model scale that allowed greater spatial resolution of concentration data. It was noticed that the dispersion route is quite sensitive to both the source location and the wind direction, and dispersion trends were found similar to the first stage experiment results. In particular, the region of influence in both vertical and horizontal directions, together with contamination degrees induced by cross-contamination was determined. Moreover, comparisons were made between open-window and no-window situations. The mean concentration distributions under both configurations were found to be similar, implying that the presented window-wall-ratio was not large enough to

influence the basic flow pattern. The concentration fluctuations were also examined to illustrate the unsteady dispersion characteristics.

The study on this physical process is not only helpful to reduce the hazardous effect of routine release of harmful indoor air pollutants, but also useful for the purpose of prevention and control of accidental infectious diseases outbreak. The features revealed by the investigation indicate that early intervention for high-rise residential blocks may be implemented in terms of diagnosis and isolation if an emerging, highly infectious disease is suspected. The identification of this transmission path also shed light on both architectural and ventilation design in high-rise residential blocks to avoid cross indoor air contamination, which deserves further investigations.

## Publications arising from the thesis

### I. Journal Papers

- **Liu, Xiaoping**, Niu, Jianlei, Perino, Marco & Heiselberg, Per. Numerical simulation of inter-flat air cross-contamination under the condition of single-sided natural ventilation. *Journal of Building Performance Simulation*, 1 (2), pp.133-147. (2008) (Based on Chapter 4)
- **Liu, X.P.**, Niu, J.L., Kwok, K.C.S., Wang, J.H., Li, B.Z. Investigation of indoor air pollutant dispersion and cross-contamination around a typical high-rise residential building: Wind tunnel tests. *Building and Environment*, 45(8), pp.1769-1778. (2010) (Based on Chapter 6)
- Wang, J.H., Niu, J.L., **Liu, X.P.** Yu, C.W.F. Assessment of Pollutant Dispersion in the Re-entrance Space of a High-rise Residential Building, Using Wind Tunnel Simulations. *Indoor and Built Environment*. 19(6), pp.638-647. (2010). (Based on Chapter 5)

### II. Manuscripts

- **Liu, X.P.**, Niu, J.L., Kwok, K.C.S. Local characteristics of hazardous gas dispersion around high-rise building due to wind effect: Mean concentration and infection risk assessment. Submitted to *Journal of Hazardous Materials*. (Based on Chapter 6)
- **Liu, X.P.**, Niu, J.L., Kwok, K.C.S. Analysis of concentration fluctuations about hazardous gas dispersion around high-rise building due to wind effect. Submitted to *Journal of Hazardous Materials*. (Based on Chapter 6)

### III. Conference Papers

- **Liu, X.P.**, Niu, J.L., Gao, N.P., Perino, M., Heiselberg, P. CFD Simulation of Inter-flat Air Cross-Contamination—A Possible Transmission Path of Infectious Diseases. The 10<sup>th</sup> International Building Performance Simulation Association Conference and Exhibition. *BUILDING SIMULATION 2007*.

September 3-6, 2007. Beijing, China. (Based on Chapter 4)

- **Liu, Xiaoping**, Niu, Jianlei, Wang, Jianhui. Experimental Investigation of Air Cross-Contamination around One Typical High-Rise Residential Building in Hong Kong. The 9th International Healthy Buildings Conference and Exhibition. Healthy Building 2009. September 13-17, 2009. Syracuse, NY, USA. (Based on Chapter 5)
- **Liu, Xiaoping**, Niu, Jianlei. Experimental investigation of cross-contamination in high-rise residential building, 2010 Asian Workshop on Indoor Environment and Health-The First ISIAQ Asian Regional Conference 2010. August 19-25, 2010. Tainan City , Taiwan. (Based on Chapter 6)
- **Liu, X.P.**, Niu, J.L. Wind tunnel test of indoor air pollutant dispersion around high-rise building. IAQ 2010: Airborne Infection Control - Ventilation, IAQ & Energy. November 10-12, 2010, Kuala Lumpur, Malaysia. (Based on Chapter 6)

## **Acknowledgements**

First of all, I would like to deeply thank my chief supervisor Prof. Niu Jianlei, for his thoughtful consideration and invaluable guidance throughout this study. His continuous support, encouragement and faith in me was the driving force that kept me going. It is my great honor to join his research team, and learn from him how to conduct scientific research.

I would also like to express my gratitude to my Co-supervisor, Dr. Mak Cheuk-ming, for his kind help during my study.

I am grateful to Prof. K. C.S. Kwok for his extensive help for the analysis of wind tunnel test data. I also would like to thank Dr. Peter A. Hitchcock and the technical staff of CLP Wind tunnel, Hong Kong University of Science and Technology in preparing the scaled models and assisting the wind tunnel tests.

I could never find the right words to thank properly the dearest and most important people in my life, my parents, my sister and my wife. Their unconditional love, encouragement and support made all this possible.

## Table of Contents

<b>Certificate of Originality .....</b>	<b>i</b>
<b>Abstract.....</b>	<b>i</b>
<b>Publications arising from the thesis .....</b>	<b>v</b>
<b>Acknowledgements.....</b>	<b>vii</b>
<b>Table of Contents .....</b>	<b>viii</b>
<b>List of Figures.....</b>	<b>xii</b>
<b>List of Tables .....</b>	<b>xvi</b>
<b>Chapter 1 Introduction.....</b>	<b>1</b>
<b>1.1 Background.....</b>	<b>1</b>
<b>1.2 Hong Kong Environmental Conditions.....</b>	<b>3</b>
<b>1.3 Statement of the Problem .....</b>	<b>7</b>
<b>1.4 Objectives of the Present Study .....</b>	<b>9</b>
<b>1.5 Structure of the Thesis.....</b>	<b>10</b>
<b>Chapter 2 Literature Review .....</b>	<b>13</b>
<b>2.1 Natural Ventilation .....</b>	<b>13</b>
2.1.1 Introduction.....	13
2.1.2 Principles of Natural Ventilation .....	16
2.1.3 Different Types of Natural Ventilation.....	18
2.1.4 Different Methods on Natural Ventilation Study.....	20
<b>2.2 Airflow and Pollutant Dispersion around Buildings .....</b>	<b>23</b>
2.2.1 Introduction.....	23

2.2.2 Investigation Methods.....	28
<b>2.3 Related Studies aimed at Hong Kong Environment .....</b>	<b>34</b>
<b>2.4 Summary .....</b>	<b>36</b>
<b>Chapter 3 Research Methodology .....</b>	<b>38</b>
<b>3.1 Introduction.....</b>	<b>38</b>
<b>3.2 Wind Tunnel Method.....</b>	<b>39</b>
3.2.1 Wind Tunnel Modelling Theory .....	39
3.2.2 The CLP Power Wind/Wave Tunnel .....	43
3.2.3 Building Model Design.....	45
3.2.4 Approaching Wind Profile.....	47
3.2.5 General Arrangement of Wind Tunnel Experiment.....	48
3.2.6 Measurement Methods.....	50
<b>3.3 Computational Fluid Dynamics Method.....</b>	<b>53</b>
3.3.1 Governing Equations .....	53
3.3.2 Turbulence Models .....	54
3.3.3 Other Related Issues .....	58
<b>3.4 Summary.....</b>	<b>60</b>
<b>Chapter 4 Air Cross-contamination Under Buoyancy Effect.....</b>	<b>61</b>
<b>4.1 Introduction.....</b>	<b>61</b>
<b>4.2 Model Validation.....</b>	<b>63</b>
4.2.1 Introduction.....	63
4.2.2 A Brief Description on Previous Experiment Used for CFD Model Validation .....	64
4.2.3 CFD Simulation Setup .....	66
4.2.4 Comparisons between CFD Results and Experimental Data.....	69
<b>4.3 CFD Study on Buoyancy-Driven Cross-contamination .....</b>	<b>73</b>
4.3.1 Analysis and Simplification of the Model .....	73

4.3.2 Transient-State Contaminant Transmission.....	77
4.3.3 Steady-state Contaminant Transmission with Constant Release .....	82
4.3.4 Further Discussion and Analysis .....	84
<b>4.4 Possible Optimization Design.....</b>	<b>86</b>
4.4.1 Building Structure Optimization.....	86
4.4.2 Ventilation Design Optimization .....	91
<b>4.5 Summary.....</b>	<b>93</b>
<b>Chapter 5 Investigations on Air Pollutant Dispersion around Sealed Building</b>	<b>95</b>
<b>5.1 Introduction.....</b>	<b>95</b>
<b>5.2 Experiment Configuration .....</b>	<b>95</b>
5.2.1 Simulated Wind Profile in High Speed Wind Tunnel .....	96
5.2.2 Detailed Setup.....	97
<b>5.3 Measurement Results.....</b>	<b>99</b>
5.3.1 Mean Pressure Coefficient Distributions .....	99
5.3.2 Tracer Gas Concentration Profile .....	102
<b>5.4 Evaluation of CFD Method Performances .....</b>	<b>105</b>
5.4.1 Computational Domain Design and Grid Generation.....	105
5.4.2 Turbulence Models and Numerical Methods.....	110
5.4.5 Comparisons between CFD Results and Wind Tunnel Data .....	111
5.4.4 Further Discussions.....	132
<b>5.5 Summary.....</b>	<b>133</b>
<b>Chapter 6 Experimental Study on Large Scale Building Model with Openable Windows.....</b>	<b>135</b>
<b>6.1 Introduction.....</b>	<b>135</b>
<b>6.2 Experiment Setup.....</b>	<b>136</b>
6.2.1 Concentration Measurement Setup .....	136
6.2.2 Quality Assurance of Statistical Results.....	140

6.2.3 Pressure Measurement Setup .....	141
6.2.4 Simulated Wind Profile in Low Speed Wind Tunnel .....	143
<b>6.3 Mean Pressure Distribution and Mean Concentration Profile.....</b>	<b>144</b>
6.3.1 Results under Prevailing Wind Direction with Closed-window.....	144
6.3.2 Results under Other Wind Directions with Closed-window .....	151
6.3.3 Further Discussions.....	154
6.3.4 Results under Prevailing Wind Directions with Open-window.....	156
6.3.5 Results under Other Wind Directions with Open-window .....	159
<b>6.4 Concentration Fluctuation Characteristics .....</b>	<b>162</b>
6.4.1 Concentration Fluctuation Intensity.....	162
6.4.2 Cumulative Distribution Function .....	165
6.4.3 90-Percentile .....	171
6.4.4 Infection Risk Assessment.....	175
<b>6.5 Summary .....</b>	<b>180</b>
<b>Chapter 7 Concluding Remarks and Recommendations .....</b>	<b>183</b>
<b>7.1 Conclusions .....</b>	<b>184</b>
<b>7.2 Recommendations for the Further Works.....</b>	<b>189</b>
<b>References .....</b>	<b>191</b>

## List of Figures

Figure 1.1 Typical building types in Hong Kong (a. Typical building shape I, b. Typical building shape II) .....	4
Figure 1.2 The floor plan of the two building types. (a. Typical building shape I, b. Typical building shape II) .....	5
Figure 1.3 Thesis related research areas and methods .....	8
Figure 2.1 Flow Patterns around Rectangular Building.....	25
Figure 2.2 Surface flow along different rectangular building.....	26
Figure 3.1 The plan view of the CLP Power Wind/Wave Tunnel in HKUST.....	44
Figure 3.2 Plan view of the experiment model. ....	46
Figure 3.3 The sketch of the experiment configuration .....	49
Figure 4.1 Hypothetical contamination transmission path at one-sided ventilation conditions .....	62
Figure 4.2 Geometrical features of the test room and the layout of the typical points for comparison.....	65
Figure 4.3 Schematic geometry of the simulation model with grids layout in XY plane .....	67
Figure 4.4 Comparison between simulation and measured results of ACH values ...	70
Figure 4.5 Comparison between simulation and measured results of velocity magnitude at typical points: (a) $\Delta T = 20^\circ\text{C}$ and (b) $\Delta T = 10^\circ\text{C}$ .....	73
Figure 4.6 The schematic of free decay unsteady case and the measuring points location in plan .....	74
Figure 4.7 Predicted ACH values of each room versus time .....	78
Figure 4.8 Predict Volume-averaged $\text{CO}_2$ concentrations of each room versus time	79
Figure 4.9 Simulated $\text{CO}_2$ mass fractions at different points versus time.....	81
Figure 4.10 Simulated $\text{CO}_2$ concentration distributions at the centre plane ( $X=1.6\text{m}$ ) .....	82
Figure 4.11 Simulated path line colored by velocity magnitude .....	83
Figure 4.12 Variations of the measured mass fractions of $M_{2-4}$ and $M_{2-6}$ with the monitored local wind speed (From Niu and Tung 2008) .....	86
Figure 4.13 Simulated $\text{CO}_2$ concentration distributions at the centre plane with ledge effect ( $X=1.6\text{m}$ ) .....	87

Figure 4.14 Simulated path line colored by CO <sub>2</sub> mass fraction near the upper window: (a) without the ledge and (b) with the ledge above the window .....	89
Figure 4.15 Mass fraction in the lower part of the upper window versus time.....	90
Figure 4.16 Comparison of $f_p$ between with and without the ledge at different outside temperature .....	90
Figure 4.17 Simulated CO <sub>2</sub> concentration distributions at the centre plane with individual mechanical exhaust (X=1.6m).....	92
Figure 5.1 Photos of the experiment setup in high speed wind tunnel .....	96
Figure 5.2 Simulated approaching wind profile in high-speed wind tunnel.....	97
Figure 5.3 Plan view of the model and pressure measurement point locations .....	98
Figure 5.4 Tracer gas source location and concentration measurement points.....	99
Figure 5.5 Measured pressure coefficients along the building surface at different building heights at three approaching wind incident angles .....	101
Figure 5.6 Normalized tracer gas concentration distribution. (D0, D45 and D90 are the results obtained under wind direction of 0°, 45° and 90°, respectively.) .....	103
Figure 5.7 Computational domain and boundary conditions.....	106
Figure 5.8 Grid generated for this study .....	109
Figure 5.9 wall unit distribution on the building surfaces .....	110
Figure 5.10 Comparisons of mean pressure coefficients between CFD results and the wind tunnel measurements ( $\theta = 0^\circ$ ). .....	113
Figure 5.11 Comparisons of mean pressure coefficients between CFD results and the wind tunnel measurements ( $\theta = 45^\circ$ ). .....	115
Figure 5.12 Perspective view of the model and sections. ....	118
Figure 5.13 Mean velocity contour distributions with streamlines on: a) Section1; b) Section 2 .....	121
Figure 5.14 Mean velocity contour distributions with streamlines on Section 1 under oblique wind direction. ....	122
Figure 5.15 Comparisons of normalized concentration between CFD results with different turbulence models and wind tunnel measurement results ( $\theta = 0^\circ$ , the source was located in the 26 <sup>th</sup> floor). ....	124

Figure 5.16 Comparisons of normalized concentration between CFD results with different turbulence models and wind tunnel measurement results ( $\theta = 45^\circ$ , the source was located in the 26 <sup>th</sup> floor) .....	127
Figure 5.17 Streamlines colored by $K_c$ values and the iso-surface under normal wind direction: a) Source at the 6 <sup>th</sup> floor; b) Source at the 26 <sup>th</sup> floor.....	130
Figure 5.18 Streamlines colored by $K_c$ values and the iso-surface under oblique wind direction: a) Source at the 6 <sup>th</sup> floor; b) Source at the 26 <sup>th</sup> floor.....	131
Figure 6.1 The photo of the experiment configuration. ....	136
Figure 6.2 Plan view of the experiment model .....	139
Figure 6.3 Detailed positions of tracer gas concentration measurement points and source location in one single floor.....	140
Figure 6.4 Standard deviation versus averaging time .....	141
Figure 6.5 Pressure Measurement Points and Window's Locations.....	143
Figure 6.6 Normalized wind profile of the approaching wind. ....	144
Figure 6.7 Normalized concentration distributions within the windward (W) and leeward (L) re-entrant spaces under prevailing wind condition with closed-window, when tracer released at a) the 3 <sup>rd</sup> floor; b) the 6 <sup>th</sup> floor; c) the 9 <sup>th</sup> floor. (The abbreviation "S_W" and "S_L" represent if the source located windward or leeward was active, respectively.).....	146
Figure 6.8 Contour lines of the mean pressure coefficient on the building envelopes of different flats under prevailing wind direction ( $\theta = 0^\circ$ ): a) Flat A; b) Flat B; c) Flat C; d) Flat D. (The black points "■" shown in the figure are original measurement points) .....	149
Figure 6.9 Normalized concentration distributions under other wind directions (The abbreviation "D45" and "D90" represent the wind direction is $\theta = 45^\circ$ or $\theta = 90^\circ$ , respectively) with closed-window, when tracer released at a) the 3 <sup>rd</sup> floor; b) the 6 <sup>th</sup> floor; c) the 9 <sup>th</sup> floor. ....	152
Figure 6.10 Normalized concentration distributions within the windward (W) and leeward (L) re-entrant spaces under prevailing wind condition with open-window, when tracer released at a) the 3 <sup>rd</sup> floor; b) the 6 <sup>th</sup> floor; c) the 9 <sup>th</sup> floor. ....	158

Figure 6.11 Normalized concentration distributions under other wind directions ( $\theta = 45^\circ$ , $\theta = 90^\circ$ ) with open-window, when tracer released at a) the 3 <sup>rd</sup> floor; b) the 6 <sup>th</sup> floor; c) the 9 <sup>th</sup> floor. ....	161
Figure 6.12 Concentration fluctuation intensity when source was located in the 3 <sup>rd</sup> floor .....	164
Figure 6.13 Concentration fluctuation intensity when source was located in the 6 <sup>th</sup> floor .....	165
Figure 6.14 Time series for point P1 (in windward cases) or P5 (in leeward cases) and CDF shapes at vertical adjacent floors with closed-window condition. (The abbreviation F5 and F7 represent the 5 <sup>th</sup> floor or the 7 <sup>th</sup> floor, respectively; W and L represent in windward or leeward condition, respectively.) .....	167
Figure 6.15 CDF shapes at vertical adjacent floors with open-window condition. (The abbreviation F5 and F7 represent the 5 <sup>th</sup> floor or the 7 <sup>th</sup> floor, respectively; W and L represent in windward or leeward condition, respectively.) .....	169
Figure 6.16 CDF shapes under the other two wind directions. ( $\theta = 45^\circ$ , $\theta = 90^\circ$ ). .....	171

## List of Tables

Table 1.1 Monthly prevailing wind direction and mean wind speed recorded at the observatory and Waglan Island (from 1971 to 2000).....	6
Table 3.1 The overall parameters of the CLP Power Wind/Wave Tunnel in HKUST .....	45
Table 4.1 Predicted results at different indoor/outdoor temperature differences.....	85
Table 5.1 Comparisons of solution domain size (The abbreviation “W” and “H” represent the building width and height, respectively).....	107
Table 6.1 The configuration of each case under prevailing wind condition (Closed-Window) .....	137
Table 6.2 The configuration of each case under other wind conditions (Closed-Window) .....	137
Table 6.3 The 90-percentile normalized by mean concentration under prevailing wind direction with closed-window (Source located in the 6 <sup>th</sup> floor) .....	172
Table 6.4 The 90-percentile normalized by mean concentration under other wind conditions with closed-window (Source located in the 6 <sup>th</sup> floor).....	172
Table 6.5 The 90-percentile normalized by source concentration under prevailing wind direction with closed-window (Source located in the 6 <sup>th</sup> floor) .....	174
Table 6.6 The 90-percentile normalized by source concentration under other wind conditions with closed-window (Source located in the 6 <sup>th</sup> floor).....	175
Table 6.7 The infection risk calculated by mean and instantaneous peak concentration values (Source located in the 6 <sup>th</sup> floor, windward condition).....	177
Table 6.8 The infection risk calculated by mean and instantaneous peak concentration values (Source located in the 6 <sup>th</sup> floor, leeward condition).....	178
Table 6.9 The infection risk calculated by mean and instantaneous peak concentration values (Source located in the 6 <sup>th</sup> floor, $\theta = 45^\circ$ ).....	178
Table 6.10 The infection risk calculated by mean and instantaneous peak concentration values (Source located in the 6 <sup>th</sup> floor, $\theta = 90^\circ$ ).....	179

# **Chapter 1**

## **Introduction**

### **1.1 Background**

Since 1970s, increased demand and concern for human health, serious attempts to control air pollution, and the development of research capabilities have resulted in more and more studies on pollutant transportation within building environment (Cermak, 1975; Cermak, 1978; Snyder, 1979). The pollutant emissions around a building can affect its indoor air quality if the plume impinges on air intakes of the emitting building or the surrounding buildings. Understanding the characteristics of contaminant distribution in different environments and the mechanisms of contaminated air transport in and around buildings are the prerequisite conditions for employing effective indoor air pollution control strategies (Heinsohn & Cimbala, 2003). The prediction of the pollutant concentration field near buildings is very important for building engineers to design proper intake and exhaust location to avoid unwanted consequences.

Moreover, the study of airborne transmission route of highly infectious diseases has attracted great concern in recent years, especially after the worldwide outbreak of severe acute respiratory syndrome (SARS) happened in 2003 (Li et al., 2004a, Li et al., 2004b). Individuals with certain respiratory tract infections (e.g., tuberculosis, smallpox) may transmit the infection through the air. The airborne infectious particles were often considered to be droplet nuclei. Infection via inhalation of pathogen-carrying droplet nuclei is termed “airborne transmission” (Nicas et al.,

2005). Experimental evidence suggested that droplet transmission might in fact contribute to the burden of disease (Dick et al. 1987), which may travel with the ambient air flow depending on the particle size. More recently, Yu et al. (2004) published the key findings in the *New England Journal of Medicine*, for the SARS outbreak in one real estate (Amoy Garden) in Hong Kong. Their epidemiologic analysis and experimental studies, as well as airflow simulations supported the probability of an airborne spread of the SARS virus in this outbreak. These developed concerns over the effects of pollution on human health and the requirements in preventing infectious disease transmission have increased the need for thorough studies of pollutant dispersion within and around buildings.

Many previous studies have been conducted on the behavior of plumes released near different building environments, ranging from street canyons (Vardoulakis et al., 2003; Li et al, 2006), building arrays (Macdonald et al., 1997; Shi et al., 2008) to an isolate single building (Higson et al., 1996; Li and Stathopoulos, 1997). The past research concentrated on the problem of pollutant released from the source located in a certain distance upwind of the building, with attention to the concentration distribution in the vicinity of building and especially in building wake, but to a lesser extent on air cross-contamination around a building itself. It is known that the air exchange process during natural ventilation could transport the outdoor pollutant into indoor environment. Under crowd living conditions, the air pollutant exhausted from one household could probably re-enter into the neighbouring households, traveling with ambient airflow. Such pollutant dispersion process is defined as air cross-contamination in this study. The changes in building design devised to improve land

use efficiency, led to more complex dispersion routes of contaminants and infections that have not been observed before.

Air-cross contamination in residential building environment can have a wide range of negative consequences for the residents' health and productivity. For example, the cooking smell released from one household could be easily detected by other households through this kind of cross-contamination, which probably resulted in neighborhood nuisance problems. In particular, the possible serious threat of highly infectious disease outbreak or the growing threat of bioterrorism attack through deliberately releasing highly toxic agents have also highlighted the need of study focused on pollutant dispersion within modern residential building environment. Especially in those buildings that natural ventilation is widely used, air cross-contamination could lead to undesirable results through the open windows. The study on this physical process is not only helpful to reduce the hazardous effect of routine release of harmful pollutant near the building, but also useful for the purpose of prevention and control of accidental infectious diseases outbreak, including SARS, TB (tuberculosis) and the growing threat of H1N1 influenza.

## **1.2 Hong Kong Environmental Conditions**

High-rise buildings became possible with the invention of the elevator (lift) and cheaper, more abundant building materials. Buildings between 23 m to 150 m high are considered high-rise.

- The *International Conference on Fire Safety in High-Rise Buildings* defined a high-rise as "any structure where the height can have a serious impact on evacuation".
- Most building engineers, inspectors, architects and similar professions define a high-rise as a building that is at least 23 m tall.
- Chinese Standard, GB 50352—2005 (Code for design of civil buildings) (GB50352-2005, 2005) defines a high-rise as a building that is at least 24 m tall.



a. large slab-shaped building

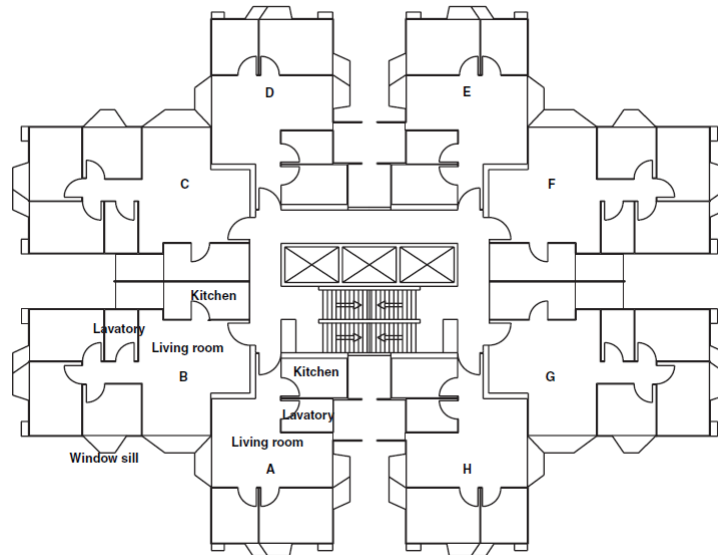


b. Cross-shaped building

**Figure 1.1 Typical building types in Hong Kong (a. Typical building shape I, b. Typical building shape II)**



a)



b)

**Figure 1.2 The floor plan of the two building types. (a. Typical building shape I, b. Typical building shape II)**

Two kinds of typical building shapes are shown in Figure 1.1 and Figure 1.2. Typical building shape I is slab-shaped building. The building has flat façade and the windows are flush with the walls. For building shape shown in Figure 1.1 II, each floor contains eight units. It comprises a central core, and the residential units extending outward from the core in eight directions. A pair of adjacent residential units is separated with an outdoor recessed space formed by their external walls. This design is to fulfill the relevant building regulations and code of practice in force in Hong Kong, allowing individual flats to have more external wall and window areas

(Anonymous, 1984). Consequently, four semi-enclosed, so-called re-entrant spaces are formed in each high-rise block, into which the exhaust air from all the floors are discharged, and it can lead to a high possibility of cross-contamination.

The recessed space design allows individual residential units to have more walls and windows that are external. Then, each room in a unit may be provided by an external wall, which increases availability of daylight and natural ventilation to the units, and availability of openings for installation of air-conditioners, and for kitchen, toilet, and gas heater exhausts. Plumbing and drainage pipes may be installed at all the external side of the wall within the recessed space to ease maintenance and repair.

**Table 1.1 Monthly prevailing wind direction and mean wind speed recorded at the observatory and Waglan Island (from 1971 to 2000).**

Month	Observatory		Waglan Island	
	Prevailing Direction (deg.)	Mean Wind Speed (km/h)	Prevailing Direction (deg.)	Mean Wind Speed (km/h)
January	090	11.0	070	25.4
February	090	12.1	070	25.1
March	090	12.6	070	23.5
April	090	11.7	070	21.2
May	090	10.8	080	20.2
June	090	11.0	230	23.3
July	090	10.9	230	21.9

August	090	10.2	240	20.0
September	090	11.0	090	22.8
October	090	12.4	080	28.7
November	090	10.9	080	27.9
December	090	10.3	070	26.5
Year	090	11.2	070	23.9

As to the meteorological conditions, Hong Kong's climate is sub-tropical, tending towards temperate for nearly half the year. The monthly prevailing wind direction and mean wind speed recorded at the Observatory and Waglan Island from 1971 to 2000 is shown as Table 1.1 (Hong Kong Observatory, 2008). Hong Kong Observatory is located in the center of Hong Kong, and its elevation of ground above mean sea-level is 32m. Waglan is located in the southeast part of Hong Kong with the elevation 56m.

### **1.3 Statement of the Problem**

It has been well known that the contaminant distribution and transmission route near building can be extremely complicated due to the interaction between plumes of pollutants and building structure. This presented work was first raised by an attractive phenomenon observed during SARS epidemic in 2003, consequently further extended to the air cross-contamination characteristics around two typical kinds of high-rise residential (HRR) building in Hong Kong with complicated building shapes. The unfortunate SARS outbreak has called for the need for

ventilation and indoor air quality professionals to investigate the links between the indoor environment affected by pollutant dispersion characteristics and public health.

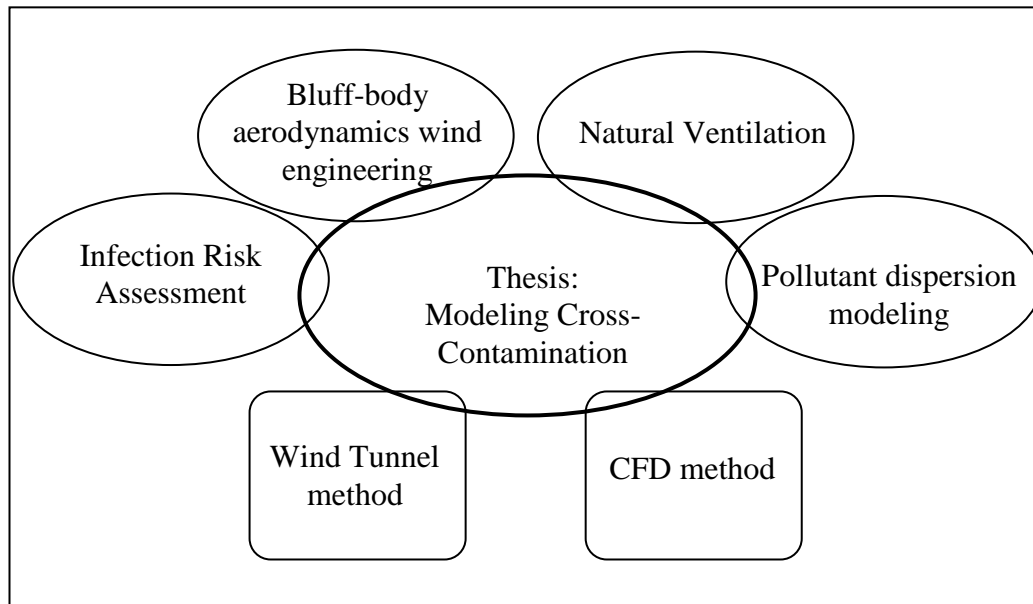


**Figure 1.3 Thesis related research areas and methods**

This dissertation focuses on the study of transport and diffusion of pollutants in and around complex buildings. The main goal is to gain a better understanding of how contaminants originating from one household travel with the ambient airflow and spread into neighboring residential units. The region of influence, the dispersion route under different driving forces, the strength of contaminant concentration and its exposure risks due to this kind of dispersion are investigated in this study. Based on the obtained results and the risk estimations, it is hoped that the corresponding strategies and optimization plan can be established.

The scope of research defined above involves a variable of research areas and techniques. As shown in Figure 1.3, this thesis crossed over building ventilation, urban air pollution modelling, wind engineering and infection risk assessment.

Basically, two complementary methods, physical modeling in a wind tunnel and numerical method using computational fluid dynamics (CFD) techniques, have been employed to investigate the mechanisms of air pollutant transmission within building environment.

#### **1.4 Objectives of the Present Study**

The overall objective of this study is to evaluate the risks of air cross-contamination around two typical high-rise residential building designs in Hong Kong under different naturally ventilated conditions, i.e. buoyancy-dominated and wind-dominated conditions, respectively.

The first objective of this study is to identify this possible transmission path within one typical HRR building design under buoyancy effect. This stage of study is focused on a simple, slab-shaped building, representing one common type of high rise residential block in Hong Kong. The identification combined with previous on-site field investigation (Niu and Tung, 2008) helps to strengthen the need of further investigations aimed at the air pollutant dispersion around another typical building with more complex building shape under wind effect. Moreover, based on the features of transmission route revealed by the studies, the efforts can be clearly focused on how to destroy the cascade effect introduced by one-sided ventilation via open windows. With regards to both architectural and ventilation designs, the possible optimal strategies were preliminarily evaluated by CFD methods.

The second objective is to investigate pollutant dispersion characteristics around Type II building with a more complex shape under wind effect. The physical process is determined primarily by the complicated turbulent wake flows. This resulted in difficulties in prediction of the pollutant dispersion by directly using computational method, especially with such complex building shape. Therefore, a series of experiments were designed and undertaken in a boundary layer wind tunnel with careful considerations. The wind-induced pressure and tracer gas concentration distributions are used in complements for evaluating the possibility of discharged indoor air pollutants re-entering adjacent indoor environments in the same building. The concentration fluctuations are also investigated to reveal the unsteady characteristics of the dispersion process. The values and positions of short duration peaks are estimated to check for exceedance of critical thresholds. In addition, a well known infection risk calculated model using Wells-Riley equation (Riley et al., 1978) is introduced to estimate the infection risk caused by this cross-unit contamination.

The final objective of this research is to evaluate the computational method in predicting more complex interaction between plumes of pollutants and building structure under wind effect. The wind tunnel experiment results provided the necessary information for the calibration of the numerical method via comparisons between predicted results and experimental data.

### **1.5 Structure of the Thesis**

This thesis consists of 7 chapters that include the introduction of the thesis, a literature review of the related research, numerical analysis of the situation under

buoyancy effect, experimental and CFD study of distribution pattern of contaminants around a building model under wind effect, and an estimation of infection risk of airborne transmitted diseases. The contents in each chapter are summarized as follows:

Chapter 1 introduces the background and the motivation of this study and provides an overview of the thesis.

In Chapter 2, the past works related to this study are extensively reviewed and discussed, with the main emphasis on the airflow and dispersion around buildings. The basic knowledge relevant to natural ventilation and the infection risk estimation models are also reviewed, and the significance of this study is discussed here.

Chapter 3 introduces the research methodologies in this study. Two well-established research approaches, i.e., numerical simulation based on CFD method plus experimental investigation technique are introduced. Firstly, for the numerical method, the turbulence models developed so far are briefly introduced. The differences based on different study purposes are discussed, ranging from single-sided natural ventilation that is involved in the study of buoyancy induced cross-contamination, to a larger scale urban flow and dispersion around building environment. Secondly, the detailed considerations about experiment design and arrangement of wind tunnel measurements are described.

Chapter 4 presents the CFD simulation of air-cross contamination that occurs at relatively calm days when wind speeds are low, and buoyancy force dominates. With

the aim of improving the ventilation design of high-rise residential buildings to avoid this kind of cross contamination, the effects of alternative architectural components and ventilation strategies are analyzed.

Chapter 5 describes the first stage wind tunnel studies and the comparisons between numerical results and experimental data. A 1:150 scale Type II HRR building model was constructed to illustrate the basic features of pollutant dispersion under wind effect. The performances under different configurations of CFD methods are evaluated.

Chapter 6 reports the wind tunnel test results and analysis of tracer gas concentration distributions together with its fluctuation characteristics. To obtain a higher spatial resolution of the experiment data, a 1:30 scale model with openable windows was constructed and the related experiments were carried out in a larger wind tunnel. The wind-induced pressure and tracer gas concentration distributions are used in complements for evaluating the possibility of discharged indoor air pollutants re-entering adjacent indoor environments in the same building.

The final chapter, Chapter 7 gives a general conclusion drawn from the present work, and states the limitations of this study as well as the suggestions for future researches.

## **Chapter 2**

### **Literature Review**

The scales involved in this study are from part of a HRR building to the entire building, with different emphasis. Firstly, CFD simulation method was employed to study the cross-contamination between two vertical adjacent units that belong to one typical high-rise residential building, under the condition of single-sided natural ventilation. Subsequently, more complicated pollutant dispersion process driven by wind forces around the entire building was investigated. The wide range of scales in this study requires different knowledge and approaches used to adequately solve the problem. Therefore, a literature review was undertaken to cover these related issues.

#### **2.1 Natural Ventilation**

##### **2.1.1 Introduction**

The ventilation of a space can be considered as two distinct processes. The first process is to introduce the outdoor air into and out a space through openings, while the second is the motion of the air inside the space (Etheridge & Sandberg, 1996). It is one of the most important factors for maintaining acceptable indoor air quality in buildings. Proper ventilation design can help to improve indoor air quality and contribute to human health. There are several types of pollutants that must be removed from the building, such as pollutants related to human occupancy and to human activities, as well as that related to building itself, including those from

building materials and furniture etc. The tight relationship between indoor air pollutants and health was reviewed by Jones (1999). Air exchange between indoor and outdoor is happened during the first process, while the second process is related to internal air movement.

The volumetric flowrate of outside air being introduced into building is normally called ventilation rate. Apparently, ventilation plays a dual role in providing a health indoor environment due to the air exchange process. On one hand, it is known that ventilation is effective to remove indoor-generated pollutants from indoor air or to dilute their concentration to acceptable levels. But on the other hand, pollutant could also be introduced into indoor environment due to this air exchange process. For example, the contaminated outdoor air pollutants caused by traffic (Chan and Chung, 2003; Zhu et al., 2005) could enter into the building without a good ventilation control strategy. Kraenzmer (1999) compared a calculated exhaust air concentration to a measured exhaust air concentration about various gaseous pollutants to determine where the studied pollutant comes from. The results identified that some of the pollutants are originating from the outdoor air and penetrating into the building through ventilation air. Chao and Tung (2001) presented an empirical model for outdoor air contaminant transmission into residential buildings, and revealed that the air exchange rate plays an important role in influencing the contaminant transmission. Furthermore, strong and sufficient evidence to demonstrate the definite association between ventilation, air movements in buildings and the spread of infectious agents was revealed in a multidisciplinary systematic review conducted by Li et al. (2006).

The importance of ventilation highlights the need of investigations on building ventilation. The governing feature of this flow is the air exchange between an interior space and the external ambient. The flow of air through building openings is caused by either natural forces such as buoyancy and wind, or by mechanical fans. Based on these different driving forces, ventilation in a building can be defined as natural ventilation or mechanical ventilation. Both natural ventilation (Ayad, 1999; Jiang and Chen, 2001) and mechanical ventilation (Chow, 2001) have been thoroughly studied before. Particularly, Niachou et al. (2005) performed ventilation measurements within the 24-hour period on a circular basis, the comparisons between different ventilation strategies show natural ventilation can be more effective with regard to ventilation rate. The experimental results pointed out that in the presence of cross ventilation and with sufficient ambient wind speed, appreciable ventilation rates can be obtained with natural ventilation. In addition, summaries showed that buildings with natural ventilation are associated with less SBS-symptom, than buildings with traditional ventilation systems, (Seppanen and Fisk, 2002; Wargocki et al, 2002). Thus, with an increased awareness of the cost and environmental impacts of energy use, natural ventilation has become an increasingly attractive method for providing acceptable indoor environment rather than the more prevailing approach of using mechanical ventilation.

The advantages of using natural ventilation for energy conservation and the successful applications in providing human comfortable environment encouraged a large body of works aimed on this subject. Due to the scope of presented study, only some of the key issues are addressed and discussed here.

### 2.1.2 Principles of Natural Ventilation

In general, natural ventilation is created by pressure differences between the inside and outside of a building caused by wind and air temperature differences. For wind driven natural ventilation, the airflow through the opening is determined by the surface pressures on the building envelopes generated by the wind. Khan et al. (2008) gave a review on various wind driven ventilation designs with respect to traditional means to more modern techniques. The time-mean pressure due to wind flow on to or away from a surface is given by (Santamouris and Wouters, 2006):

$$p_w = \frac{1}{2} \rho C_p U^2 \quad (2.1)$$

where  $p_w$  is the surface pressure relative to outdoor static pressure in undisturbed flow,  $\rho$  is the air density,  $U$  is the time mean wind speed at a given level,  $C_p$  is the pressure coefficient. The dimensionless pressure coefficient is an empirical parameter that describes the changes in wind-induced pressure on building surface affected by prevailing local wind characteristics. The values can be either positive or negative depending on the building shape and orientation.

For buoyancy-driven natural ventilation, the air exchange is determined by the air density differences due to different temperature levels of air. When the inside building temperature is greater than outside, warm indoor air will rise and exit, subsequently be replaced by cooler, denser outdoor air. These kinds of ventilation are driven by buoyancy effect, or namely stack effect. Stack pressure is the hydrostatic pressure caused by the weight of a column of air located inside or outside a building. For an increase of temperature with height, there will be a corresponding decrease in pressure. If the temperature has a linear variation on vertical direction, and assuming

temperature and barometric pressure are constant over the height of interest, the stack pressure can be calculated as:

$$p_s = p_r - \rho gH \quad (2.2)$$

where  $p_s$  is the stack pressure,  $p_r$  is the stack pressure at reference height,  $\rho$  is the indoor or outdoor air density and  $H$  is the height above reference plane. The pressure difference at different height can then be determined from a definition of the neutral plane (ASHRAE Fundamentals, 2005).

Furthermore, when both wind and thermal buoyancy are present simultaneously, the driving force for natural ventilation becomes the pressure differences induced by the combination of both wind and buoyancy effects. The total driving forces are found as the sum of both forces. Under such situation, the wind can either assist the buoyancy force or oppose the airflow (Li and Delsante, 2001). The relationship between the buoyancy and wind effects could be complex due to the interaction between these two forces. Hunt and Linden (1999) tried to identify the form of the nonlinear relationship between the buoyancy and wind effects. It is shown that there is a Pythagorean relationship between the combined buoyancy and wind-driven velocity, and the velocities which are produced by buoyancy and wind forces acting in isolation. Li et al. (2001) revealed that multiple solutions for the flow rate exist in a natural ventilation system, induced by the interaction between both wind and buoyancy forces. It was found that under certain physical simplifications, the system is governed in steady state by a non-linear algebraic equation.

The pressure drop across an opening caused by wind and buoyancy effect dominates the airflow rate through that opening. The airflow through an opening can then be determined from the pressure difference by:

$$Q = C_D A \sqrt{2 \frac{\Delta P}{\rho}} \quad (2.3)$$

where  $A$  is the area of the opening,  $\Delta P$  is the pressure drop across the opening, and  $C_D$  is a discharge coefficient associated with the opening. Linden (1999) made an extensive review about the detailed flow mechanics of natural ventilation.

### **2.1.3 Different Types of Natural Ventilation**

Natural ventilation may be considered as single-sided or cross ventilated depending on the configuration of openings in the building. The openings can be designed on either opposite sides (cross-ventilation) or the same side of the building (single side ventilation).

Cross-ventilation is mainly caused by approaching wind effect. The wind airflow over a building tends to induce positive pressures on windward surfaces and negative pressures on leeward surfaces and on the roof, thereby creating a net pressure difference across the section of the building. Such pressure difference drives a flow within the building from the higher pressures side to the lower pressure side. Cross ventilation is strongly affected by the incident angle of the oncoming flow because the pressure at the openings can be varied due to changes of the separated flow patterns around the building (Ohba et al., 2001). Detailed mechanism of cross ventilation with open windows was investigated by Kato et al. (2003), employing

both wind tunnel method and CFD technique. The velocity and pressure fields of airflows in and around building models were analyzed in detail.

The ventilation potential is the possibility of providing outdoor air for indoor environment. An analytical model for this ventilation potential has been presented by Yang et al. (2005), aiming at Chinese residential buildings, and then developed by Luo et al. (2007). For cross ventilation potential estimating, the wind incidences and environment density significantly influence the pressure gradients across the building (Moeseke et al., 2005). Burnett et al. (2004) employed CFD simulation method to address how to get a maximum cross-ventilation based on the evaluations of pressure at external surfaces of a typical high-rise residential building in Hong Kong. The ventilation potential is related to the maximum air flow rate together with the flow trend, which is also in connection with pollutant dispersion around building. This also increases the need of studies on surface pressure distribution on building facades.

Single-sided ventilation is another common form of natural ventilation. It occurs when there is a single opening into a space. Both experimental and numerical methods have been used to study this kind of ventilation (Eftekhari et al. 2003). Larsen and Heiselberg (2008) revealed that the dominating driving force differs between wind speed and temperature difference depending on the ratio between the forces and the wind direction. For wind-induced single-sided natural ventilation, the ventilation rate is affected by both mean wind speed and the fluctuations of the wind. Experimental study has shown that the turbulent features of the approaching wind are also responsible for single side ventilation (Allard, 1998). Haghighat et al. (2000)

developed several correlation methods for the calculation of wind driven single-sided ventilation.

As to temperature-driven single side ventilation, where one opening separates two connected volumes of air at different temperatures, gravity currents occur when the outlet to the outdoors with another temperature is opened (Etheridge & Sandberg, 1996). This transient behavior is investigated by both theoretical/numerical prediction models and experimental methods (Fracastoro et al. 2002). The volume flow rate through one single large opening is approximated as (Awbi, 1996)

$$Q = \frac{C_d A}{3} \sqrt{\frac{gH\Delta T}{T_{out}}} \quad (2.4)$$

where  $H$  is the height of the window,  $g$  is the gravity acceleration and  $C_d$  is taken to be the discharge coefficient. As one of the prediction methods, this empirical model involves applying simple equations from Bernoulli theory for buoyancy-driven flow induced by temperature differences, together with an empirical discharge coefficient (Allard, 1998). The discharge coefficient  $C_d$  is influenced greatest by the dimensions and position of the opening, and is also influenced by the temperature difference between inside and outside air (Favaro & Manz, 2005). Most designs for single-sided ventilation focused on the effect caused by different driving forces individually, since there is a lack of information on the combined effects of wind and buoyancy on single-sided condition.

#### **2.1.4 Different Methods on Natural Ventilation Study**

A wide range of methods have been developed for natural ventilation studies. Presenting a detailed review of these studies is out of the scope of the present work. As mentioned above, the air exchange process happened during ventilation is the main concern which is closely related to pollutant dispersion studies. With regard to this aspect, the overall methods can be divided into two categories. The first is experiment method, and the second is prediction method. In this section, only prediction methods are briefly reviewed and discussed.

Simplified empirical methods provide general correlations to calculate the air flow rate. The expressions usually combine the air flow with the driving forces in order to give a bulk evaluation of the air flow rate in a building. It has been used for various kinds of situations (Linden, 1999). The main advantage of these methods is that they can immediately give an approximation of the situations. However, the models have been deduced either from theory or from specific experimental data and cannot be considered of general validity.

Network method is another common method in ventilation studies. A literature review undertaken in 1992 (Feustel and Dieris, 1992) identified 50 different multi-zone models that have been developed since 1970. For example, Conjunction of Multizone Infiltration Specialists (COMIS), a simulation tool developed at Lawrence Berkeley Laboratory, can be used to simulate air flow patterns in a multizone structure. The network method is based on the application of the Bernoulli Equation to determine the pressure difference and hence flow rate across each opening. It can be used to predict the overall ventilation rate of the entire building, and the individual air flow rate and direction through each opening. The prediction results obtained by

this model on both single-sided and cross ventilation have been compared with full scale measurements, and they were in good agreement with the experimental data (Dascalaki et al., 1999).

After reviewing the applications of CFD method on building environmental design, Jones and Whittle (1992) concluded that CFD codes can successfully be applied to building air flow prediction based on careful consideration and validation. CFD solves a set of partial differential equations for the conservation of mass, momentum, energy, and species concentrations, which govern the transport phenomena during ventilation process. Allocca et al. (2003) applied CFD techniques to determine the effects of buoyancy, wind and their combination on ventilation rates and indoor conditions. They revealed that the CFD model is an appropriate tool for single-sided ventilation design and research upon validation with analytical and empirical results. The performance of CFD for modeling natural ventilation driven by thermal buoyancy in two connected spaces has been evaluated through comparisons with the analytical models and small-scale experiments (Ji et al. 2007). The numerical results showed the ability of CFD for modeling natural ventilation flows driven by thermal buoyant plumes in connected spaces. Evola and Popov (2006) employed Reynolds averaged Navier-Stokes approach on wind driven natural ventilation in a cubic building under both single-sided and cross ventilation configurations. The results were then compared with experimental data provided in literature and well established empirical expressions for the prediction of the ventilation rate. It was shown that the simulation results were in good agreement with the data obtained by the other two methods.

Generally speaking, each method has its special place in ventilation analysis and design, and there are no universal tools. Experimental method gives the first hand information about natural ventilation studies, and its results can be used to validate other prediction methods. CFD method is capable of predicting flows in the building with great detail, but it is more time consuming to execute than multi zone method. Multi-zone methods offer opportunities for whole-building performance modelling, or a building with a large number of rooms. Li and Heiselberg (2003) presented a critical review of the literatures and recent developments in analysis methods for natural ventilation in buildings. More recently, Chen (2009) provided a comprehensive review on the overall methods about ventilation performance studies. It was found that CFD models become more and more popular in recent years for natural ventilation studies.

## **2.2 Airflow and Pollutant Dispersion around Buildings**

### **2.2.1 Introduction**

Characteristics of bluff body flow and dispersion of pollutants around building in urban environment are discussed here. There are several issues involved: atmospheric boundary layer flow, airflow around buildings, and pollutant dispersion around buildings.

Urban boundary layer flow at high velocities is a very typical flow condition of broad applicability for the rough surface of urban areas. From the standpoint of aerodynamics, the wind field of an urban area is a boundary layer flow along a rough

surface. Changes in the roughness of the surface cause internal boundary layers to develop within the planetary boundary layer, with different velocity profiles and turbulence characteristics. There are two kinds of expression to describe the mean velocity profile of atmospheric boundary layer. One is a power law and another is a log law. The detailed velocity and turbulence intensity profiles of the simulated atmospheric boundary layer in the present wind tunnel study are given in Section 3.2.4.

The contaminant transmission route within building environment is highly related to the airflow pattern near the buildings. The flow pattern that develop around individual building govern the wind forces on the building, the distribution of pressure on the building envelope, the scalar dispersion around the building and subsequently ingress of outdoor contaminant entering into indoor environment. Besides, observations indicated that the flow pattern around the building significantly affected the ventilation flow rate (Hu et al., 2008), which had been proved strongly related to airborne pollutant dispersion and infectious diseases transmission. Therefore, the study of the mechanisms of flow around buildings is the prerequisite to investigating the potential spread path of cross-contamination around building.

Figure 2.1 (ASHRAE, 2007) shows the interaction between contamination transport and the approaching wind when the pollutant is released from the roof of a rectangular building. As wind reaches a building, airflow separates at the building edges, generating recirculation zones over downwind surfaces and extending into the downwind wake. The flow pattern near the windward wall could be divided into three regions. The wind flow comes to the windward wall and rests at about two-

thirds of the height of the buildings to form a front stagnation region. Above this stagnation region, the wind flow passes the upper part of the building over the roof (**upwash**) and forms a recirculation region behind the building. Below the stagnation region, the flow goes down until it reaches the ground (**downwash**), and then moves forward against the wind. In this region, the flow rolls up and forms a horseshoe vortex on the ground in front of the windward face.

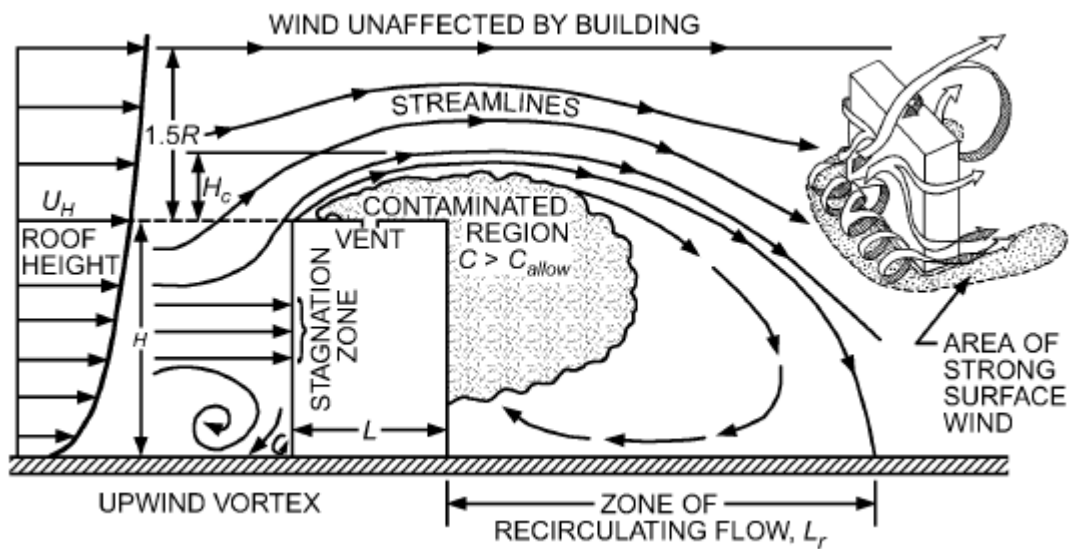


**Figure 2.1 Flow Patterns around Rectangular Building**

**((From: ASHRAE Handbook-HVAC Applications 44.3, 2005))**

Near the sidewalls, due to the flow separation along the edge of the windward surface, the sidewalls are under the action of negative pressure. The flow pattern at lower part of the sidewalls is associated with the horseshoe vortex. At leeward walls, it was found due to the flow from the horseshoe vortex through the shear layers on each side of building, one kind of vertical vortices could be formed with a rough flow direction from bottom to top behind the building (Cook, 1985). A circulation region could also be found behind the building driven by the shear layer over the roof. A relatively uniform pressure distribution is found in the region close to the vertical

sides of the leeward face. Figure 2.2 (ASHRAE, 2007) further illustrates the surface flow pattern along the building surface. It should be noticed that the surface flow patterns mainly depend on the building shape and upwind conditions. Because of the three-dimensional flow around a building, the shape and size of the recirculation airflow are not constant over the surface.

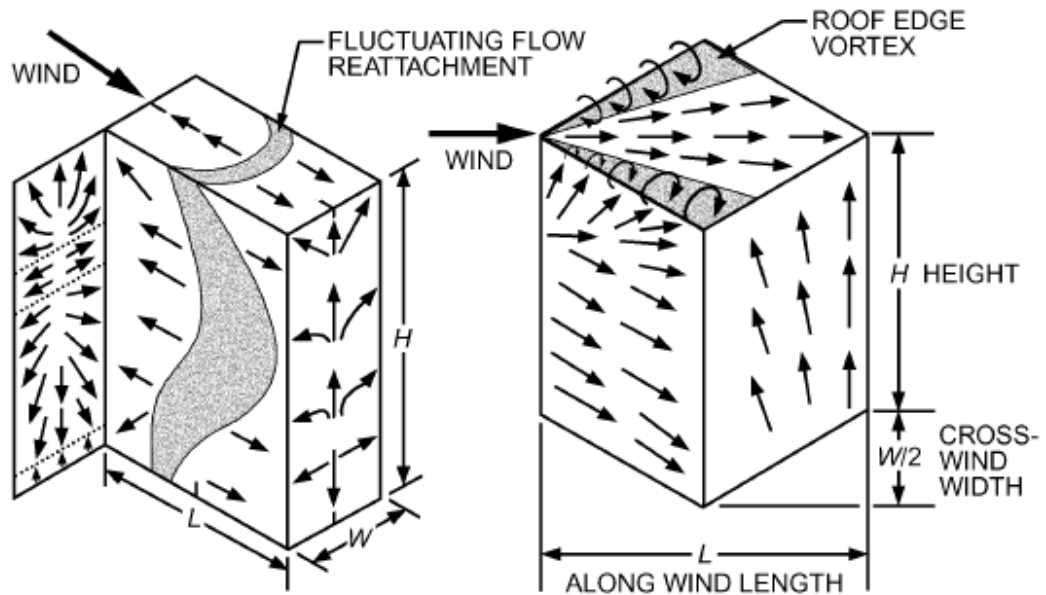


**Figure 2.2 Surface flow along different rectangular building**

**(From: ASHRAE Handbook-HVAC Applications 44.3, 2007)**

For pollutant dispersion around building environment, a substantial body of literature exists on this subject due to its specific importance for human health. Many previous studies have been conducted on the behavior of plumes released near different building environment ranging from street canyons, building arrays to isolated single building. Field measurement (Qin and Kot, 1993), wind tunnel method (Kastner-Klein et al., 2004) and CFD techniques (Liu et al., 2005) have been performed on the studies of pollutant transport inside and over urban street canyons. Vardoulakis et al. (2003) reviewed the measurements and modelling techniques for wind flow and

pollutant transport within street canyons. In particular, the recent progress in CFD modelling and wind tunnel method of wind field and pollutant transport in street canyons was summarized by Li et al. (2006) and Ahmad et al. (2005), respectively. Moreover, many researchers have contributed to the growth of our understanding of the features of pollutants movement within a group of buildings. The results obtained by scaled field measurements (Macdonald et al., 1997) illustrated that, when a plume was released upwind of regular arrays under different plan area density, the lateral concentration profiles, defined as the pollutant concentration distributions along a horizontal direction normal to the approaching wind, were generally Gaussian except that, close to the source, the concentration level was higher in the dense array than that in an open terrain. Mfula et al. (2003) employed wind tunnel method to determine the region around the building from which pollution sources affect the building. The region size depends on the density of the building array. The reduction in the spacing between buildings with each increment in area density encouraged lateral plume spread. More recently, Shi et al. (2008) presented numerical simulation of wind field and contaminant dispersion in the flow over a group of buildings, using the latest CFD techniques with large eddy simulation (LES) model. The prediction results of mean concentration field illustrated that numerical method also became a powerful tool for simulating contaminant dispersion inside building array by carefully considering a number of issues in the application.

Besides these studies for the pollutant dispersion within group structures, the information on flow and dispersion around an isolated obstacle is also useful for revealing the fundamental characteristics of the interaction between plumes of pollutant and building structure. The broad features of dispersion around isolated

simple building have been studied extensively (Higson et al., 1996; Li and Stathopoulos, 1997). A comparison was presented between dispersion around an isolated building and around the same building embedded in a building array (Mavroidis and Griffiths, 2001). The studies revealed that enhanced lateral spread occurred within the array while reduced concentration appeared in the building wake comparing with that of isolated building situations. In general, aimed at various kinds of building environment, the contributions recorded in a lot of literatures enhance the capability to deal with the contaminant dispersion in urban area, and broaden the method in predicting the complex interaction between plumes of pollutants and building structures in real situations.

### **2.2.2 Investigation Methods**

#### **Air flow around building**

The airflow around building is defined by impingement, separation, reattachment, circulation, vortices, etc., and all those phenomena increase the difficulty of study on such process. The majority of the studies focused on the basic cube shape, because of its geometrical simplicity yet representing the complex features of building aerodynamics. These include full-scale low-rise building structures such as Silsoe Cube (Wright and Easom, 2003) and Texas Tech University (Senthoran et al. 2004). When a building is exposed to a boundary layer type flow, the building causes a disturbance in the wind. The attempts to study wind effects on a tall building have been made by applying both experimental and CFD methods. Building surface pressures, which were affected by the approaching wind profile, were measured by

Melbourne (1980) on the Commonwealth Advisory Aeronautical Council (CAARC) standard tall building at different situations. Its full scale dimensions are: side 30.8 m (100 ft) by 45.72 m (150 ft) and height 183.88 m (600 ft). It has been intensively studied as one of the standard models to investigate the wind effects on tall buildings, and several wind tunnel measurements for this building were reported (Melbourne, 1980; Tanaka and Lawen, 1986; Goliger and Milford, 1988). However, the weakness of physical modelling is its high cost and thus limited cases can be studied in detail with this method.

Computational Wind Engineering (CWE) as a branch of Computational Fluid Dynamics (CFD) has been developed rapidly over the last three decades to evaluate the interaction between wind and structures numerically. The techniques of CFD have been widely used to predict wind flows around bluff bodies. Stathopoulos and Baskaran (1996) studied on computer simulation technique for the evaluation of mean wind environmental conditions around buildings. The computed results were compared with wind tunnel experimental data, and it was shown that the most significant features of the wind environmental conditions around buildings can be predicted with reasonable accuracy, indicating high potential for CFD application to wind environmental design. After that, the available computational results at that time and its comparisons against that of wind tunnel measurements were summarized by Stathopoulos (1997).

With rapid development in computer hardware and numerical algorithms, computational fluid dynamics techniques are now widely utilized to study the wind field around high rise buildings. Murakami (1998) reviewed the CFD applications in

wind engineering and commented that the LES with a dynamic subgrid-scale (SGS) model is a promising tool for accurately predicting the flow field around a bluff body. RANS (Reynolds averaged Navier-Stokes) turbulence models were compared with LES model about the performance in predicting the turbulent flow features around building, and it was shown that acceptable results can be also obtained by these models (Lubcke et al., 2001). More recently, Tominaga et al. (2008a) compared computational fluid dynamics (CFD) results using various revised  $k-\epsilon$  models and large eddy simulation (LES) applied to flow around a high-rise building model. It revealed that the results obtained by Durbin's revised  $k-\epsilon$  model and the LES with inflow turbulence show generally good agreement with experimental results. The wind effects on a tall steel building was numerical evaluated by Huang et al. (2007), and illustrated it is necessary to correctly simulate both the incident wind velocity profile and turbulence intensity profile in CFD computations for successful predicting wind effects on tall buildings. Aimed at Hong Kong building characteristics, Burnett et al. (2005) numerical investigate the wind-induced pressure at external surfaces of a high-rise residential building. The results revealed that an optimal building orientation relative to the wind can be found through the comparisons of different cross-ventilation potential at various kinds of situations. Yang et al. (2005) examined different design of estates for good cross-ventilation in high-rise residential buildings in Hong Kong through CFD simulation studies. The outputs from wind field models can be used with pollutant transport models to calculate the pollutant distribution around buildings.

In general, CFD method has been widely used in predicting the airflow pattern around buildings since 1990s, after the CWE Conferences in 1992. Some countries

have already established working groups to investigate the practical applicability of CWE and develop recommendations for the applications, such as the Architectural Institute of Japan (AIJ) (Tamura et al. 2008, Tominaga et al. 2008b). There have been several successful applications using CFD method, and the predication results are in good agreement with experimental data. The solution variability is affected by a wide range of possible user-inputs and decisions, such as meshing choices, source conditions, turbulence models, inflow conditions and representation of the geometry. Stathopoulos (2002) concluded that in spite of some interesting and impressive results obtained by CWE, the numerical method is still virtual rather than real. More parallel studies-numerical and experimental-will be required to increase the level of confidence in the computational results.

### **Pollutant dispersion around building**

There have been a wide range of methods that exist for predicting pollutant dispersion. Generally speaking, there are two categories of methods to study pollutant dispersion around building: experimental methods including full-scale measurements and scale modeling method, prediction methods including empirical models and computational fluid dynamics simulations. The purpose of this section is not to list models or go into the detail of their content. Rather, the modelling types used to investigate pollutant dispersion around building are described, along with a brief introduction about the pros and cons of each type.

Experimental dispersion modeling can take place either in the field or in the laboratory. Field experiments such as tracer releases in real urban sites provide the closest approximation to the dispersion process. Several field tests have been

conducted in the past (Davidson et al., 1995; Mavroidis and Griffiths, 2001; Stathopoulos et al., 2002). These are valuable because they are conducted in the real environment conditions and provide information on the real complexity of the phenomenon. However, in general, field measurements are limited by their low spatial resolution, uncontrollable meteorological conditions and the results are totally different with various individual buildings. Also, due to the inherent natural variability found in the field, measurements must be taken over sufficiently long periods to draw statistically significant conclusions.

Laboratory scaled modelling is a key dispersion modelling tool. The majority of dispersion studies have been carried out in the laboratory. It is usually carried out either in a wind tunnel or a water tank. Scale modelling is based on theoretical assumption that flow and dispersion around scaled obstacles is dynamically similar to that at full scale. This method allows controlled physical simulation of dispersion processes (Davidson et al., 1996; Meroney et al., 1999; Mavroidis et al., 2003). But this physical modeling method is still time consuming and costly while detailed information of flow and concentration field can not be obtained. More on wind tunnel modelling techniques can be found in Section 3.2.1.

Semi-empirical models express pollutant concentration as a function of several input variables. An example of such model is a Gaussian plume model (Pasquill and Smith, 1983). The advantage of these models lies in their simplicity, which makes them relatively easy and quick to use. The disadvantage of this approach is this formula can only be used to do a rough estimate of the pollutant dispersion in atmospheric environment. The accuracy of its calculation can not be ensured, and this method is

not appropriate for complex situations with dispersion field affected by complicated building structures.

With the increasing computational speed of computer and better computer graphic tools, numerical simulation with CFD techniques has become a powerful tool in predicting contamination spread in and around building environment (Mavroidis et al., 2007; Shi et al., 2008; Blocken et al., 2008). This approach is generally less expensive than field and wind tunnel tests, and the results of the flow and concentration field can be obtained in great detail. However, CFD requires specific care in order for the results to be reliable. Ranging from grid resolution, boundary conditions to model selection and iterative convergence should be taken into consideration based on careful analysis of the flow features about the presented problems, together with estimation about the computational cost. More on CFD modelling techniques can be found in Section 5.4.1 and 5.4.2.

By definition, any modelling method is a simulation of reality based on particular assumptions, simplifications and approximations, and these determine the degree of accuracy and uncertainty inherent in any type of modelling. It should be noticed that different processes are important at different scales, and consequently different models are required. A comprehensive review (Meroney, 2004) has been made on the methods that exist for predicting pollutant dispersion, ranging from field tests and wind tunnel modeling to semi-empirical methods and numerical simulations with CFD techniques.

### **2.3 Related Studies aimed at Hong Kong Environment**

The contamination spread path around building is strongly affected by the air flow characteristics near to the building. The air flow pattern near a building can be particularly complex caused by the interaction between meteorological conditions and building structures, which can be varied by different environmental conditions.

The presence of more and more high rise residential buildings have led to some problems. One of the problems is the quality of air. Especially in modern developed cities where high rise residential buildings are common, the residents would usually suffer from the indoor air quality problem if the ventilation system were not properly designed. Hong Kong's environmental issues are typical of those in many densely populated cities (Burnett, 2005), and new problems present because of the presence of high-rise residential (HRR) buildings while the housing problem is solved (Niu, 2004). A questionnaire survey carried out by Lin and Deng (2006) shows that most of the respondents are not satisfied with the indoor air quality in bedrooms in Hong Kong.

From infectious disease transmission point of view, Hong Kong was the hardest-hit area during the SARS epidemic in 2003, with 1,755 residents infected, of whom 299 died (WHO, 2003). Two serious case clusters, one in a residential estate, and the other in hospital wards, drew much attention to the mode of transmission of SARS virus and the role of environmental factors. A detailed investigation using a multi-zone model was conducted to explore the association between the spatial infection pattern and the predicted virus-laden aerosols dispersion pattern in the most affected

block (Block E) of Amoy Gardens (Li, et al, 2004a). The largest nosocomial outbreak in the Hospital wards was also studied in detail by Li et al.(2004b), using retrospective on-site inspections and measurements combined with CFD simulations.

Comparatively, smaller scale SARS clusters that occurred in several other high-rise residential buildings in Hong Kong have not attracted sufficient attention. In Wing Shui house (Lek Yuen Estate, Sha Tin District), 11 infection cases residing in 5 households were reported with no presence of SARS virus detected in the sewage system and common areas after a prompt investigation, also there does not exist the re-entrance space as had been highly publicized in the Amoy Garden case (HWFB of the HKSAR, 2003). In Hing Tung House (Tung Tau Estate, Kowloon City), 6 confirmed SARS cases involving 3 families were reported along one vertical block with findings showing that this building did not have any structural factors similar to those of the Amoy Gardens that would lead to an outbreak (DH of the HKSAR, 2003). In the case of Wing Shui house, adjacent upper floor residents were infected after those on the lower floor, and bio-material of the SARS virus was found within the deposits on the window-sill and floors on two other upper floors. In view of these facts, it is well justified to suspect that the virus-containing contaminants can travel with ventilation air from a lower flat to the adjacent upper flat in high-rise residential blocks at certain environmental conditions, forming a spread path of infectious diseases. Also, the vertical spreading was extremely similar to an airborne outbreak of smallpox disease in a German hospital, which relied on open-window to obtain natural ventilation (Schaelin et al., 1992). Using smoke test, they identified that there was a vertical air flow coming out of the index room on the ground floor and re-entering the upper three floors, via open windows located on the same facade.

In light of these previous studies, the present study is focused on the new pollutant transmission path related to Hong Kong environmental conditions, which has been overlooked so far. It is the hope of the author that the new problem about HRR building environment introduced in this thesis will prove a useful basis for future HRR building environment research.

## **2.4 Summary**

In this chapter, several key issues related to the topic of this thesis have been reviewed. The investigation on cross-contamination includes both the ingress of outdoor pollution into indoor environment and the estimation of pollutant concentrations around building. Therefore, firstly the important role of air exchange between indoor and outdoor environment was discussed and the fundamental principles of natural ventilation was presented. The review of the literature presented in this section focused on the studies related to the air exchange process between inside and outside. In particular, mainly concern is put on the modelling method about the ventilation performance of high-rise residential buildings, which has been mainly driven by the associated high energy costs.

Next, pollutant dispersion was placed in an urban context, and a number of issues about both airflow and pollutant dispersion around building were introduced. The state of the art in terms of near building dispersion modelling was reviewed.

Empirical model can be very useful in modelling dispersion. Many dispersion studies have concentrated on the comparisons against empirical model and made modification on the model parameters aiming at different problems. But in complex situations such as near-field urban dispersion, the model is not feasible for specific cases. Besides, it can hardly handle the complicated interaction between complex building shape and upcoming wind profile, resulted in an unsuccessful prediction of pollutant dispersion. For the current study, both the near building pollutant dispersion and modelling of wind interacting with complex building are the key issues need to be solved. Therefore, the empirical model is probably not appropriate for the current study.

Field measurement is a valuable tool for dispersion studies since it can provide first-hand information under specific environment conditions. The on-site experiment results can reveal the transport process in real situation and it can be used to check the empirical model and to determine the parameters. However, the results from field experiments are hard to generalize, since it is difficult to tell how much influence for each single parameter has on the observed flow and dispersion behavior. It is not possible to control environmental conditions such as wind speed and wind direction in the field. Furthermore, the cost of full-scale measurements of concentration profile around an entire building is beyond the resources available for this investigation.

In the next chapter, the methods by which this investigation is carried out are presented.

## **Chapter 3**

### **Research Methodology**

#### **3.1 Introduction**

In this chapter, the investigation methods used in this study are described. The choice of methods and the main points of each method are outlined. The overall objective of this study is to investigate the possible cross-contamination in complex building environment dominated by natural forces. It can be divided into two main categories. Firstly, aimed at relatively simple HRR building and under buoyancy dominated environmental condition, the cross-contamination between two vertical adjacent flats is studied and evaluated. This stage of work is mainly focused on part of the HRR building and to analyze the consequences of pollutant re-enter into indoor environment caused by air exchange between indoor and outdoor environment. Next, based on the identification of this transmission path, the study is therefore extended to the entire building under more complex situation. The main concern of wind-induced cross-contamination in more complicated building shape is to evaluate the pollutant dispersion near the building surfaces. The selection of investigation method for each stage is based on different characteristic and purpose of the study.

The study on buoyancy-induced cross-contamination between two vertical adjacent households is carried out by CFD techniques. Benefiting from CFD advantages, enough experiment cases for validation and the rapid progress on ventilation studies, the problem could be solved based on a careful calibration or validation between

simulation results with related experimental case. Also, the outcomes based on various kinds of performance design could be numerically evaluated.

As to the investigation on cross-contamination under wind effect, the purpose is to estimate the dispersion process around entire building affected by atmospheric boundary layer flow. Due to the limitation of reliable information about this problem, a hybrid approach combining both physical modelling and numerical modelling methods is applied for this study. A series of experiments are designed and undertaken in a boundary layer wind tunnel. In the mean time, the wind tunnel experiment results could provide the necessary information for the calibration on the numerical method via comparisons between predicted results and experiment data.

Both experimental techniques used in the wind tunnel and a framework of CFD method are introduced in the following sections of this chapter.

## **3.2 Wind Tunnel Method**

### **3.2.1 Wind Tunnel Modelling Theory**

Wind tunnel modelling is a type of physical scaled modelling method. Scaled modelling is based on the fundamental premise that by reducing the geometrical scale of a given flow domain, and by adjusting reference parameters such as flow velocity, fluid density etc., the original scale flow can be reproduced correctly.

To accurately simulate the dynamics of the flow in the physical model, similarity criteria are derived through analysis of the equations of motion. With the earth as a reference frame rotating at an angular velocity, the fluid motion is described by the continuity, conservation of momentum and energy equations. These equations of motion for a fluid in a turbulent boundary layer can be expressed in a nondimensional form by using the scaling factors (Snyder, 1979). One set of requirements for exact similarity is equality of the nondimensional coefficients for the physical model and the atmosphere. In summary, the requirements may be stated as follows (Cermak J.E. 1975):

- Undistorted scaling of geometry
- Equal Rossby Number
- Equal Gross Richardson Number
- Equal Reynolds Number
- Equal Prandtl Number
- Equal Eckert number

Unfortunately, all similarity requirements cannot be satisfied simultaneously and we must use partial or approximate similitude. Hence model conditions must be chosen which are designed to simulate most accurately those scales of motion that are of greatest significance for the application. Fortunately, several of the dimensionless parameters can be neglected due to their low relative importance when simulating transport and dispersion about buildings.

Geometric similarity will be automatically satisfied by a correctly scaled model with all lengths equally scaled in 3 dimensions. The Rossby Number is a representation of the ratio of inertial forces to Coriolis forces, reflecting the inertial effects of transport in a rotating coordinate system (the Earth). To exactly simulate this number, the effects of the Earth's rotation should be simulated in the wind tunnel. However, this criterion could be relaxed because the effects of the Earth's rotation are negligible in the prototype for the short traced distances and velocities considered in this experiment. The Richardson number represents the relative significance of buoyant forces and inertial forces. This criterion could also be relaxed since atmospheric stratification effects are small because that the presented experiment is conducted in room temperature. The Prandtl number is expressed as the ratio of molecular viscosity to thermal diffusivity, which involves only the properties of the fluid. Because the target fluid in both the model and the prototype is air, Prandtl number similarity is automatically achieved in this experiment. The Eckert number represents the ratio of heat generated by friction to heat compression. It can not be made similar of two flows if the Richardson number equality exists. However, the range of velocities considered in these experiments is much smaller than the speed of sound. Thus, the Eckert number criteria may be neglected because Eckert number is generally small compared to unity for subsonic flows.

The Reynolds Number is defined as the ratio of convective inertial forces to viscous forces. If strict Reynolds number equality is required, no atmospheric phenomena could be modeled since scale reduction of 1:100 to 1:1000 commonly result in model Reynolds numbers two to three orders of magnitude smaller than those found in the atmosphere. Meroney (2004) made a detailed review about Reynolds number

independence happened in different kinds of situations. It was said that for a flow system in which thermal and Coriolis effects were absent and whose boundary conditions were similar when normalized by the appropriate characteristic length  $L$  and velocity  $U_R$ , the turbulent flow structure would be similar at all sufficiently high Reynolds numbers. The Reynolds number independence criterion is based on the premise that “geometrically similar flows are similar at all sufficiently large Reynolds numbers”. Above a certain Re threshold a flow becomes turbulent and then the gross structure of the turbulence becomes similar over a wide range of Re numbers. For modeling of plumes interacting with structures, it is now known that the criteria are affected by source location, building orientation, and measurement location. Simulations for measurement locations in the middle to far wake region ( $x > 1H$  downwind) may only require  $Re = U_H H/\nu > 3,000$  if a truly turbulent exhaust plume exists. However, concentration distributions on the building surface itself may vary with wind speed until Re values exceed 15,000. With respect to our investigations, even if the wind velocity at model height is as low as 1m/s, the Reynolds number of wind tunnel modeling is about  $4 \times 10^4$  at room temperature, which is much larger than the criteria. Thus the Reynolds independence can be satisfied.

Besides the similarity requirements mentioned above. The approaching wind profile obtained in wind tunnel and that of prototype should also be similarity. The similarity of the approach-flow characteristics requires similarity of the following flow features:

- Distributions of mean and turbulent velocities,

- The longitudinal pressure gradient (should be zero),
- Distributions of mean and fluctuating temperatures, and
- Equality of the ratio  $H_2/H_1$  if the flow is layered.

The present experiment is not focused on the buoyancy effect on the flow pattern and contamination dispersion. Therefore, the last two criteria could be neglected. The wind characteristics are achieved by a combination of turbulence generating spires, a barrier at the entrance of the wind tunnel, and roughness elements along the wind tunnel floor upstream of the model. The longitudinal pressure gradient over the model is set to be zero by adjusting the wind tunnel roof height to make the flow as non-accelerating as it is in the atmosphere, or through the use of vented wind tunnel boundaries. An alternative to this requirement is the application of blockage corrections which is satisfied during the presented experiments. The blockage ratio, defined as the projected area of the near field simulation and the wind tunnel cross sectional area, should be less than 5% to minimize the requirements for blockage correction (Barlow, 1999). In addition, the building model under study does not exceed half the wind tunnel height during the experiments

### **3.2.2 The CLP Power Wind/Wave Tunnel**

In conducting wind tunnel model studies of wind effects on tall buildings and other structures on the surface of the Earth, it is necessary to adequately simulate the atmospheric boundary layer. The experiment in this study is undertaken in the CLP Power Wind/Wave Tunnel (WWT) in the Hong Kong University of Science and

Technology. The CLP Power Wind/Wave Tunnel Facility has a state-of-the-art subsonic boundary layer wind tunnel with two parallel wind tunnel test sections (high-speed and large cross-section) for civil/structural engineering and environmental engineering applications. It can be used to simulate atmospheric boundary layer flow over various types of terrain, ranging from open terrain, such as open water, to urban or mountainous terrain.

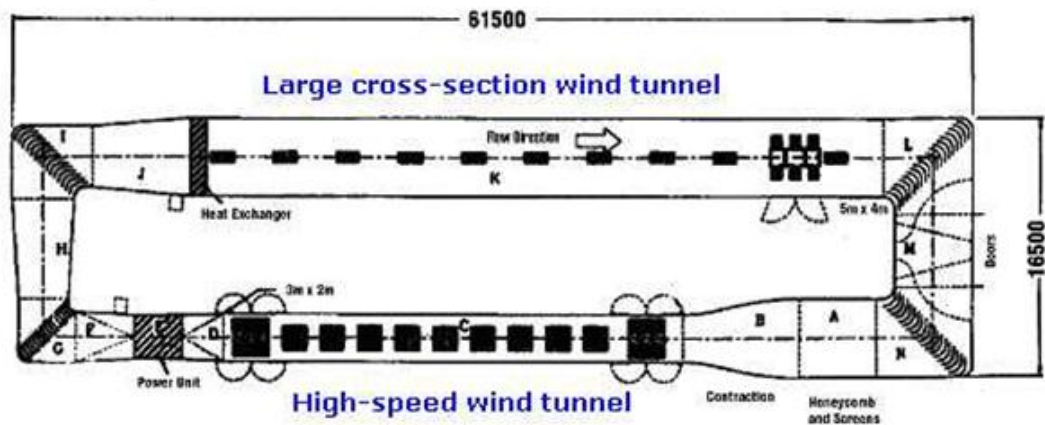


**Figure 3.1 The plan view of the CLP Power Wind/Wave Tunnel in HKUST**

Figure 3.1 and Table 3.1 show the plan view and facts of this wind tunnel. The 28 m long high-speed test section has a 3 m wide  $\times$  2 m high working section and a maximum free stream wind speed of approximately 30 m/s. The 40 m long low-speed test section has a 5 m wide  $\times$  4 m high working section and a maximum free stream wind speed of approximately 10 m/s. Various terrain simulations can be modelled in either test section at different length scales. In its basic configuration, the wind tunnel forms a closed-loop for enhanced efficiency. For gas dispersion studies, the wind tunnel can be converted from closed-loop to open-circuit by using purge doors in the return leg connecting the low and high-speed sections.

**Table 3.1 The overall parameters of the CLP Power Wind/Wave Tunnel in  
HKUST**

Overall size	61.5 m long x 16.5 m wide x 7.5 m high
High-speed wind tunnel	29.2 m long x 3 m wide x 2 m high
Turbulence intensity	< 0.5%
Flow uniformity	< $\pm 0.5\%$
Flow angularity	< $0.5^\circ$
Contraction ratio	3.33 : 1
Large cross-section wind tunnel	41 m long x 5 m wide x 4 m high
Flow conditioning elements for both test sections	Honeycomb/screens
Water tank	41 m long x 5 m wide x 3 m water depth
Fan type	Axial flow
Fan diameter	2.5 m
Power	170 kW
Speed regulation	variable speed + manually variable pitch
Heat exchanger	$\pm 1^\circ\text{C}$

### 3.2.3 Building Model Design

The objective of this research is to study the pollutant dispersion in and around typical-shaped high rise residential buildings in Hong Kong. The models were constructed based on the shape of type II mentioned in section 1.2. Model A represents a 33 stories HRR building with height equal to 100m in prototype. Model B represents a 10 stories HRR building with height equal to 30m in prototype, and is constructed with effective opening area equal to 20% of a normal window area. The first stage experiment is undertaken in the high speed section of CLP Power wind

tunnel with model A. The second stage experiment is undertaken in the low speed section with model B.

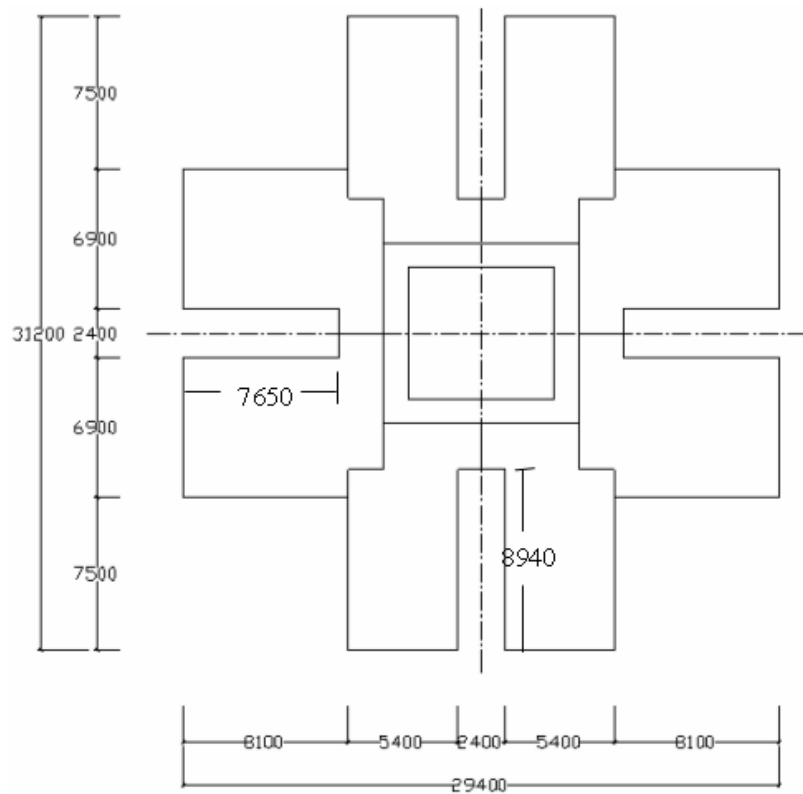


**Figure 3.2 Plan view of the experiment model.**

A plan view of the simplified building model is shown in Figure 3.2, and each floor contains eight units. The first building model A is constructed as a block without any openings on the building envelope. For this stage of experiment, the main purpose is to reveal the basic characteristics of airflow and pollutant dispersion around the HRR building under wind effect, and to evaluate the cross-contamination risk from an entire building point of view. For this kind of building shape, it is very common in Hong Kong with a height usually over 30 floors. Moreover, at scales near 1:100, simulation is achieved only down to scales associated with the maximum turbulent energy resulting from local surface roughness. When local diffusion near buildings

and building-plume interactions are under investigation, a model scale of approximately 1:100 simulates the important scales of motion (Cermak, 1975). Also, for time consuming consideration, the first stage of experiment is designed to be undertaken in the high speed section of CLP Power wind tunnel. The experiment data can also be used to evaluate the performance of CFD methods.

The second stage of experiment is designed to further study the detailed pollutant dispersion mechanisms around high rise residential building in detail. Therefore, it should be undertaken in the low speed section of CLP Power wind tunnel due to the use of large-scale models can eliminate unwanted problems and also allow greater spatial resolution of concentration data (Saathof et al., 1995). Therefore, both mean concentration and concentration fluctuations could be intensively studied based on the results obtained in this stage. And the risk of cross-contamination under wind effect can be therefore estimated and evaluated.

### **3.2.4 Approaching Wind Profile**

The velocity profile of the atmospheric boundary layer in the wind tunnel test takes the following power law

$$\frac{U(Z)}{U_{ref}} = \left( \frac{Z}{Z_{ref}} \right)^\alpha \quad (3.1)$$

where  $U_{ref}$  is mean velocity at the height of the building model,  $Z_{ref}$  is the model height, and  $\alpha$  is the power law exponent, which is 0.2 for present experiments. For the turbulence intensity profile in the approaching flow, at present, only Japan, ECCS

(The European Convention for Constructional Steelwork) and Australia provide the longitudinal turbulence intensity profile at different terrain conditions. HKSAR Planning Department (2008) pointed out that the conduct of the wind tunnel test should comply, as far as practicable, with established international best practices. Therefore, the turbulence intensity profile of the approaching wind flow was simulated in accordance with Terrain Category 2 stipulated in Australian/New Zealand Standard (1989). For high-speed section of wind tunnel, computer controlled, pneumatically operated roughness elements are used to develop the turbulent boundary layer flow. For low-speed section of wind tunnel, the atmospheric boundary layer flow is generated by a combination of turbulence generating spires, a barrier at the entrance of the wind tunnel, and roughness elements along the wind tunnel floor upstream of the model.

The characteristics of the ABL were examined by measuring longitudinal wind velocity and turbulence intensity profiles at the windward face of the building model. The mean velocity profile was presented by wind velocity ratio (VR) defined as  $U_z / U_{\text{Ref}}$  to achieve the boundary conditions similarity criteria through normalized by the appropriate characteristic velocity  $U_{\text{Ref}}$ , which was selected as the wind velocity at building height in this experiment.

### **3.2.5 General Arrangement of Wind Tunnel Experiment**

The general sketch of the experiment configuration is shown in Figure 3.3. The density difference between this tracer gas and air is within 5 percent, thus the

buoyancy effect is negligible during the experiment. Tracer gas was released through a flow-meter at a constant flow rate at a nozzle exit, which was flush with the building surface. The flow rate of the tracer gas was low enough to ensure that source momentum effects were not significant.

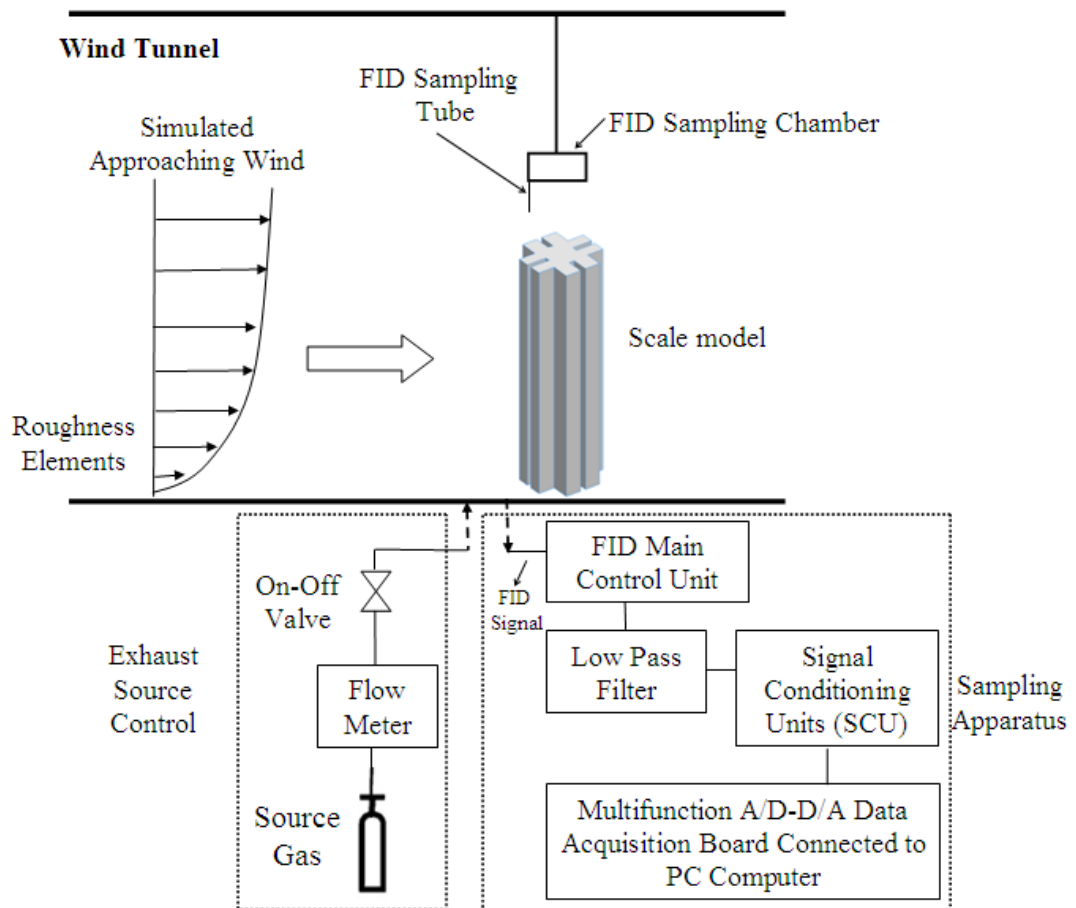


**Figure 3.3 The sketch of the experiment configuration**

The tracer gas was released from different points. At any one series of measurements, tracer gas was only released at one of these locations. Compared with a line source which is usually used to produce the dispersion characteristic within streets induced by traffic pollutant, a point source provides more clear information on pollutant fluxes and dispersion within complex building environment. A point source

represents a situation where a single source of pollution is dominant, such as hazardous release. The tracer gas used during the experiment is propane in air with known constant concentration.

### **3.2.6 Measurement Methods**

For the wind profile calibration, the wind characteristics are measured by Cobra Probe due to its advantages and reliability (Watkins et al. 2006). It was supplied by the manufacturer already calibrated for velocity and frequency response and required only static calibration to check the transducer Volts-to-Pressure ratio before use. The Cobra Probe is a four-hole pressure probe that provides dynamic, 3-component velocity and local pressure measurements in real-time. It is able to measure flow fields within a range of  $\pm 45^\circ$  at frequencies of more than 2000 Hz, making it ideal for the measurement of turbulent flow fields.

Surface pressures were measured simultaneously by pressure taps (diameter of 0.5mm), which were mounted on the model and connected to 16-channel electronic pressure scanners manufactured by Pressure System Inc. (Csiba and Martinuzzi, 2008). Both the tubes and the pressure scanners were concealed in the building model and connected to the data acquisition system under the wind tunnel floor. This arrangement makes sure that the tubes and scanners have no interference to the airflow. The pressure measurement points were arranged along the exteriors of the building, thus the pressure coefficient distribution along the whole building could be established. The pressure coefficient is defined as:

$$C_p = (p - p_{ref}) / 0.5\rho U_{ref}^2 \quad (3.2)$$

The difference between the surface pressure  $p$  on the building envelope and the static pressure  $p_{ref}$  measured at the reference position by a Pitot-static probe was then non-dimensionalized using  $U_H$ , the velocity at the building height to give the pressure coefficient,  $C_p$ , in the usual form.

For the tracer gas concentration measurement, the detection of propane concentrations was achieved with fast flame ionization detectors (Pavageau and Schatzmann, 1999; Baker and Hargreaves, 2001) (FID, model HFR400 manufactured by Cambustion Ltd). A FID works by counting the ions generated when a sample, containing a hydrocarbon, is burnt in a hydrogen flame. The leakage current from a high-voltage collector is proportional to the number of ions produced, and hence to the concentration of hydrocarbon in the sample. For each stage of experiment, concentration measurements were taken at each floor at different facades within the re-entrant space to enable dispersion patterns to be mapped out in detail. Four FID sets were used to simultaneously sample the building surface concentrations. Samples of air were collected via sampling tubes which had an inside diameter of 1.2mm. The signal was then passed through a low pass filter which effectively eliminates the alias errors. The background concentration in the wind tunnel was measured upstream of the model and subtracted from the measured concentrations.

Careful considerations have been made on how to minimize the effect induced by experimental uncertainty. The first is to minimize the equipment error. The calibration of the fast FID was carried out using a series of standard gas with a series of known concentrations. Two selectable gains were used in order to enable the instrument to be operated at different levels of sensitivity, aimed at different concentration ranges (i.e. using gain A for high-concentration measurement, and gain B for low-concentration measurement.). The calibration was repeated to ensure that the calibration error is generally within 10% before each experiment, and the detectors were found to have linear calibration curves in both gains. Second, the unavoidable random variation that occurs when making repeated measurements was attempted to minimize by carefully selecting the sampling time for concentration measurements. Numerous repetitions of the same case were made in order to determine the inherent variability of the dispersing characteristics.

The measured concentrations at different locations were scaled using the usual form of non-dimensional concentration  $K_c$  :

$$K_c = \frac{CU_H H^2}{Q} \quad (3.3)$$

where  $C$  is the measured mean concentration,  $U_H$  is the mean wind speed at building model height  $H$ , and  $Q$  is the volumetric flow rate of the tracer gas. This scaling accounts fully for all aspects of plume dispersion at any scale, wind speed or source flow rate. The dimensionless concentration expresses the absolute differences of concentrations for different configurations. The equation can also be presented as another form:  $K_c = C/(Q/U_H H^2)$ , in which the term  $Q/U_H H^2$  represents the

concentration when the emitted pollutant is assumed to be evenly distributed within the sectional area of the building. Thus this index also indicates the dilution ratio at various positions compared with source strength.

For detailed setup of each stage experiment, the measurement points and source location arrangement will be presented in the following chapters.

### **3.3 Computational Fluid Dynamics Method**

Advanced technology has produced faster and more powerful computers, which allows computational fluid dynamics (CFD) method to be used in different engineering applications. Besides the scale-modelling method, with increasing computational resources and the widespread availability of commercial codes employing the CFD approach, numerical method is gradually being adopted as an attractive alternative tool to predict contaminant dispersion and concentration distribution. Numerical simulation is especially useful for providing detailed flow visualization that is difficult for physical simulation to perform.

#### **3.3.1 Governing Equations**

CFD modelling is based on the numerical solution of the governing equations of fluid flow. The general form of conservation equation for mass, momentum, energy and scalar quantities such as the concentration of pollutants is given by:

$$\frac{\partial}{\partial t}(\rho\phi) + \text{div}(\rho\vec{u}\phi) = \text{div}(\Gamma_{\phi}\text{grad}\phi) + S_{\phi} \quad (3.4)$$

The source term  $S$  of quantity  $\phi$  takes the appropriate form for momentum, energy, turbulent kinetic energy, dissipation rate and concentration.

These equations pertain to both laminar and turbulent fluid flow. When the flow is laminar, a discretized form there equations can be solved easily via various numerical techniques. If the flow is turbulent, simulations will require modeling and high-performance computational techniques.

### 3.3.2 Turbulence Models

The most common CFD techniques are direct numerical simulation (DNS), large-eddy simulation (LES), and Reynolds averaged Navier-Stokes (RANS) equations with turbulence. Each technique handles turbulence in a different manner. DNS compute the mean flow and all turbulent velocity fluctuations. The unsteady N-S equations are solved on spatial grids that are sufficiently fine that they can resolve the Kolmogorov length scales at which energy dissipation takes place and with time steps sufficiently small to resolve the period of the fastest fluctuations. It is known that applying DNS is not realistic at present since this method is still excessively costly and can be used only for fundamental academic research. Also, the need to resolve the full spectrum of scales is not necessary for most engineering applications. Therefore, a successful simulation of turbulent flow should use approximations, namely, turbulence models.

There are generally two categories of turbulence modelling approaches, in which the governing equations are either time-averaged (RANS-based models) or spatially-averaged (LES), respectively. LES is an intermediate form of turbulence calculations which tracks the behavior of the larger eddies. The premise of LES is to simulate the large-scale turbulent motions and approximate the small-scale motions through modeling. The effects on the resolved flow (mean flow plus large eddies) due to the smallest, unresolved eddies are included by means of a so-called sub-grid scale model. The success of the LES stems from the fact that the main contribution to turbulent transport comes from the large-eddy motion. In the mean time, because small-scale turbulence is modeled, LES requires considerably less computational resources than DNS. With the increasing numerical capability of modern computer, LES is more and more widely used in predicting airflow field. The key to successfully predicting airflow by the LES is to accurately represent the unresolved subgrid-scale (SGS) motion. It should be noticed that under present computational conditions, such applications employing LES are mainly focused on simple geometry of buildings. To study the problems with a complex geometry or a large-scale site, LES has difficulty due to limitations of available memory and computing speed.

RANS models have been the mainstay of engineering flow calculations over the last three decades, due to the modest computing resources required for reasonably accurate flow computation (Versteeg and Malalasekera, 2007). The attention of RANS models is focused on the mean flow and the effects of turbulence on mean flow properties. Prior to the application of numerical methods the N-S equations are time averaged. Extra terms appear in the time-averaged flow equations due to the

interactions between various turbulent fluctuations. These extra terms are modeled with different models. The most common RANS turbulence models are classified on the basis of the number of additional transport equations that need to be solved along with the RANS flow equations. Reynolds-stress models, which have seven extra transport equations, are superior to the eddy-viscosity models, because the RSM do not use the Bousinesq approximation. However, there is a penalty in terms of model complexity, computing requirements, and numeric algorithm stability with the Reynolds-stress models. At present, the most widely used models are still two equation eddy-viscosity turbulence models, especially the  $k-\varepsilon$  model developed by Launder and Spalding (1974). Recently, two revised model, i.e., the RNG  $k-\varepsilon$  model (Yakhot et al. 1992) and Realizable  $k-\varepsilon$  model (Shih et al., 1995), have also been widely used.

The standard  $k-\varepsilon$  model is a semi-empirical model based on model transport equations for the turbulence kinetic energy and its dissipation rate. The RNG  $k-\varepsilon$  model was derived using a rigorous statistical technique (called renormalization group theory). It is similar in form to the standard  $k-\varepsilon$  model. One difference between the standard and RNG  $k-\varepsilon$  models is the calculations of turbulent viscosity. In the standard  $k-\varepsilon$  model,  $\mu_t$  is defined as  $\mu_t = \rho C_\mu (k^2 / \varepsilon)$  which denotes gas phase turbulent viscosity. In the RNG  $k-\varepsilon$  using differential viscosity model,  $\mu_{eff}$  which denotes effective viscosity is calculated by

$$d\left(\frac{\rho^2 k}{\sqrt{\varepsilon \mu}}\right) = 1.72 \frac{\hat{v}}{\sqrt{\hat{v}^3 - 1 + C_v}} d\hat{v} \quad (3.5)$$

where  $\hat{\nu} = \mu_{eff} / \mu$  and  $C_\nu \approx 100$ . Equation (2) is integrated to obtain an accurate description of how the effective turbulent transport varies with the effective Reynolds number (or eddy scale), allowing the model to better handle low-Reynolds-number and near-wall flows. Another visible difference between the standard and RNG  $k-\varepsilon$  models is that RNG  $k-\varepsilon$  model has an additional term  $R_\varepsilon$  in its  $\varepsilon$  equation that significantly improves accuracy for rapidly strained flows. The model constants in each model were different, too, with  $C_{1\varepsilon}^{RNG} = 1.42$  and  $C_{2\varepsilon}^{RNG} = 1.68$  derived analytically by the RNG theory, while  $C_{1\varepsilon}^{Standard} = 1.44$  and  $C_{2\varepsilon}^{Standard} = 1.92$  were determined from experiments.

The realizable  $k-\varepsilon$  model differs from the standard  $k-\varepsilon$  model in two important ways. Firstly, it contains a new formulation involving a variable  $C_\mu$  for the turbulent viscosity. Also, a new transport equation for  $\varepsilon$  has been derived from an exact equation for the transport of the mean-square vorticity fluctuation.

The accuracy of the predictions of each method is inversely related to the degree of approximation introduced. However, the cost in terms of computational resources is very high for DNS and LES simulations, which typically require large amounts of supercomputer time. Comparatively, RANS solving CFD methods with turbulence models are much less demanding, and are therefore widely used for practical applications. The performance of different turbulence models is case-sensitive for solving different problems. Thus, the validation of CFD simulations against similar experimental results is necessary. During the following studies, the validation and evaluation of CFD method are carefully performed and discussed.

### 3.3.3 Other Related Issues

#### Grid Generation

The first step (and arguably the most important step) in a CFD solution is the grid generation process, which defines the nodes or cells at which flow variables (velocity, pressure, etc.) are calculated throughout the computational domain. Most CFD codes can run with either structured or unstructured grids. A structured grid consists of planar cells with four edges (2-D) or volumetric cells with six faces (3-D). An unstructured grid consists of cells of various shapes, but typically triangles (2-D) and tetrahedrons (3-D) are used. For complex building geometries, an unstructured grid is usually much easier for the user to generate. The correctness and accuracy of a simulation result depend very much on the grid quality. The grid design is closely related to the selection of turbulence model and near wall treatment. In addition, Non-uniform grids are preferable in flows with solid boundaries to resolve the rapid changes in the near-wall region. However, this would require different filter cutoff width in the core flow and near-wall regions. In non-uniform grids the cutoff width would vary along with the control volume size. As for different methods of near wall treatment, the grid resolution near to the boundary should also be examined. For example, standard wall function cease to be valid in the viscous sublayer due to the logarithmic law for mean velocity is known to be valid for  $30 < y^+ < 300$ , which means inappropriate fine grids should be avoided. For enhanced wall treatment that combines a two-layer model with so-called enhanced wall functions with the intention of resolving the laminar sublayer,  $y^+$  at the wall-adjacent cell should be on

the order of  $y^+ = 1$ . However, a higher  $y^+$  is acceptable as long as it is well inside the viscous sublayer ( $y^+ < 4$  to  $5$ ).

In general, since the coarse grid introduces more numerical viscosity, grid-refinement study is essentially necessary to achieve a grid-independent solution. Although it may not be realistic to conduct grid refinement for the complete system, such a grid refinement should be conducted for benchmark cases, in order to estimate the errors introduced in the complete system.

### **Boundary Conditions**

While the equations of motion, the computational domain, and even the grid may be the same for two CFD problems, the imposed boundary conditions are the factor that leads to a unique CFD solution. For instance, as to buoyancy-driven ventilation studies, both indoor and outdoor environments are probably included in one computational domain, thus the predicted results could be very sensitive to the boundary conditions (Allocca et al., 2003). Users can specify different values for the variables of the incoming flow along the inlet, such as pressure or velocity values, depending on the driving forces of the airflow. If energy and/or turbulence equations are being solved, the temperature and/or turbulence properties of the incoming flow need to be specified as well. Outflow boundary is where fluid flows out of the computational domain. As to solid boundaries such as the wall boundary, fluid cannot pass through a wall, thus the normal component of velocity at a wall is zero. If the energy equation is being solved, either wall temperature or wall heat flux must also be specified (but not both). If turbulence equations are being solved, wall

roughness must be specified. Other boundary conditions also include symmetry, periodic conditions. The boundary condition settings are closely related to the problems, while further considerations are required due to the selection of turbulence models.

### **3.4 Summary**

In this chapter, the methods that commonly used to investigate flow and dispersion around HRR building have been presented. The fundamentals of these methods have been introduced.

The methods selected for this study are wind tunnel experiment method and numerical method with CFD techniques, aiming at different characteristics of the study objectives. The CFD simulation setup will be further described in each related chapter. For the wind tunnel studies, the overall arrangement and measurement methods are presented, the detailed experimental setup for different stages of purpose will be introduced in Chapter 5 and Chapter 6, respectively.

## **Chapter 4**

### **Air Cross-contamination Under Buoyancy Effect**

#### **4.1 Introduction**

The cross-contamination process under a certain weather condition is numerically studied in this chapter. Firstly, started from an attractive phenomenon that was observed during SARS epidemic, as mentioned in 2.3, one possible pollutant dispersion route caused by inter-flat airflow near the building is proposed. Next, based on the validation of CFD methods, the mechanisms of this kind cross-contamination around typical HRR building type I is numerically simulated. Finally, the possible optimization designs are analyzed and evaluated.

The contaminant transmission route within building environment is highly related to meteorological conditions. For the present study in this chapter, the certain weather condition that would probably lead to cross-contamination is analyzed. During the SARS epidemic period, the temperature of the outdoor environment was mildly low. The mean temperature especially during night time can be observed around 20°C (Hong Kong Observatory, 2005). However, the indoor temperature of modern buildings is usually higher than outdoor due to isolation and numbers of electronic devices even though they are not in use (Linden, 1999). In view of the moderate weather conditions at that time, instead of using air conditioners, the residents are most likely to open the windows in order to provide night time cooling. Thus, with doors closed, and the residents' behavior of window opening, the flats become

single-side ventilated, and the open windows function as both inlet and outlet of natural ventilation air.

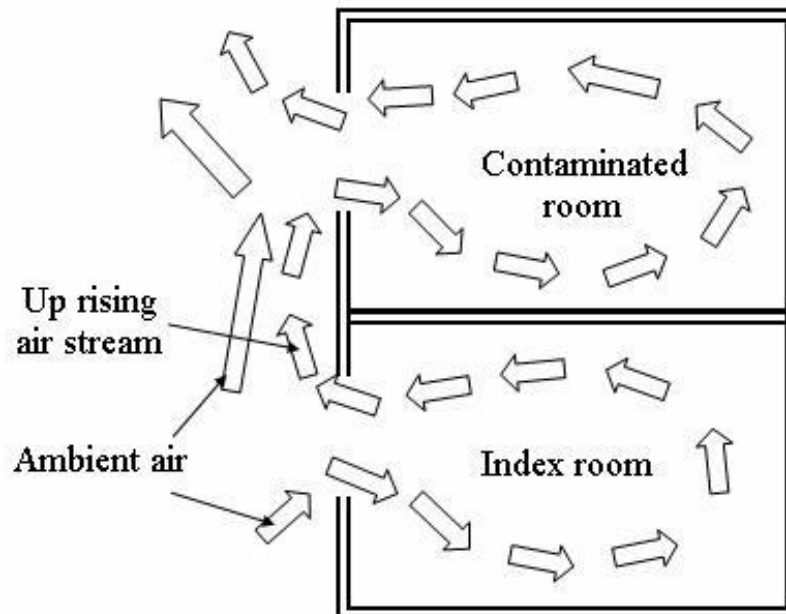


**Figure 4.1 Hypothetical contamination transmission path at one-sided ventilation conditions**

The hypothetical flow pattern in adjacent two flats in the vertical direction is shown in Figure 4.1, assuming the building has flat façade and the windows are flush with the walls, based on the features of the buildings with the SARS case clusters (e.g. Wing Shui house). The exhaust air coming out from the upper part of the window on the lower floor will re-enter the lower part of the open window at the immediate upper floor. Our hypothesis is that, on relatively calm days when the wind speed is low, buoyancy-driven single side natural ventilation through the open windows dominates the air flow pattern from one flat to another flat, and can be a possible major route in virus-laden aerosol transmission. Earlier on-site measurements using the tracer-gas technique have revealed that the room upstairs could contain up to 7%

of the exhaust air from the immediately adjacent flat downstairs due to this kind of inter-flat airflow (Niu and Tung, 2008). In this chapter, computational fluid dynamics techniques are employed to examine the likelihood of contaminated air exiting from lower flat entering a flat above through the open windows due to the buoyancy forces. Through the validation of the simulation methods with experimental data and consequently the applications in predicting the contamination spread in hypothetical cases, one of the possible transmission routes of airborne disease is to be identified. The identification of this transmission path in the high-rise residential blocks with flush windows in the same vertical façade will be useful in improving ventilation and building design for high-rise residential blocks to minimize the inter-flat air flow via open windows.

## **4.2 Model Validation**

### **4.2.1 Introduction**

Based on the summary of the meteorological conditions from the nearby meteorology stations of the buildings with SARS case clusters, it can be observed that the wind speed can low to  $0.1ms^{-1}$  (Niu and Tung, 2008). When the wind velocity is relatively low, the room exhaust air, which is typically not centralized and not stacked, was left to drift freely around the building without being blown away. From the point of view of air pollutant dispersion, this consequently leads to the “worst scenario”, which means the exhaust air flow subsequently moves upward to the intake of upper floors through open windows caused by buoyancy effects, and

becomes part of the incoming flow of the upper floors with windows flush on the same side.

Under such circumstance, the buoyant force induced by indoor/outdoor temperature differences will be the dominant driving force for building ventilation. The assumed transmission route of infectious contamination generated by SARS patients can be dominated by such buoyancy-driven single-sided natural ventilation on a moderate day without wind or with a gentle breeze. The airflow pattern and the velocity flow field play significant roles in the dispersion method of contamination in buildings. Therefore, the study of the mechanisms of single side natural ventilation is the prerequisite to investigating the potential spread path of infectious diseases on a moderate day without wind or with a gentle breeze. In particular, the main concern will first be focused on the buoyancy-driven single side natural ventilation.

#### **4.2.2 A Brief Description on Previous Experiment Used for CFD Model Validation**

Heiselberg et al.(2003) performed a full-scale experiment to analyze the characteristics of single side natural ventilation provided by a window opening, which is highly related to the transmission process we attempt to work on. The experiment was conducted in a large thermostatic chamber including a test room with openable window. The set-up was used to investigate the air flow through a window when it is suddenly opened. A constant temperature difference was maintained within the test chamber, which was cooled down to simulate an outside environment, and the test room inside the chamber was heated to a higher

temperature. Cold air was supplied via a ventilation sock while warm air was exhausted through two outlets in the ceiling.

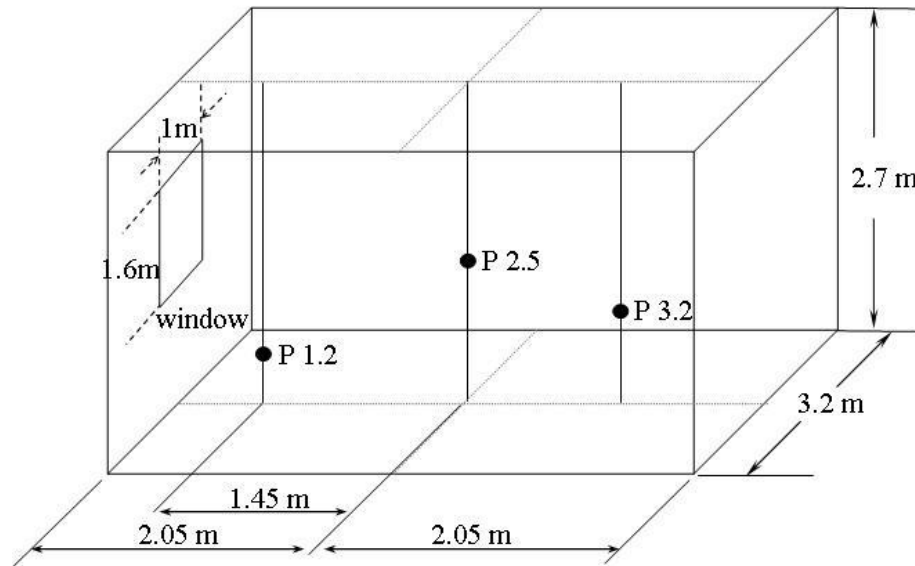


**Figure 4.2 Geometrical features of the test room and the layout of the typical points for comparison**

The geometrical features of the test room and the typical points for comparison are shown in Figure 4.2. In the experiment, the hot sphere transducers were placed in an array on the inside of the opening, which have been calibrated between 0 and 1 m/s in a wind tunnel with an accuracy of  $\pm 3$  cm/s and are also dependent on the horizontal direction of the air flow. Velocity measurements were taken every 0.1s. The measured velocities were multiplied by  $\cos(\pi/4)$  to get the horizontal velocity component, and the angle was adjusted near to the edge of the window, then the air flow was calculated as the area under the velocity profile multiplied by the width of the opening. The air flows were converted into air change rates, which are then averaged over 1.0s. The experimental results were used to evaluate the accuracy of

the two turbulence models. Consequently we can get to know the approximate error range between simulation results and the realistic flow parameters from this calibration in advance.

### **4.2.3 CFD Simulation Setup**

The test chamber which was regarded as an outdoor environment was simulated by means of a fictitious volume that was suitably ventilated and enclosed by solid walls, similar to the earlier study (Perino and Heiselberg, 2003). Fixed temperatures were imposed on the internal wall of the test room in view of the lag effects in the experiments after the heater was switched off. The inlet air flow (cold air) with the same ventilation quantity as the experiment was set up on the narrow zonal areas far away from the test room, in order to minimize influences on the air exchange through the opening by the outside flow (Figure 4.3). The zero diffusion flux condition was applied at outlet, while the conditions of the outlet plane were extrapolated from within the domain and had no impact on the upstream flow. The density differences due to temperature variations that occur in buildings are sufficiently small. Hence, buoyancy was modeled using the Boussinesq approximation in which density is assumed to be constant except in the momentum equation which gives rise to the buoyancy term in the modified pressure. A symmetry boundary bisecting the flow domain was used to reduce computational time, and up to 592205 tetrahedral finite volume cells were used. The grid size was set from  $0.02m$  close to the window to catch detail information near the opening, and up to  $0.2m$  in the overall flow domain on the account of reducing the computational costs.

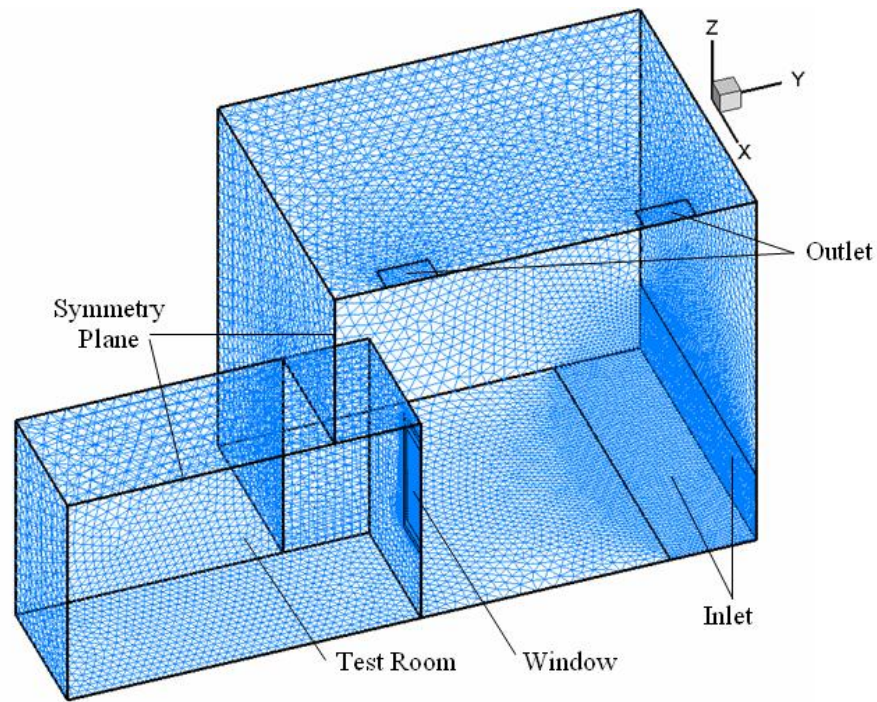


**Figure 4.3 Schematic geometry of the simulation model with grids layout in XY plane**

A widely used commercial CFD program (Fluent 6.2) was employed. For the natural convection in a single room with the characteristic length of approximately  $3m$ , even if the temperature difference is as low as  $1^{\circ}C$ , the Rayleigh number can be of the order of  $1 \times 10^8$ . The onset of turbulence is known to occur in the range  $10^6 < Ra < 10^9$  (Jones and Whittle, 1992). It is therefore reasonable to assume that the flows investigated here are turbulent. Considering the characteristics of indoor air flow, the overall flow features are considered as turbulent based on the analysis above. However, in some regions of an indoor space, the air flow can be weakly turbulent (Chen and Srebric, 2002). Two equation eddy-viscosity turbulence models are generally suitable for modeling indoor air flows when the indoor environment is not complex and the secondary recirculation of indoor air flow is not the main interest (Chen, 1995). Therefore, the likelihood of a considerably low-Reynolds-number flow

occurring in the indoor environment should be taken into account. The standard  $k-\varepsilon$  model and the RNG based  $k-\varepsilon$  model are used and the results obtained by each method are compared in this study. In the RNG  $k-\varepsilon$  using differential viscosity model, the calculation method on effective viscosity provides an accurate description of how the effective turbulent transport varies with the effective Reynolds number (or eddy scale), allowing the model to better handle low-Reynolds-number and near-wall flows.

All the discretized equations are solved in a segregated manner with the implicit formulation. The implicit method is recommended for general purpose transient calculations because of its robustness and unconditional stability, except other unsteady processes such as the characteristic time scale of problem is on the same order as that of the acoustics. For explicit scheme, the time step is usually very small due to the restriction of the Courant-Friedrichs-Lewy (CFL) condition (Courant et al., 1928) and a large number of time steps are required for a given time period. Hence, the implicit scheme was applied in the presented studies on the ground of its superior stability and allowance for large time discretization.

During the first 5 seconds after the beginning of the simulation, the results of different time steps at  $\Delta t = 1s$ ,  $\Delta t = 0.5s$ ,  $\Delta t = 0.25s$  and  $\Delta t = 0.2s$  were compared to find the differences induced by the different size of time step. The discrepancy of the predicted ACH between  $\Delta t = 1s$  and  $\Delta t = 0.2s$  was around 1%. It was found that the velocities at typical points were more sensitive to the time step, the difference was around 30% between  $\Delta t = 1s$  and  $\Delta t = 0.2s$ , but about 10% between  $\Delta t = 0.5s$  and

$\Delta t = 0.25s$ , finally became around 1% when the time step is low to 0.2s. This comparison was also conducted after 20 seconds from the beginning, till the time of 30s, at the time steps of  $\Delta t = 2s$  and  $\Delta t = 1s$ . The ACH had the discrepancy about 1% and become almost the same when it was low to 1.25s, while the difference of velocity was around 7% and decreased to 3% when the time step is lowered to 1s. In addition, this time-dependent problem caused by window opening has a very fast "startup" transient that decays rapidly during the latter period. It is thus acceptable to choose a conservatively small  $\Delta t$  for the first period of the process. Therefore, to capture characteristics of flow field at the early beginning and also give attention to the simulation efficiency, the time step was chosen varying from 0.2s in the first 20 seconds and up to 1s.

#### 4.2.4 Comparisons between CFD Results and Experimental Data

Comparisons between experimental and simulation results were performed for the 600 second period after the window was opened. The simulated air change rate per hour (hereafter denoted ACH) at anytime can be directly computed by integrating the velocity (Y direction) at the opening.

$$ACH = \frac{3600 \times \frac{1}{2} \int |U_j| dA}{V_{room}} \quad (4.1)$$

where  $U_j$  denotes the velocity magnitude in Y-direction,  $A$  is the opening of the room and  $V_{room}$  is the total volume of the test room. This parameter represents the ventilation rate through the window which acts an important role in indoor contaminants dilution and transmission. On one hand, it points out the quantity of

fresh air entering the contaminated room; on the other hand, exhaust air leaving the opening leads to potential contaminants re-entry into adjacent rooms. Hence, predicted results of ACH together with velocity magnitudes at typical points which reflect the characteristics of the indoor flow field were compared with experiment results. Two indoor/outdoor temperature differences, respectively 20 °C and 10 °C, were simulated and compared.

Figure 4.4 plots the measured ACH and the predicted results respectively obtained by the standard and RNG  $k-\varepsilon$  models under the two temperature differences. The flow characteristics are basically illustrated by the numerical results. High-ACH is obtained after the windows were opened, decreasing gradually over time, and finally turned into the quasi-steady state that did not change much in the later period of the process.

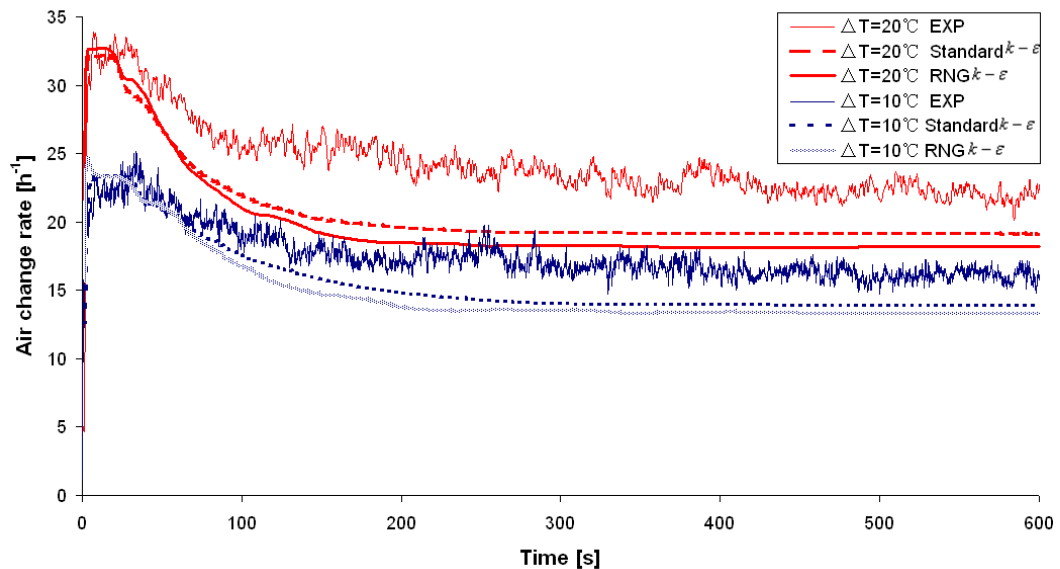


**Figure 4.4 Comparison between simulation and measured results of ACH values**

It is shown that CFD results calculated by both models agree well with the experimental data in the initial period of the process, while deviating up to around 20% in later periods. Both measured and predicted results appeared to decrease when the cold fresh air entered into the test room after the initial stage of this process, which led to the reduced driving forces. ACH is under-predicted by both models in this process. It is suspected that the thermodynamics of the simulations and the experiments are not completely alike. In the experiments, internal heaters were used to enable the average indoor and outdoor air temperature difference to reach the desired value, while fixed wall surface temperatures were set in the simulations. In addition, the dependency of the calibration method of the hot sphere transducers can give inaccurate measurements up to  $\pm 4.0$  %. At the same time, the calculation methods of ACH between experiments and simulations are different, together with the inaccuracy of experiment itself possibly also contributed to the discrepancy.

The velocity magnitude in different typical points is shown in Figure 4.5. Good agreement was achieved between both model predictions and the experiment data despite the fluctuation characteristics, which could not be revealed by the inherent time-averaging modeling approach. It appears that the results obtained by RNG  $k-\varepsilon$  model are more close to the measurements, especially in the low-velocity field such as point 2.5 and 3.2. The possible explanation is that the RNG  $k-\varepsilon$  model using a differential viscosity model takes the effective Reynolds number and that the standard  $k-\varepsilon$  model inadequately predicts the turbulence energy  $k$  in recirculation zones (Versteeg and Malalasekera, 2007). Through its effect on the viscosity, the local velocity distribution predicted by the standard  $k-\varepsilon$  model may be different from the actual distribution. Therefore, in the centre of the room, where large

recirculation exists in the case of an empty room (Nahor et al, 2005), RNG model provides better predictions than the standard  $k - \varepsilon$  model.

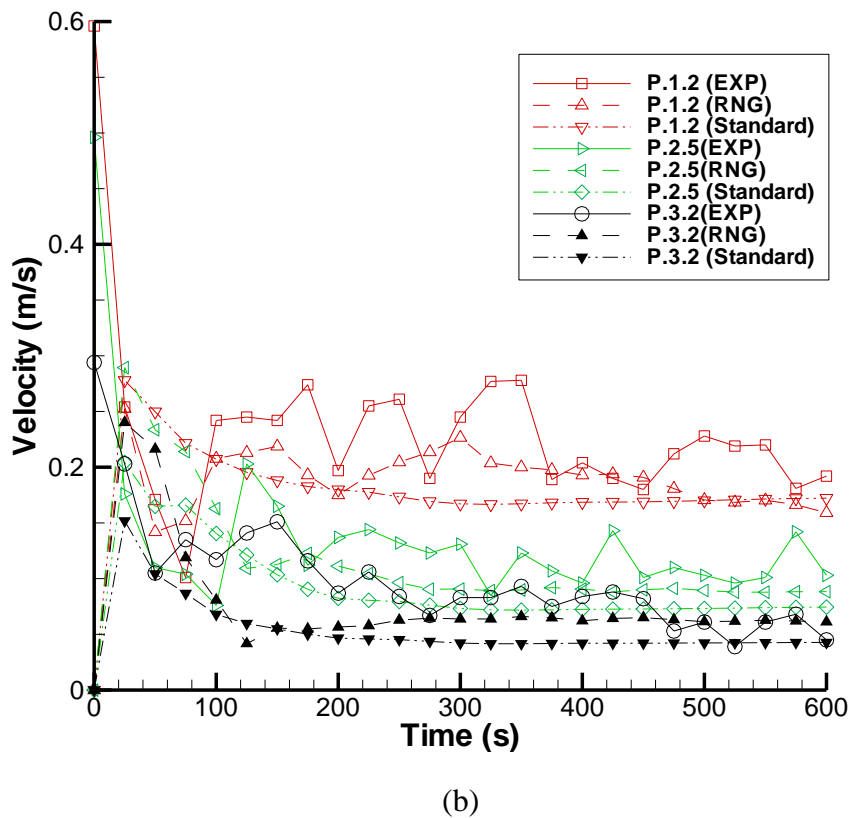
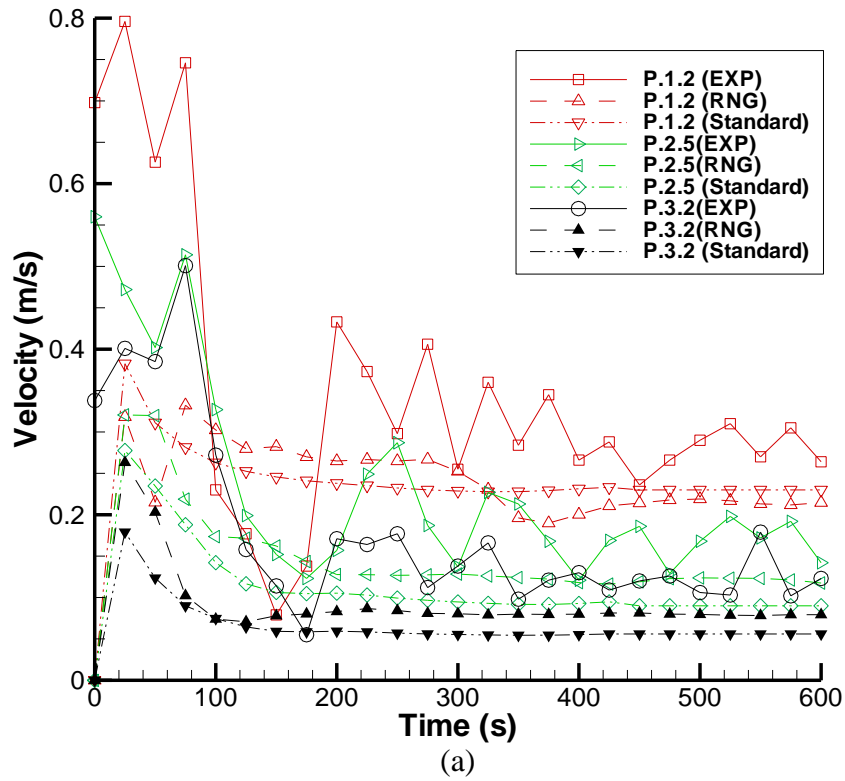


**Figure 4.5 Comparison between simulation and measured results of velocity magnitude at typical points: (a)  $\Delta T = 20^\circ\text{C}$  and (b)  $\Delta T = 10^\circ\text{C}$**

Such experimental case used for comparison has close thermal buoyancy and geometrical conditions with the cases we attempt to work on. The comparisons illustrate that both the standard and RNG  $k-\varepsilon$  model can capture the basic characteristics of temperature driven single-sided natural ventilation. In particular, the RNG  $k-\varepsilon$  model gave a better performance than standard  $k-\varepsilon$  model in velocity prediction, especially in the centre of the room, where a large recirculation exists in the case of an empty room. The indoor velocity field strongly influenced the spread of indoor contamination. Therefore, the RNG  $k-\varepsilon$  model is employed in the following application studies.

### **4.3 CFD Study on Buoyancy-Driven Cross-contamination**

#### **4.3.1 Analysis and Simplification of the Model**

In this section, several assumed scenarios were simulated based on the selected turbulence model, to evaluate the transmission mechanisms of the contaminants between two vertical flats with flush windows on the same side. The schematic of geometry is shown in Figure 4.6. To simplify, sample room in the absence of any furniture was simulated. This model stacked two identical rooms vertically above one another to simulate the two adjacent floors belonging to one typical high-rise residential building, including the outdoor environment in a combined model. The

extension of the computational domain to the outdoor environment allows us to consider the outside air flow conditions.

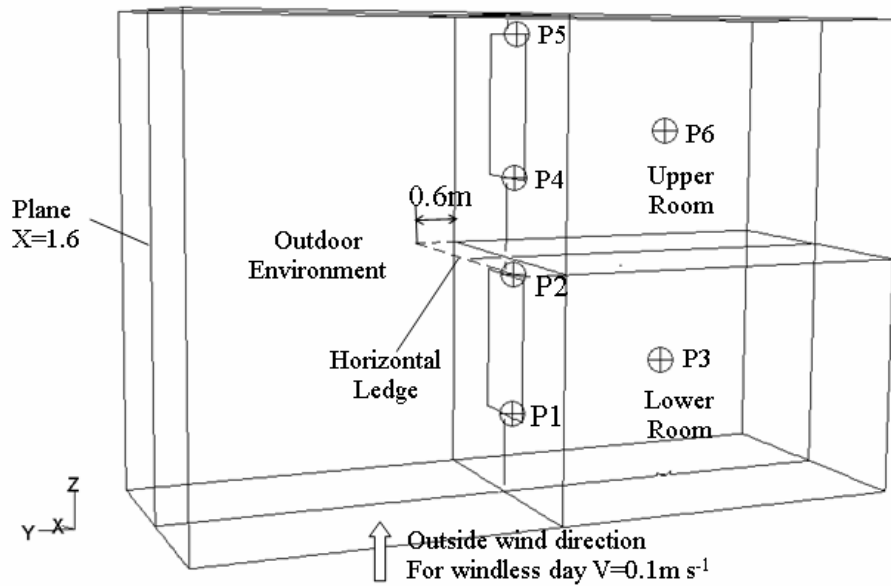


**Figure 4.6 The schematic of free decay unsteady case and the measuring points location in plan**

(A hypothetical ledge is also illustrated to investigate its blockage effects)

Carbon dioxide had been employed to evaluate the risk of indoor airborne infection transmission based on the key assumption that airborne infectious particles are droplet nuclei that remain suspended in air for long periods of time (Rudnick & Milton, 2003). For gas-particle flows, the particle inertia is presented by a dimensionless number, Stokes Number, defined as  $S_t = \tau_p / \tau_n$ , where  $\tau_p = \beta \sigma^2 / 18\nu$  is the particle relaxation time,  $\sigma$  the particle diameter,  $\beta$  the particle-to-fluid density ratio,  $\nu$  the fluid kinematic viscosity, and  $\tau_n = L/U_0$  is the system response time,  $L$  the characteristic length,  $U_0$  the characteristic velocity. This important dimensionless parameter in particle dynamics determines whether or not they are

traveling with the surrounding gas. Considering that indoor airflows are always a feature with low characteristic velocities and the contaminant particles are with small diameters, the Stokes Number for the contaminant particles flow indoor is far less than unity and the particles act like gas tracers (Tian et al., 2006). Hence, it is appropriate to employ CO<sub>2</sub> as a gas tracer to investigate the possible transmission path of infectious contaminants.

It is known that the air flow pattern near a tall building can be particularly complex caused by the interaction between meteorological conditions and building structures. The idealized model is assumed to be only part of one high rise residential buildings, which means it is difficult to define the upwind profile based on the terrain characteristics. Furthermore, it is observed that the wind profile near the opening of a flat, including both wind direction and wind speed, vary at high frequency from our previous on-site measurements. Thus, it is difficult to correctly represent the upwind profile for such cases. Considering that the wind velocity is relatively low during SARS epidemic period especially during the night, the outside wind speed along negative y direction was neglected in the following simulations, and slip boundary condition was used at the vertical domain boundary at x-z plane. According to the classification criteria of wind speed in meteorology, wind speed lower than  $2\text{km hr}^{-1}$  can be seen as nearly no wind condition. Therefore, low to  $0.1\text{m s}^{-1}$  wind speed along the positive direction of Z axis was set as the inlet of the whole domain to approach the natural outdoor environment. This treatment takes the characteristics of the surface flow patterns into account.

Considering about air flow patterns around a building, surface flow near to the building always can be found in the windward wall of the building. On the upper part of the building, the surface flow along building façade can be directed upward over the roof. In addition, upward air movement can be found in the vicinity of a building because of the thermal effects due to radiative heating on the ground and building surface (Smith, et al., 2001). The air flow near to the building can be warmed up and move upward. The turbulence intensity of this inlet boundary was set as 6%. Periodic conditions were imposed on the vertical domain boundaries at y-z plane in view of the possible characteristics of the building structures. It means that the building is extended in the negative and positive y direction. This treatment is owing to the fact that in the high-rise buildings with SARS case clusters, the shape of the buildings are like a vertical slab (e.g. Wing Shui house). In buoyancy driven single side natural ventilation, air is driven in and out due to the pressure differences produced by buoyancy forces. The air density plays a significant role to induce the buoyancy forces, and it was set as a piecewise-linear profile function of temperature to introduce the driving forces caused by temperature differences. During SARS epidemic period, cooling and heating devices were most likely not in use. Therefore, the air temperature difference between inside and outside was set to different value that ranged between 4.5 °C and 8.2 °C, based on the weather conditions. The building surface temperatures of internal walls were set to a constant value on account of a relative stable indoor environment. Hexahedral grids were used for discretization in order to reduce the computational cost. Individual cells were carefully examined to avoid unsatisfied skewness which could lead to convergence difficulties and inaccuracies in the numerical solution.

Numerical tests were first performed to wipe off the effects introduced by the outside domain size, until only small and insignificant changes in the numerical results. It was found that the ACH can vary with the outside domain size, and the discrepancy can up to 30% when the outdoor space was reduced by half. It is suspected that the inadequate outdoor space does not fully involve the exhausting flow field when the boundary conditions close to the opening. To ensure that the air exchange through each window was not influenced by the outside domain size and air inflow of the domain, the outdoor space was enlarged to make sure that the total air input of the whole domain is over 10 times larger than the air ventilation rate of each room.

#### **4.3.2 Transient-State Contaminant Transmission**

A transient case is first performed to illustrate the transient spread of contaminants from the index room located on the lower floor. The CO<sub>2</sub> concentration of the lower room is set to 3000ppm initially, while the air on the upper floor is considered clean from CO<sub>2</sub>. The outdoor temperature was set to 19°C, according to the mean air temperature in March, 2003, observed by Hong Kong Observatory. Both the indoor initial air temperature and the internal wall surface temperatures were set to 25.5°C during the simulation. The infectious contaminants were simulated by carbon dioxide (CO<sub>2</sub>) as a passive tracer. The simulation starts when the windows of both rooms are suddenly opened, and lasts for 600 seconds.

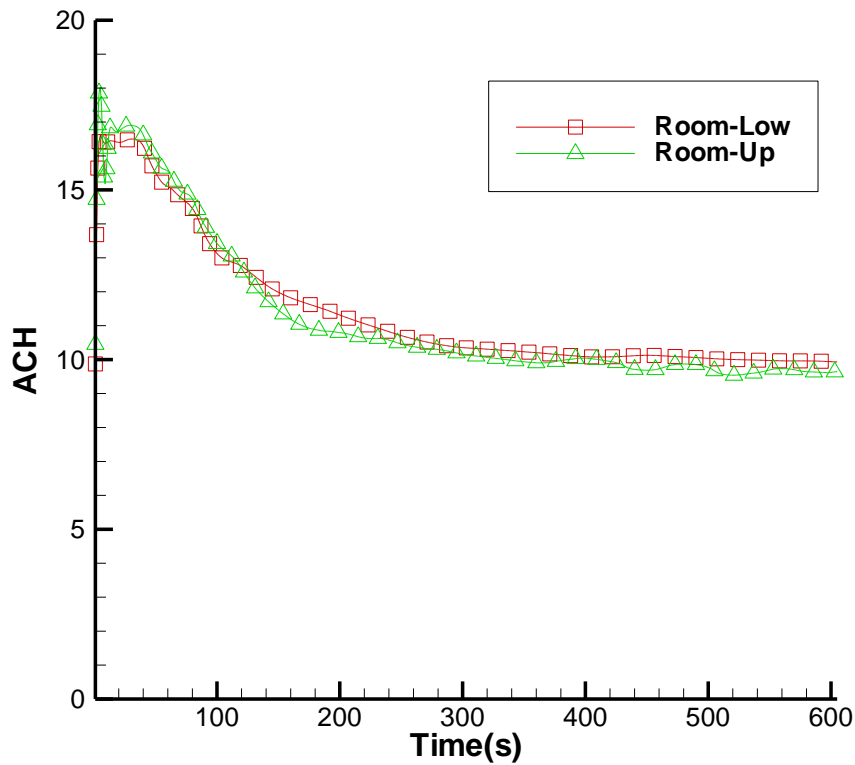


**Figure 4.7 Predicted ACH values of each room versus time**

As can be seen from Figure 4.7, ACH of each room rapidly reached the max values after the windows were opened, and quickly decreased over time, then turned into slowly descending period in the second half of the simulation. This is mainly because the driving forces induced by temperature differences between outdoor and indoor change over time. With time elapsed, the indoor air temperature decreased gradually due to the mixing effect of ingoing outdoor air, which resulted in the reduction of the temperature difference. The ACH of each room at any time was approximately the same due to almost the same difference of temperature between outdoor and indoor on each floor, which leads to the same driving force. It can be observed that the ACH of lower room is slightly higher than that of the upper room, since the outside air around the upper window combined the exhaust air from lower window with a slightly higher temperature.

A significant concentration of CO<sub>2</sub> in the upper room can be obviously detected through the predicted results (Figure 4.8). Since CO<sub>2</sub> was only initially present in the lower room, it is evidently suggested that the contaminated air of the lower room exhausted from the window could re-enter the upper room. The contaminant concentration in the upper room continuously increased in the first half of the period, but subsequently decreased in the second half of the period, which means the dilution effect of ACH was dominant in this part. The concentration of contaminants in the lower room was continuously decreasing owing to the diluting effect.

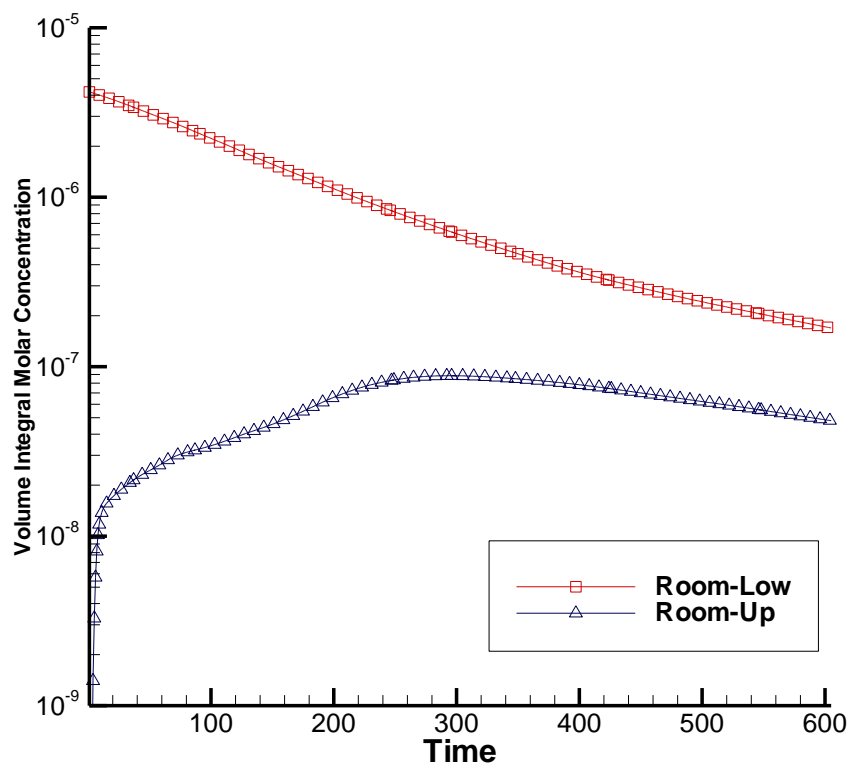


**Figure 4.8 Predict Volume-averaged CO<sub>2</sub> concentrations of each room versus time**

Figure 4.9 illustrated the changing CO<sub>2</sub> concentrations at several points within the rooms. The concentrations in the upper room at P4, P5 and P6 are much lower than

those in the index room at P1, P2 and P3. In general, the concentrations of different points changed rapidly in the initial period except P2, and changed relatively slowly in the latter period. At initial stage, the flow was better developed and the air speed sufficiently high to allow good mixing due to high air temperature difference, consequently a rapid transportation of CO<sub>2</sub>. With time lapse, the air temperature difference decreased due to mixing effect, and therefore a slower spread of CO<sub>2</sub>. The concentrations at P4 increased immediately after the simulation began, while a delay of 10s and 60s in the concentration increased at P6, and P5 can be noticed. That is mainly because P4 is near to the inflow area, which was immediately influenced by the exhaust air exiting from the lower room. P5 is near to the outflow area which was not influenced at the beginning of the process. These predicted results indicate that gradients in pollutant concentration could be maintained within a room during the initial minutes of the contaminating process (Richmond-Bryant et al., 2006). After an elapsed time of about 5 minutes, the concentration of these three points reached approximately the same level due to the mixing effect of the upper room. The CO<sub>2</sub> concentrations at Point P1, P2 and P3 in the lower room decreased due to the air change from outside.  $C_{p_1}$  evidently reduced at the very start since it was near to the entrance of the fresh air.  $C_{p_2}$  remained little changed at the beginning of the process, as a result of the contaminant stratification induced by the temperature differences. It can be explained that the buoyancy effect tends to make the original higher temperature indoor air with higher CO<sub>2</sub> concentration “float” in the upper part of the room.  $C_{p_3}$  began to decrease after a little delay, since P3 was located in the middle of the room and the flow velocity in this area is weak. As a result of the airflow patterns, the changing process of concentration in each typical point is different. The results

are mainly because that the contaminant is transported with the room air, which is displaced from the bottom to the top induced by a vertical temperature gradient.

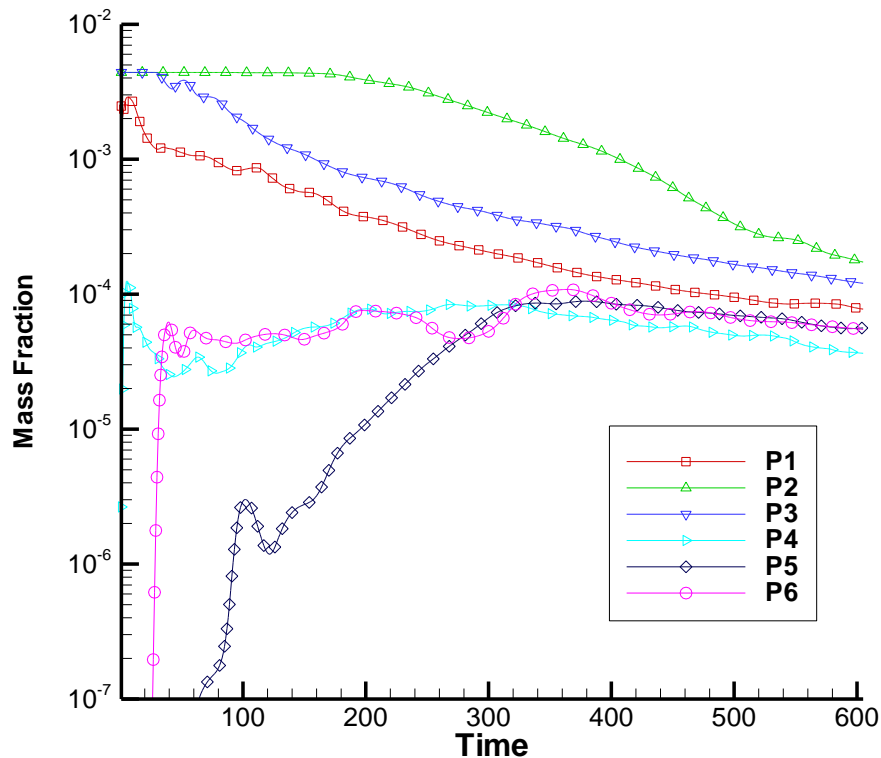


**Figure 4.9 Simulated CO<sub>2</sub> mass fractions at different points versus time**

These results illustrated the potential transmission path from the contaminated lower room to the adjacent upper room in the vertical direction. The variations of overall concentration in each room, together with the concentration changing at individual points, demonstrate that in high-rise residential buildings under certain meteorological conditions, the upper room could be influenced by the lower room with a significant contaminant concentration. These prediction results possibly explain the presence of bio-material of SARS virus at the adjacent upper floors of two index rooms of a high-rise residential building in Hong Kong, during the 2003 SARS epidemic period.

### 4.3.3 Steady-state Contaminant Transmission with Constant Release

The objective of this case is to evaluate the possible infection risk when there is a continuous contaminant source located in the lower room, which could probably happen when an infectious patient lives in that room. The layout of the simulation domain is the same as described above (Figure 4.6). The windows of both rooms were opened during the simulations. The contaminant ( $\text{CO}_2$ ) is constantly released from the bottom of the lower room, at a flow rate of  $5\text{ ml s}^{-1}$ . The temperatures of internal walls were set to  $25.5^\circ\text{C}$ , while the outdoor temperature was set to  $19^\circ\text{C}$ .

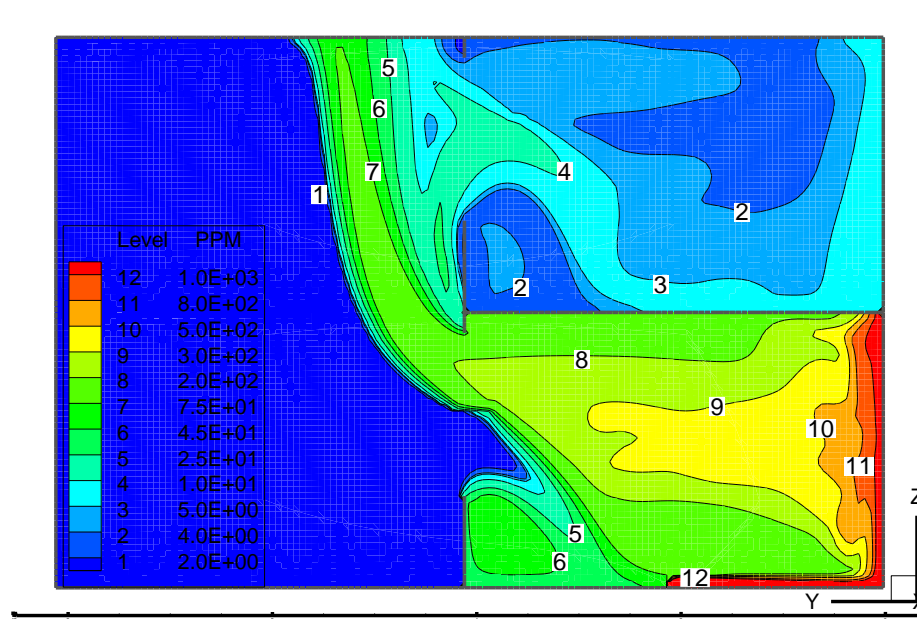


**Figure 4.10 Simulated  $\text{CO}_2$  concentration distributions at the centre plane  
( $X=1.6\text{m}$ )**

Figure 4.10 shows the predicted distribution of  $\text{CO}_2$  concentration at the mid-plane of the domain. The predicted concentration profile was a simple representation of contaminant spread between two vertical adjacent rooms. It can be clearly observed that the contaminated air exited from the upper part of the lower window and re-

entered the upper room. CO<sub>2</sub> was emitted from the source and dispersed in the lower room, then exhausted from the window and moved upward, finally re-entering the upper room. As a result of air flow pattern dominated by buoyancy effect, the pollutant can transport from household to household in the vertical direction. The concentration in upper flat is approximately lower by about two orders of magnitude than that in the lower index room.

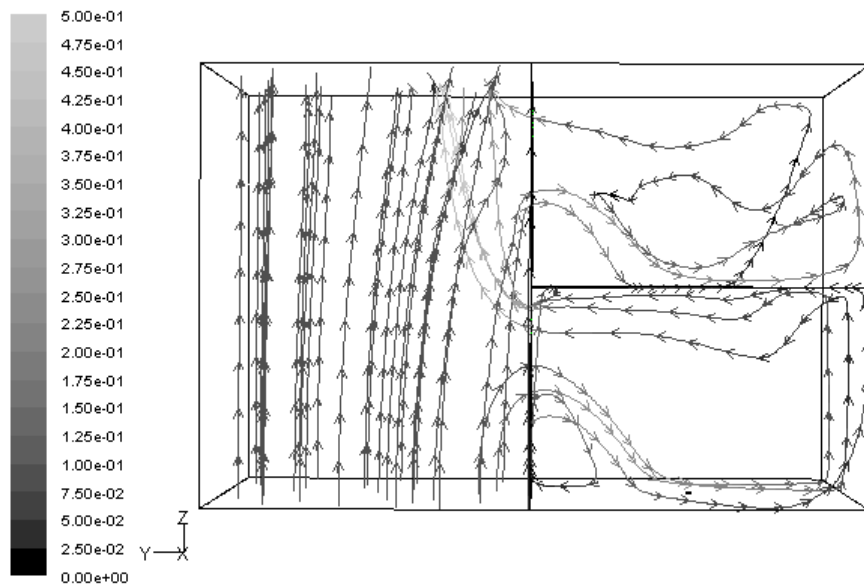


**Figure 4.11 Simulated path line colored by velocity magnitude**

Figure 4.11 presents the predicted flow path line colored by velocity magnitude at the middle plane. The distribution of CO<sub>2</sub> concentration is mainly dependent on the flow route in the simulated domain. This illustrates both the flow pattern in the simulation domain and the velocity distribution. The horizontal velocity magnitude in both rooms gradually decreased along the depth of the room, which suggested a decrease in the velocity component for the fresh air stream along the inflow direction (Gan, 2000), and the airflow moving up to the top of the rooms induced by buoyancy effects. The predicted flow pattern indicates that the hypothetical airflow route as

shown in Figure 4.1 was practically reasonable. The predicted results of flow field are consistent with the distribution of CO<sub>2</sub> concentration; the cold fresh air enters the lower room and combines with the contaminated air, then exits through the window and moved upward to the intake of the upper floor.

#### 4.3.4 Further Discussion and Analysis

The characteristics of buoyancy-driven single side ventilation are that the dominating driving force is the pressure difference generated by temperature differences between indoor and outdoor areas. Therefore, 3 more cases were conducted under the outdoor temperatures of 17.3, 20, and 21 °C, in view of the fact that the mean daily maximum and minimum air temperatures in March, 2003, was equal to 21.0 °C and 17.3 °C, respectively, while the indoor temperature was assumed to be around 25.5 °C. To estimate the risk of the upper room residents being infected by the lower room index patient, an assessment index was introduced based on the following analysis. Since the complete time history of both the ventilation air flow rate and the constant contaminant emission rate are known, the current average room concentrations can be calculated. The contaminant concentration can be expressed as:

$$C_{Up} = C_{Low} \cdot M_{U-L} = \frac{M_{U-L}}{ACH \cdot V_{room}} \cdot S = f_p \cdot S \quad (4.2)$$

where  $C_{Up}$ ,  $C_{Low}$  denote the contaminant concentration of upper room and lower room, respectively,  $M_{U-L}$  is the ratio of the concentrations,  $C_{Up} / C_{Low}$ , which can be interpreted as the mass fraction of the air originating from the lower room that is present in the upper room (Niu and Tung, 2008),  $V_{room}$  is the volume of the room and

$S$  is the release rate of the contaminant. Therefore, the factor  $f_p$  presents an index to evaluate the infection risk of upper room residents by the lower index room residents. From the indication shown by this index, prompt response such as necessary isolation could be implemented in case of an outbreak of highly infectious disease.

**Table 4.1 Predicted results at different indoor/outdoor temperature differences**

I/O temperature difference (°C)	Volume-Average Mass Fraction (Lower room)	Volume-Average Mass Fraction (Upper room)	ACH-Low	ACH-Up	$M_{U-L}$	$f_p$
8.2	1.11E-04	4.13E-06	11.54	11.22	3.72E-02	9.1E-05
6.5	1.15E-04	4.37E-06	10.65	10.24	3.80E-02	10.1E-05
5.5	1.27E-04	3.97E-06	9.87	9.40	3.13E-02	8.9E-05
4.5	1.36E-04	3.67E-06	8.97	8.60	2.70E-02	8.5E-05

The variations of assessment index  $f_p$  at the different outdoor temperatures predicted are shown in Table 4.1. ACH of each room decreased with the ascending of the outdoor temperature, since the driving force was weaker with smaller temperature differences. It can be seen that the concentration of the lower room increased owing to the negative role played by less air exchange rate, which introduced less fresh air into the lower room. On the other hand, it can also be observed from the assessment index,  $f_p$  that the concentrations of the upper room did not linearly change with the decrease of outdoor temperature. This can be explained as the increased ventilation rate played dual roles on the change of concentration—a positive role in dilution effect induced by the ventilation, and a negative role in carrying more contaminated exhaust air into the upper room.

Based on the prediction results of all the cases conducted above and the analysis, it can be seen that an indoor contaminant source located in the lower floor can be a significant contributor to concentrations in the vertical, adjacent upper room under certain meteorological conditions. The magnitude of the overall CO<sub>2</sub> concentration in the upper room could reach a few percentages of that in the lower index room. Niu and Tung (2008) also revealed similar results in their on-site experiments (Figure 4.12), and the index in terms of mass fraction  $M_{U-L}$  used to evaluate the quantity of the air that exits from the lower room and re-enters the upper room has been shown to have the same magnitude as predicted by present simulations.

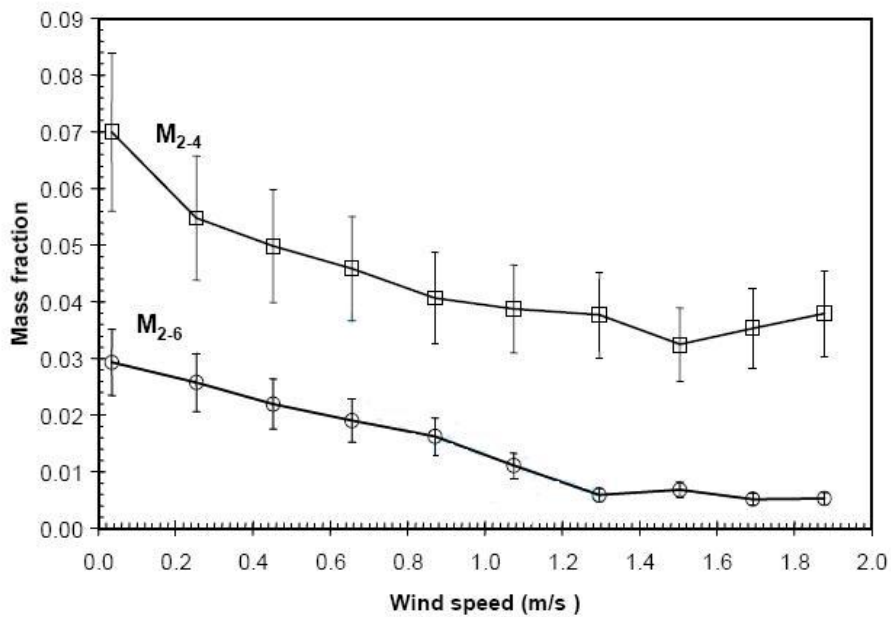


**Figure 4.12 Variations of the measured mass fractions of  $M_{2-4}$  and  $M_{2-6}$  with the monitored local wind speed (From Niu and Tung 2008)**

#### 4.4 Possible Optimization Design

##### 4.4.1 Building Structure Optimization

Based on the detailed results provided by CFD methods presented above, and also results from earlier on-site measurements, improvements in building structures could be introduced to reduce the potential risk of this kind of cross contamination.

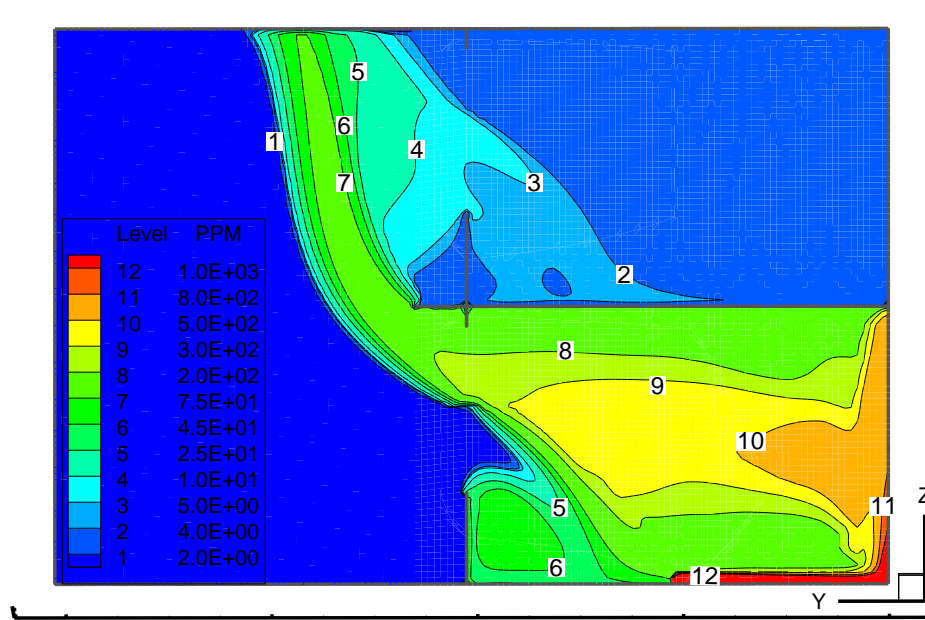
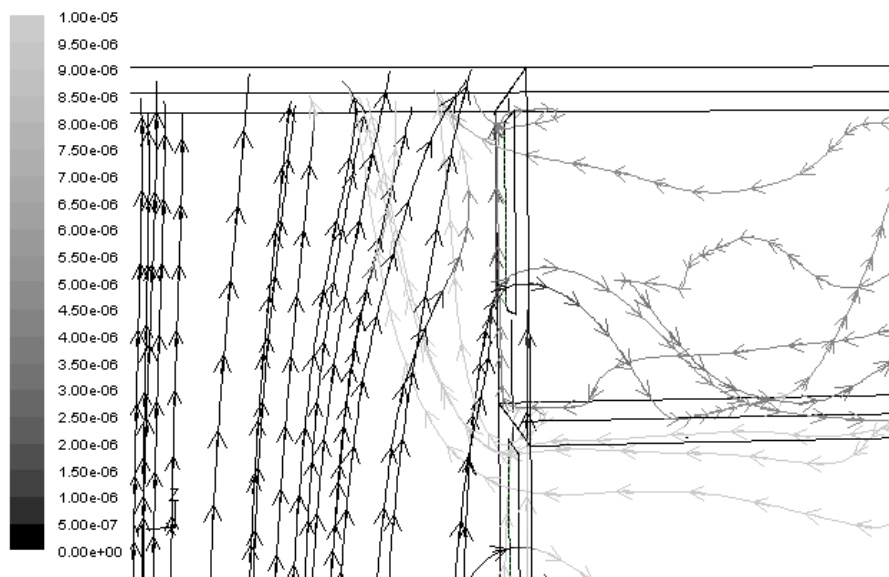


**Figure 4.13 Simulated CO<sub>2</sub> concentration distributions at the centre plane with ledge effect (X=1.6m)**

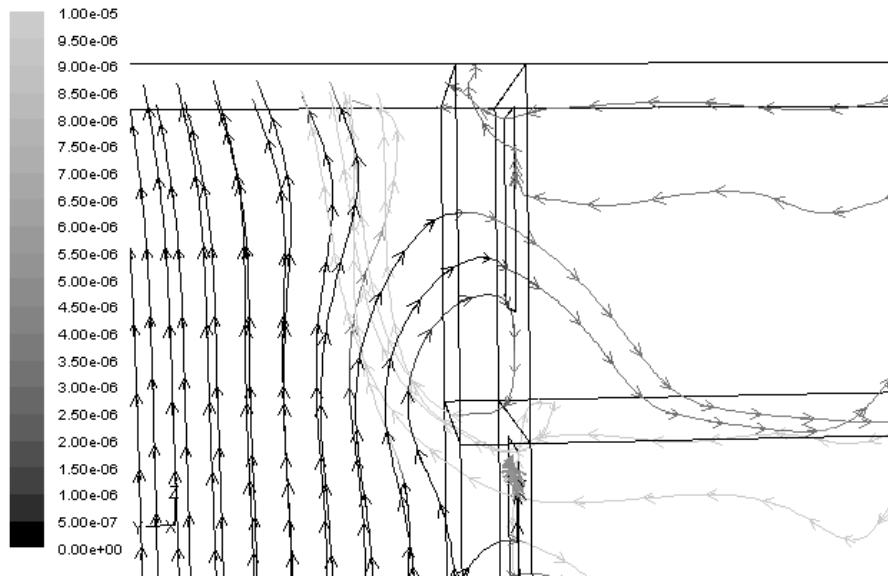
It appears that one possible way to decrease such kind of vertical upward re-entry risk could be placing a ledge above the windows. The ledge extends to the full width in the X direction, and 0.6M from the vertical wall, as shown in Figure 4.6. The models and the grids used under this circumstance are completely the same as without ledge cases, and the indoor and internal wall surface temperatures were imposed to 25.5°C, while the outside temperature was set to 19°C.

Figure 4.13 illustrated the distribution of CO<sub>2</sub> concentration at the mid-plane of the model with the effects induced by the ledge. It can be clearly seen that compared

with Figure 4.10, the distribution of CO<sub>2</sub> concentration in the index lower room did not change much after the horizontal ledge was added in the model, while the CO<sub>2</sub> concentration level in the upper room was observed to be lower. This is mainly because the ledge did not affect the air exchange of the lower room, but the contaminated air that exited from the lower window could not move vertically upward owing to the obstacle effects. Consequently, less contaminated air got to the intake area of the upper window and the concentration of CO<sub>2</sub> in the upper room was lowered due to the ledge's effect.



(a)



(b)

**Figure 4.14 Simulated path line colored by CO<sub>2</sub> mass fraction near the upper window: (a) without the ledge and (b) with the ledge above the window**

The comparison of the path line colored by CO<sub>2</sub> mass fraction near the upper window with and without ledge is shown as Figure 4.14. It is clear that with the ledge's effects, the air entering into the upper room has lower concentration of CO<sub>2</sub>. With the influence of the ledge, the ascending airflow combined with contaminated airflow escaping from the upper part window of the lower room was deflected farther from the window of upper room.

Furthermore, benefiting from the CFD advantages, a transient simulation was performed to show the differences directly. After having obtained a converged steady-state solution (with a developed air flow path, thermal field and distribution of contaminant concentration for both the indoor and outdoor air), the concentrations of contaminant in outdoor & upper room were re-set to 0, then an unsteady state simulation was started. The lower part of the window in upper room acted as the inlet

of the single-side ventilation during the process. Therefore, Figure 4.15 shows directly how long it spends that the contaminant reaches the upper room. This figure also illustrates that the flow entered in the upper room has lower concentration of contaminant under the effect of ledges.

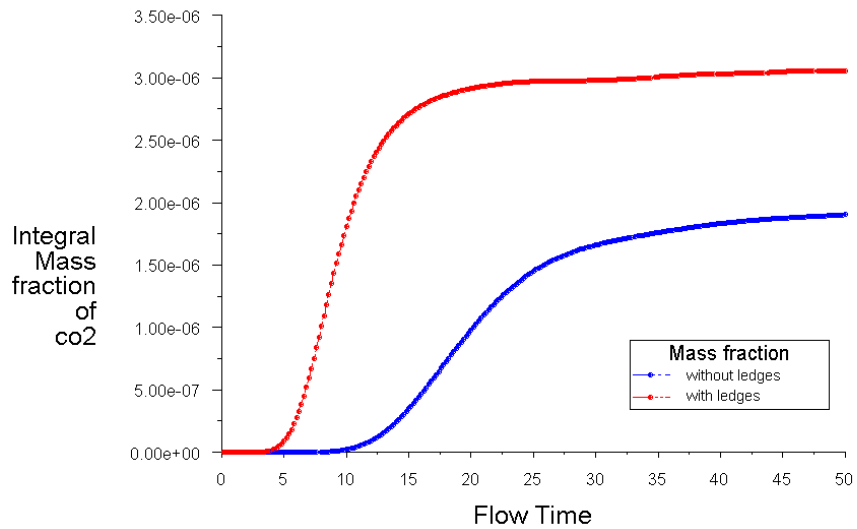


**Figure 4.15 Mass fraction in the lower part of the upper window versus time**

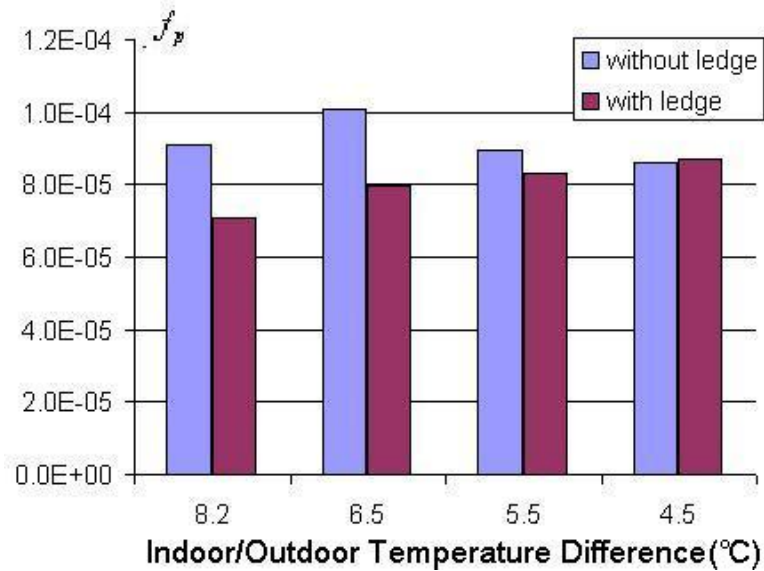


**Figure 4.16 Comparison of  $f_p$  between with and without the ledge at different outside temperature**

Finally, Figure 4.16 illustrates the differences of the assessment index,  $f_p$ , with and without the ledge at different indoor/outdoor temperature differences. The values of  $f_p$  decreased after the ledges were added, except when the outdoor temperature was close to the indoor environment. That is probably because under low temperature difference condition, the ascending airflow does not have a significant vertical velocity magnitude, so that the exhaust air tends to stick to the external wall surfaces. Consequently the difference between with or without ledge was not significant.

#### **4.4.2 Ventilation Design Optimization**

Besides the possible building construction optimization mentioned above, the improvement method to reduce such cross-contamination could also be achieved by employing optimized ventilation strategies. Using individual mechanical exhaust in each flat is an obvious option. There are ventilation standards for domestic buildings in Hong Kong – Practice Note for Authorized Persons and Registered Structural Engineer (PNAP) from Building Department (Building Department, 2005). The Building Authority recognizes that a performance-based approach to the provision of ventilation in buildings is an acceptable alternative option in satisfying the health and safety requirements. It is recommended that the ACH for kitchen could be 1.5 (Natural means) plus 5 (Mechanical means). In our numerical test, a mechanical exhaust with ACH=5 from each room was used and the results was shown to illustrate the improvement introduced by optimized ventilation strategies.

The models used under this circumstance are completely the same as shown in Figure 4.6, and the indoor and internal wall surface temperatures were imposed to 25.5°C, while the outside temperature was set to 19°C. Figure 4.17 illustrated the distribution of CO<sub>2</sub> concentration at the mid-plane of the model with the mechanical exhaust, and ACH = 5. It can be clearly seen that compared with Figure 4.10, the distribution of CO<sub>2</sub> concentration in both two adjacent rooms were reduced. This is mainly because the dilution effect introduced by mechanical ventilation. Part of the pollutant in lower index room could be exhausted from the mechanical vent. However, it could be seen from the result that the mechanical ventilation with ACH = 5 was not efficient enough to completely destroy such kind of cross-contamination. The tracer gas still can be found in upper room with a non-negligible concentration level.

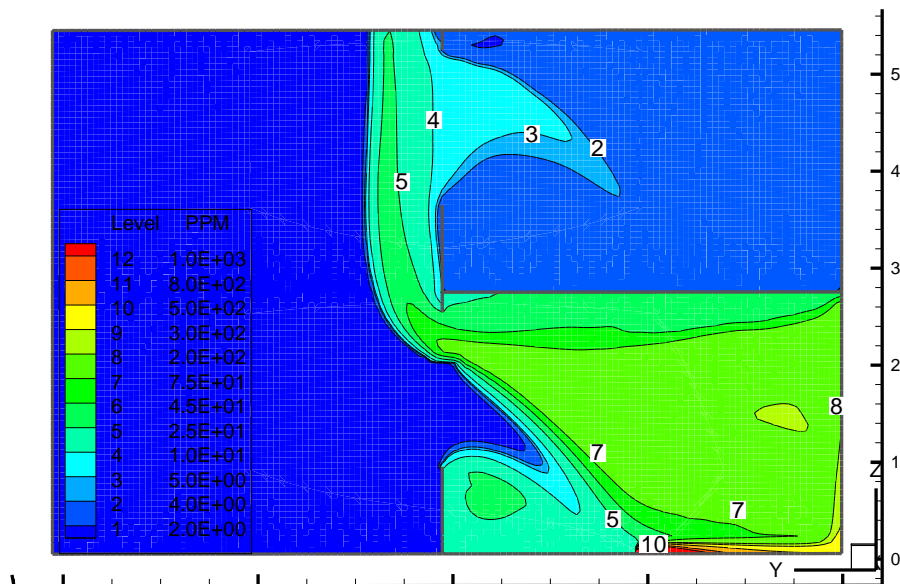


**Figure 4.17 Simulated CO<sub>2</sub> concentration distributions at the centre plane with individual mechanical exhaust (X=1.6m)**

## 4.5 Summary

In this chapter, under specific weather condition, one assumed contaminant dispersion route around a simple-shaped HRR building is identified and investigated. Due to the buoyancy effect is not easy to simulate by physical modelling method, such as a traditional wind tunnel, CFD method is employed to reveal the mechanism of this process.

First the performance of the standard and RNG  $k-\varepsilon$  models in predicting buoyancy-driven single side natural ventilation were evaluated and validated against the experimental data. The RNG  $k-\varepsilon$  model gave a relatively better performance than the standard  $k-\varepsilon$  model in predicting such kind of flow. Consequently, the RNG  $k-\varepsilon$  model was adopted to simulate the inter-flat air-flow under one-sided natural ventilation conditions, and the simulation results corroborated the hypothesis that the ventilation air from the lower flat to the adjacent upper flat via open windows can be a spread path of virus-containing bio-aerosols. It is found that under specific weather conditions, the presence of the pollutants in the immediate upper floor originating from the lower floor is generally two orders of magnitude lower than that in the lower floor. With regard to an architectural design feature, the numerical results illustrated that a window ledge between the two floors can probably reduce the contaminants spread by such inter-flat air flow.

The identification of this transmission path may also help us to reform the ventilation design in high-rise residential buildings to minimize cross contamination. Using individual mechanical exhaust in each flat is the obvious option, and is already the

practice, but without a central stack the effectiveness is less desirable. Individual mechanical exhaust into a central stack may be another effective ventilation strategy for high rise residential buildings, and the cross contamination through the open windows could be avoided or much reduced. From the perspective of infection control, early intervention may be implemented in terms of diagnosis and isolation if an emerging, highly infectious disease outbreak occurs in high-rise residential blocks.

The study presented in this chapter is focused on the air pollutant dispersion under low wind conditions. When the wind effect dominates, the transmission path may be strongly affected by the approaching wind characteristics, which deserves further investigation. In order to investigate that dispersion mechanism, it is necessary to perform the study from a whole building point of view, which will be introduced in the following chapters.

## **Chapter 5**

### **Investigations on Air Pollutant Dispersion around Sealed Building**

#### **5.1 Introduction**

The mechanisms of cross-contamination under specific weather conditions were illustrated in the earlier studies, both numerical simulation results and the previous on-site measurements identified that the possible re-entering of exhausted air pollutant could happen around a HRR building. Such identification of pollutant dispersion route and numerical analysis of the buoyancy effects under simplified weather condition with simple building layout give rise to further queries. What would probably happen if the pollutant dispersion is dominated by wind effect, and when the HRR building has more complicated building shape? Thus, the following studies are focused on pollutant dispersion under wind-effects only (without buoyancy effects), with a more complicated building layout.

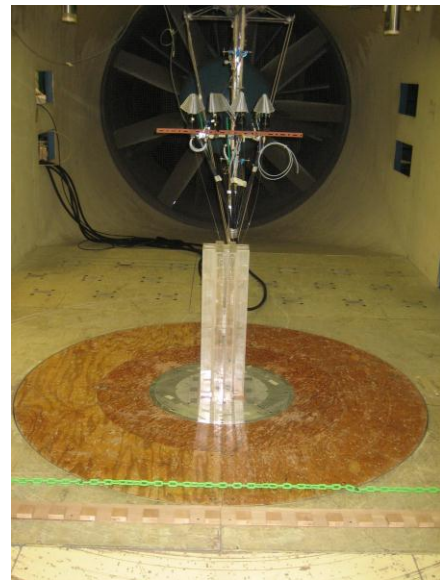
First a wind tunnel experiment was performed to obtain basic information about wind-induced cross-contamination around an entire building under different wind directions. Next, the experimental data were used to evaluate different numerical methods and turbulence models.

#### **5.2 Experiment Configuration**

The experiments were undertaken in the high speed section of UST/CLP wind tunnel. A plastic building model was constructed to a 1:150 scale. The model represents a 33 story HRR building with a height of 100m in prototype. The study is focused on the basic characteristics of air pollutant dispersion around the building, which will serve as a reference database for the validation and verification of the numerical results. Thus the model is constructed as a solid block without any openings on the building envelope. Figure 5.1 is the photos of the experiment configuration.



a) Front view



b) Back view

**Figure 5.1 Photos of the experiment setup in high speed wind tunnel**

### **5.2.1 Simulated Wind Profile in High Speed Wind Tunnel**

Roughness elements, spires and fences were used to generate the incoming boundary layer flow in the wind tunnel, which agrees with Equation (3.1). The designed and measured mean velocity and turbulence intensity profile are shown in Figure 5.4.

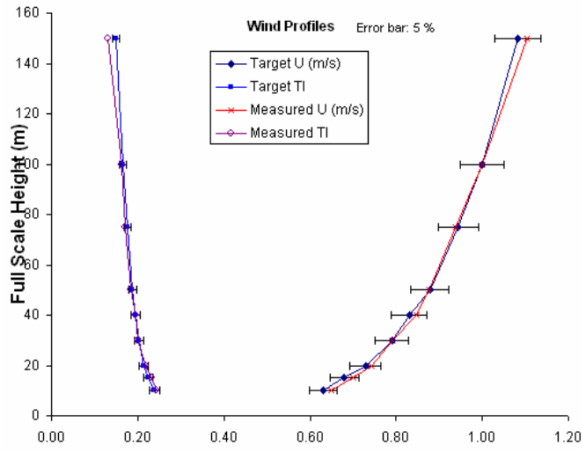
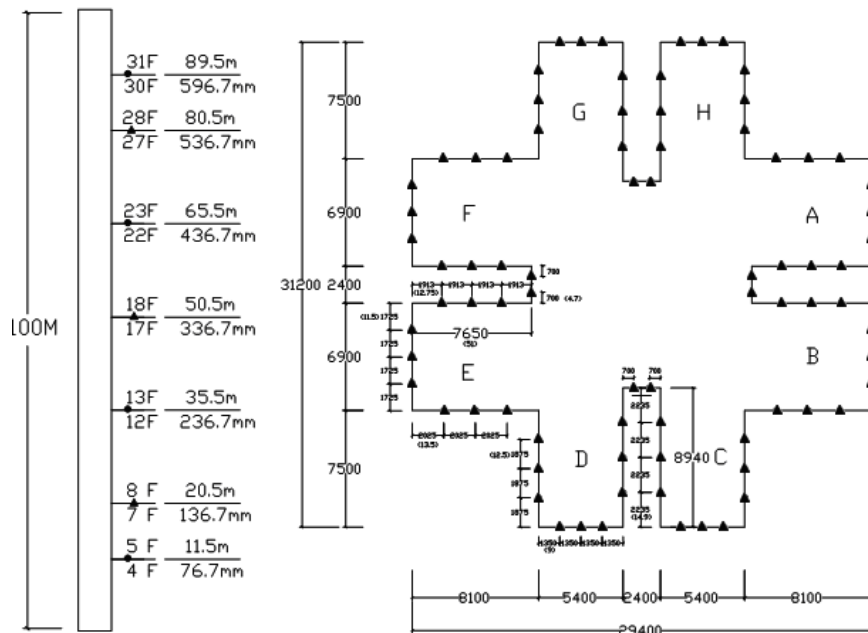


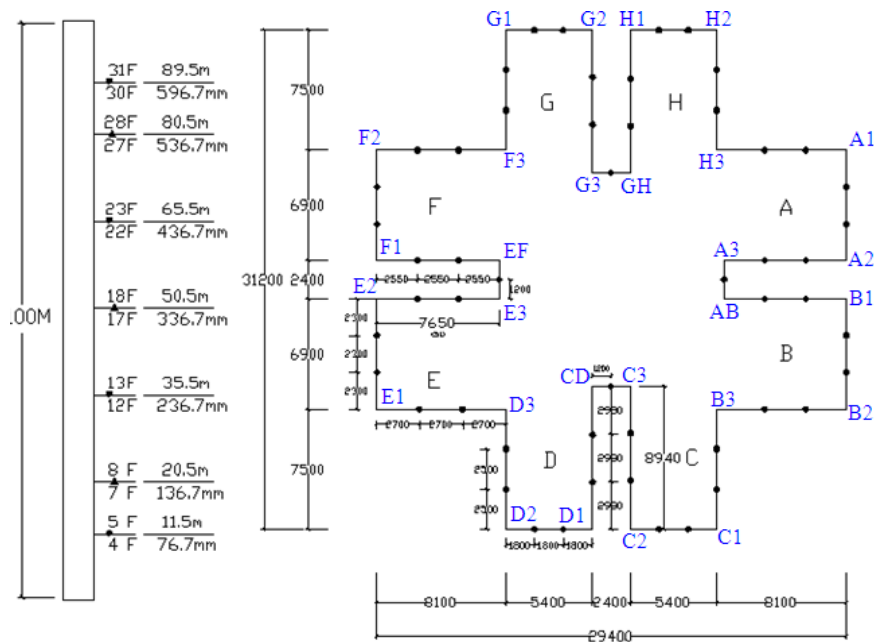
**Figure 5.2 Simulated approaching wind profile in high-speed wind tunnel**

### 5.2.2 Detailed Setup

A total 448 points were set-up for wind pressure measurement. All the measurement points are located on the building surface. Detailed pressure measurement points and the model plan view are shown in Figure 5.3. The pressure points are located at the normal position of window areas. In the 7<sup>th</sup>, the 17<sup>th</sup> and the 27<sup>th</sup> floors, 80 pressure taps were set up in each floor; and in the 4<sup>th</sup>, 12<sup>th</sup>, 22<sup>nd</sup> and 30<sup>th</sup> floors, 52 pressure taps were set up in each floor.



a) Surface pressure measurement points ( $\blacktriangle$ ) in the 7<sup>th</sup>, the 17<sup>th</sup> and the 27<sup>th</sup> floors



b) Surface pressure measurement points (●) in the 4<sup>th</sup>, 12<sup>th</sup>, 22<sup>nd</sup> and 30<sup>th</sup> floors

**Figure 5.3 Plan view of the model and pressure measurement point locations**

A gas of propane, with a concentration of 51,000ppm in air was used as the tracer to simulate an air pollutant. The tracer gas sources were located in façade H1 at the 6<sup>th</sup> floor and the 26<sup>th</sup> floor, respectively, as shown in Figure 5.4, with the source position (●) and the measurement points on the building surface (▲). The positions of the source at different height represent the exhausting air exiting from lower or higher part of the HRR building. At each measurement position, sample air was collected over a period of 48s to obtain stable estimates of mean concentration. The measurements correspond to full-scale concentrations obtained over 120 min.

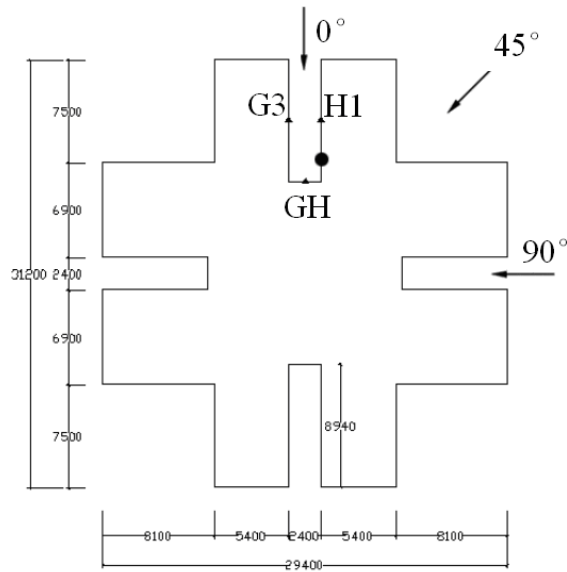
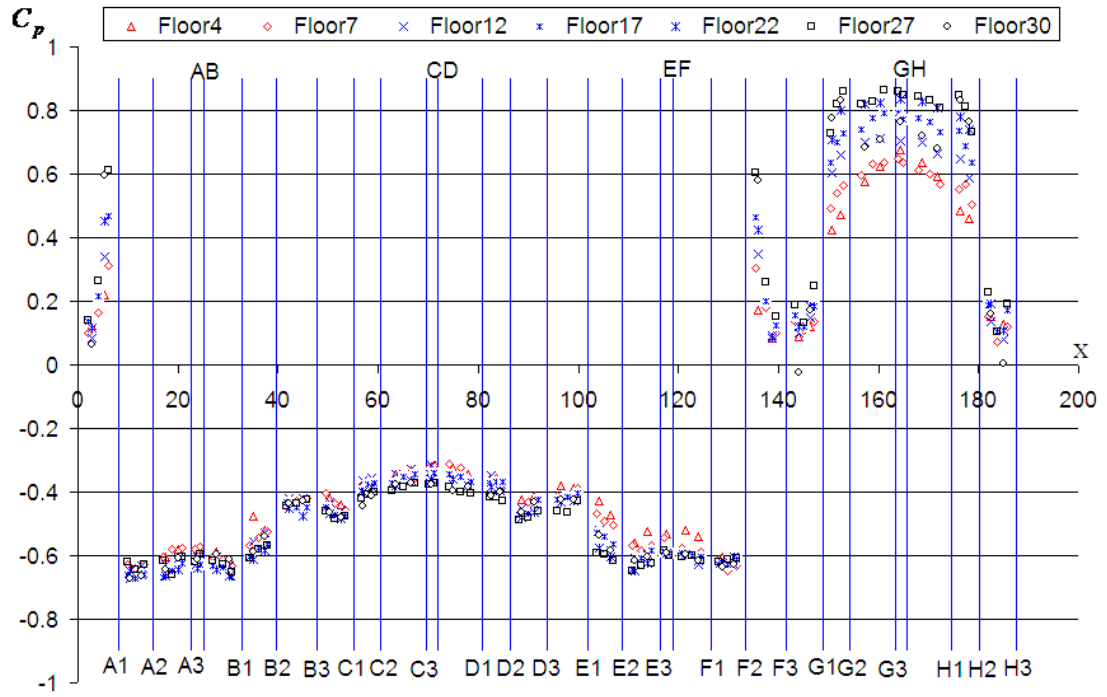


**Figure 5.4 Tracer gas source location and concentration measurement points**

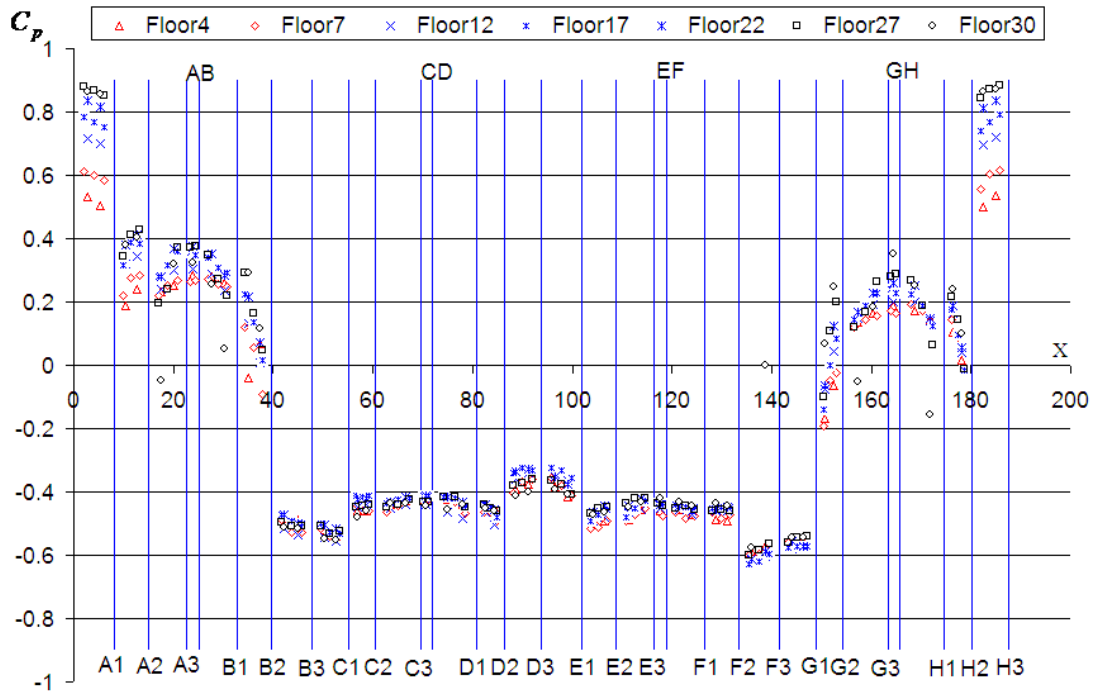
### 5.3 Measurement Results

#### 5.3.1 Mean Pressure Coefficient Distributions

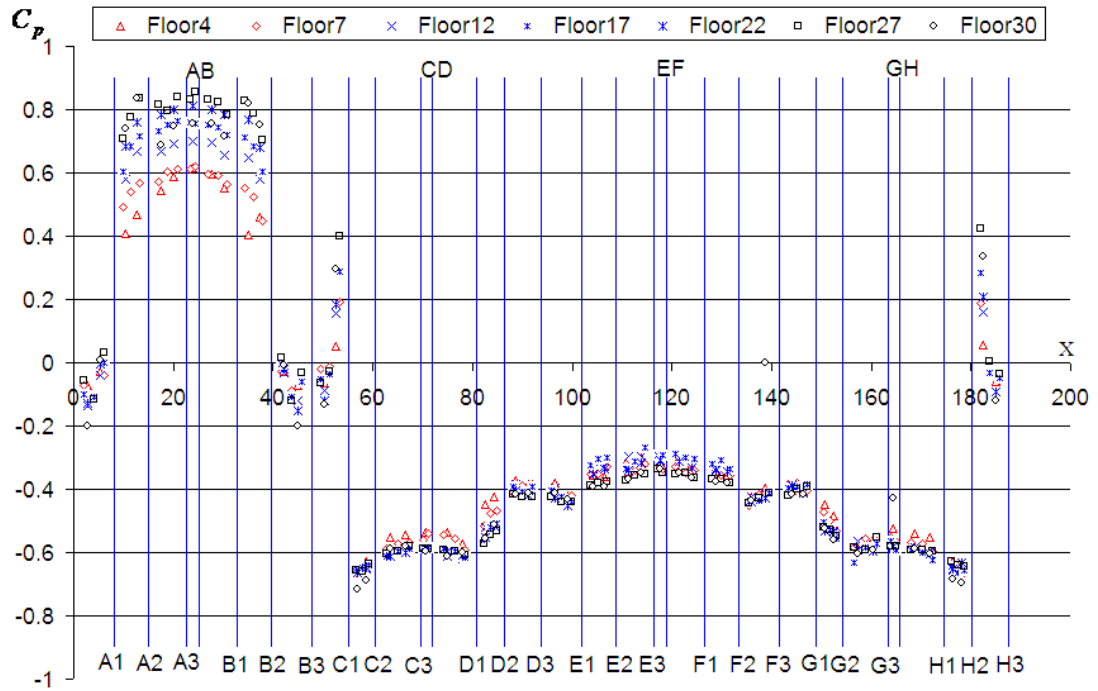
The mean pressure coefficients,  $C_p$ , calculated using Equation (3.2), along the building surface at different heights are shown in Figure 5.5, with three approaching wind incident angles. The X coordinate is the horizontal distance from point H3 shown in Figure 5.2b. The vertical blue lines indicate the positions of the building edges. The  $C_p$  value of the 3<sup>rd</sup> floor and the 7<sup>th</sup> floor that represent the lower part of the building are presented in red color, while in the middle part of the building (the results of the 12<sup>th</sup>, the 17<sup>th</sup> and the 22<sup>nd</sup> floors),  $C_p$  are presented in blue color, and in the higher part of the building (the results of the 27<sup>th</sup> and the 30<sup>th</sup> floors),  $C_p$  are presented in black color.



a)  $\theta = 0^\circ$



b)  $\theta = 45^\circ$



c)  $\theta = 90^\circ$

**Figure 5.5 Measured pressure coefficients along the building surface at different building heights at three approaching wind incident angles**

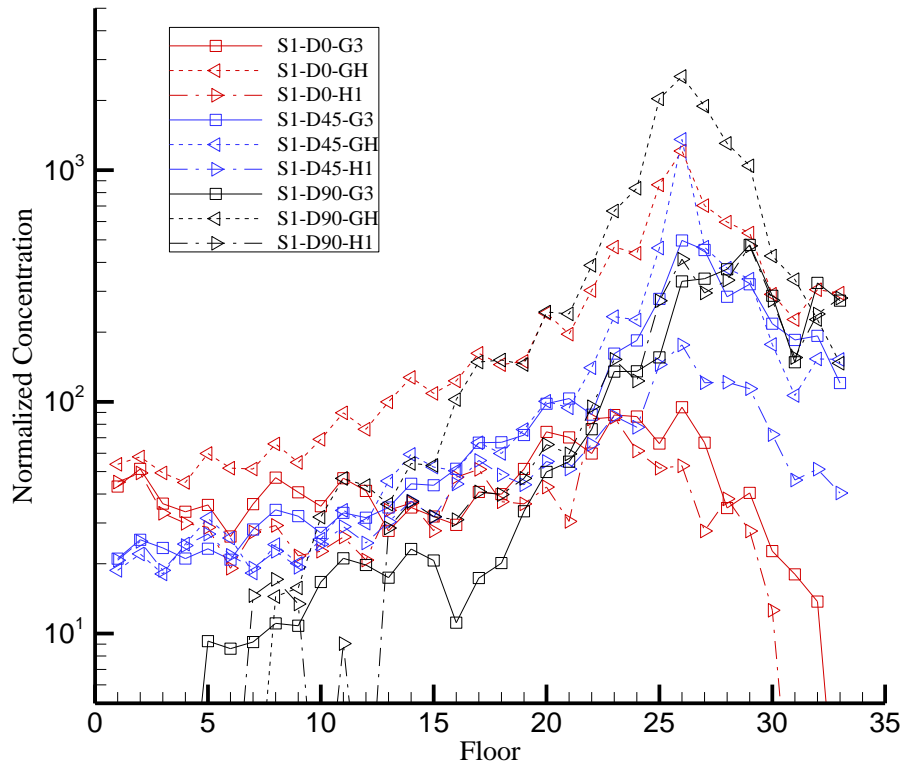
From this whole building pressure coefficient measurement, the general flow pattern characteristics around the entire building can be roughly estimated. It should be noticed that the overall pressure distribution along the building facades is complicated due to the complexity of the building shape. The pressure distributions vary with different building facades under each wind direction. As a result of the symmetrical features of the building structure, the  $C_p$  values along the horizontal building surfaces are symmetrically distributed. In view of the present study purpose, the main emphasis is given on the pressure distributions of the re-entrant spaces.

It can be observed that, under normal wind conditions ( $\theta = 0^\circ$  and  $\theta = 90^\circ$ ), the  $C_p$  values are positive only in one of the re-entrant spaces, which is in the windward side. While in the other three re-entrant spaces, which are either in the sideward or leeward side, the  $C_p$  values obtained are negative, indicating the occurrence of separate flow and recirculation flow. As to the windward re-entrant space, for example, as shown in Figure 5.5a, highest positive  $C_p$  values were found along facade G3-GH, while the other two facades (facade G2-G3 and facade GH-H1) also have positive  $C_p$  values.

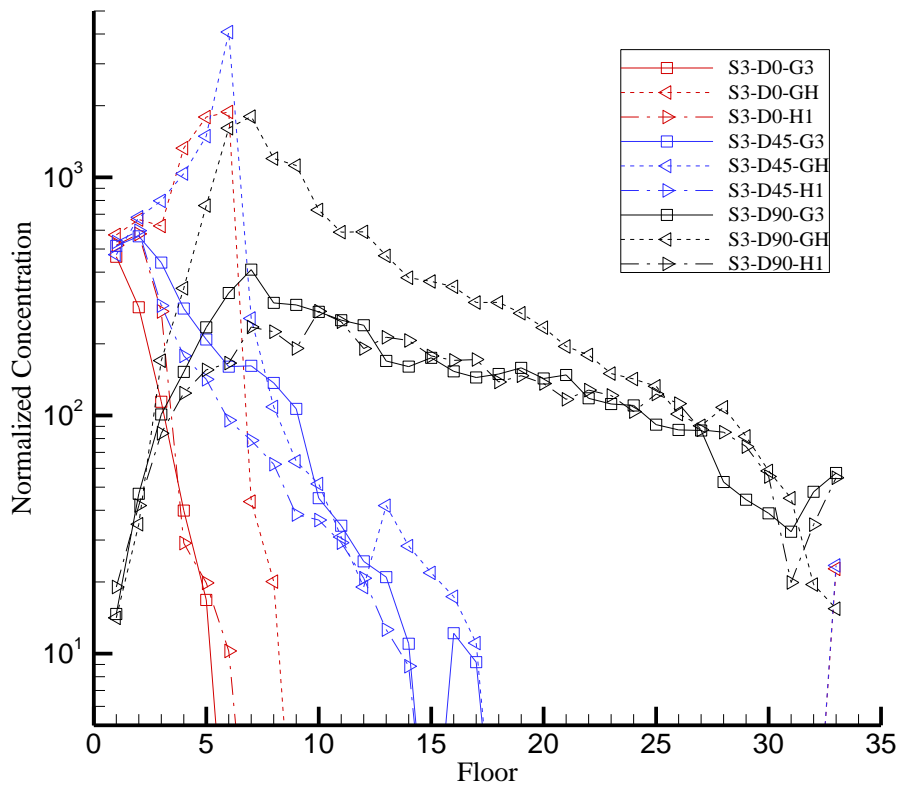
As for the  $C_p$  variations along the building height, in the windward side, the largest positive  $C_p$  values occur at the 27<sup>th</sup> floor of the building, and gradually decrease in both upward and downward directions. However, in the negative pressure facades, the variation of  $C_p$  values along the building height at a facade is not obvious.

### **5.3.2 Tracer Gas Concentration Profile**

Figure 5.6 shows the normalized concentration distribution, calculated using Equation (3.3), at each floor under three different approaching wind directions and two source locations.



a) Source at the 26<sup>th</sup> floor



b) Source at the 6<sup>th</sup> floor

**Figure 5.6 Normalized tracer gas concentration distribution. (D0, D45 and D90 are the results obtained under wind direction of  $0^\circ$ ,  $45^\circ$  and  $90^\circ$ , respectively.)**

Generally, these preliminary experimental results revealed the basic characteristics of wind-induced cross-contamination within the re-entrant space. The concentration profiles indicate the possible dispersion route of exhausted air pollutant under different circumstances. It can be observed that the concentrations generally decrease with distance from the source floor at both vertical directions. Besides, it is shown that the tracer gas can be detected not only in the source facade (facade H1), but in other facades (facade G3 and GH) within the re-entrant space, indicating a horizontal dispersion could also happen under wind effect. Comparing the concentration distributions along different façades, the concentration along façade GH is higher than other façades in all cases, which means the pollutant could be accumulated along façade GH in the deep side of this re-entrance space. Comparing different source locations, the concentration levels decrease faster from the source floor when the source was located in the lower part of the building, except when the wind direction was  $90^\circ$ . In general, with regard to different wind directions, higher risk of air cross-contamination was found when the approaching wind direction was  $90^\circ$ , i.e., when the approaching wind direction is perpendicular to the studied re-entrant space due to the symmetrical features of the building shape. It is probably because the “air curtain” effect caused by the rapid horizontal air movement across the opening of the re-entrant space, and the air pollutant can not be easily exhausted from the re-entrant space. The worst case happened when the source was located in the 6<sup>th</sup> floor with the wind direction at  $90^\circ$ , as shown in Figure 5.6b, and remarkable concentrations can be detected in the upper floors.

Moreover, it should be noticed from Figure 5.6b, when the source was located in the 6<sup>th</sup> floor, the concentration detected at façade H1 and G3 increased from the source floor to the lower floors with the coming wind direction at  $0^\circ$  and  $45^\circ$ . It is proved

that the tracer gas can be accumulated at the bottom of the re-entrance space of the building when the wind direction was 0 or 45 degree and the tracer gas was released in the lower part of the building. It could be explained by the wind induced surface flow pattern along the building surface. In lower part of a high-rise building, upwind vortex could be generated on the windward wall and thus the pollutant could be entrained and accumulated in the lower part of the re-entrant space.

#### **5.4 Evaluation of CFD Method Performances**

The basic information about wind-induced cross-contamination around the complex-shaped building can be found through the previous experimental results. Moreover, based on this preliminary exploratory study, different simulation methods can be examined for their relative suitability for the present applications. One widely used simulation software, Fluent 6.3, is used to perform the numerical experiments with the same configurations as the physical experiments. The predicted pressure coefficients and the normalized concentration values are directly compared with the previous wind tunnel experimental data. Therefore, the accuracy of the CFD simulation can be evaluated through the comparisons and analysis. Also, the mean flow fields around the target building and concentration distributions under both normal and oblique wind directions are provided here.

##### **5.4.1 Computational Domain Design and Grid Generation**

The solution domain for all the cases was a rectangular box surrounding the target building. The domain boundaries had to be positioned at sufficient distances, well

away from the building's displacement zone and re-circulation areas. The domain size designed for CFD applications on the airflow and dispersion around building plays an important role on successful prediction. The distances used in previous studies for the boundaries of the domain had been discussed and reviewed by Hall (1997). It should be large enough to generate correct flow around the building. However, if the domain is too large, the computing time will be increased significantly. The domain size used for some recent studies of flow and dispersion around building are presented and summarized in Table 5.1. Based on these data, the domain size was carefully designed and was shown in Figure 5.7, considering both accuracy and efficiency.

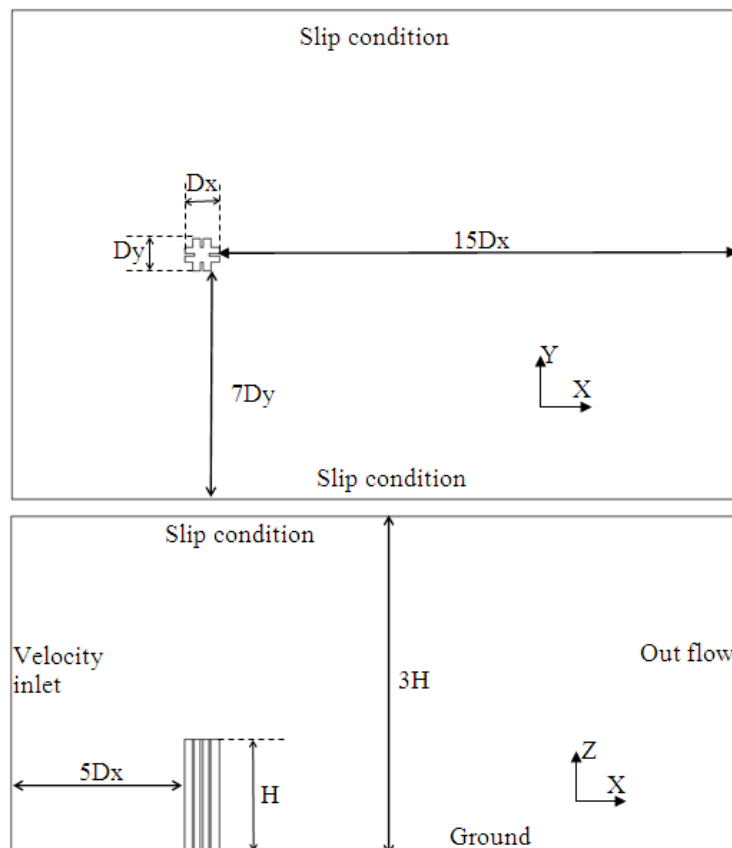
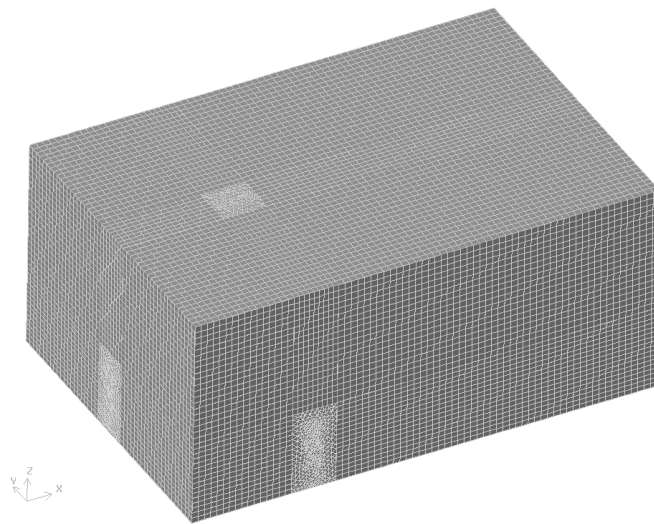


**Figure 5.7 Computational domain and boundary conditions**

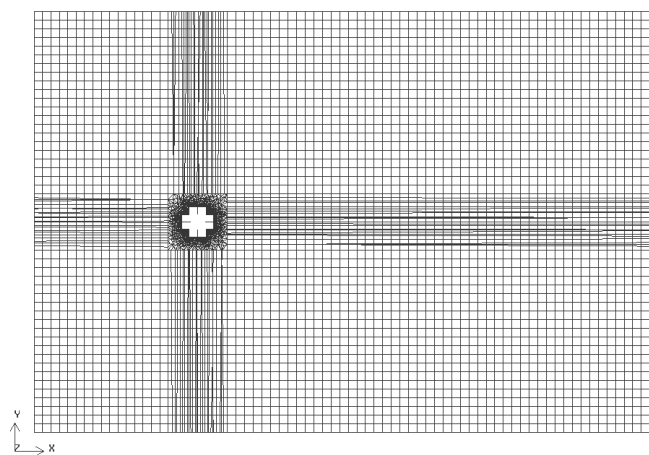
**Table 5.1 Comparisons of solution domain size (The abbreviation “W” and “H” represent the building width and height, respectively)**

Front	Behind	Side	Height	Building Features	Ref.
5H	10-16H	5H	5H	Cubic (Dispersion)	Hall, 1997
5W	15W	15W	4H	Square-Cylinder (Airflow)	Lubcke et al., 2001
6.75W	4.75W	5W	5H	Cubic (Dispersion)	Sada and Sato, 2002
2.5W	8.25W	6W	1.5H	High-rise (Airflow)	Burnett et al., 2005
4W	11W	9W	4H	Group Building (Airflow)	Yang et al., 2005
1H (4W) for Normal Wind Direction; 2H (8W) for Oblique Wind Direction	6H (25W)	15W, as Wind Tunnel	2H, as Wind Tunnel	High-rise (Airflow)	Cheng et al., 2007
6W for Normal Wind Direction; 10W for Oblique Wind Direction		6W for Normal Wind Direction; 10W for Oblique Wind Direction	4H	Low-rise (Airflow)	Asfour and Gadi, 2007
6W	22W	17W	2H	High-rise (Airflow)	Huang et al., 2007
8H	8H	6H	5H	High-rise (Airflow)	Zhang and Gu, 2008
21.5W, as Wind Tunnel		13.75W, as Wind Tunnel	5.6H, as Wind Tunnel	High-rise (Airflow)	Tominaga et al., 2008a
5.4H	10.7H	15.2 H	7.5H	Cubic (Dispersion)	Santos et al., 2009
5H	15H	13H	6.7H	Cubic (Dispersion)	Tominaga and Stathopoulos, 2009

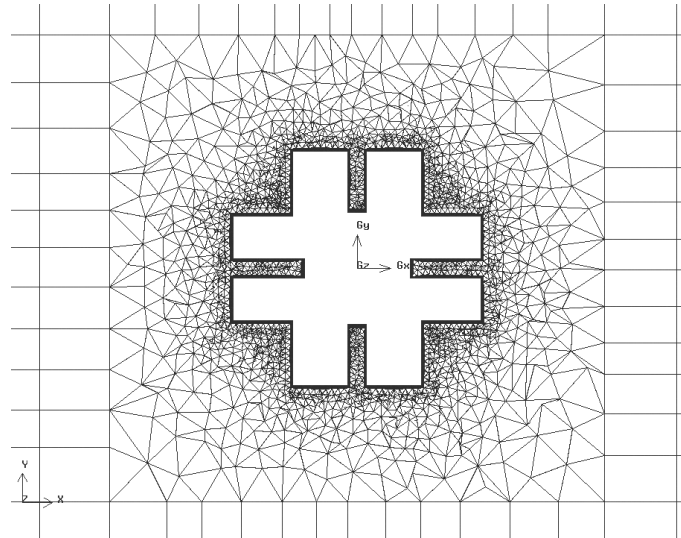
Since the commercial code used here is based on the finite volume method, with the capacity of dealing with both structured and unstructured grids in its solver, there is a variety of flexibilities of mesh generation. Figure 5.8 shows the mesh arrangement for the current studies. The building model is nested in a rectangular cylinder about eight times larger than itself. This arrangement makes it easier to generate a mesh fine enough in the neighborhood of the building surfaces while keeping the mesh in zones far away from the building in a coarser state. Total 1,768,967 meshes were generated for the cases under normal wind condition.



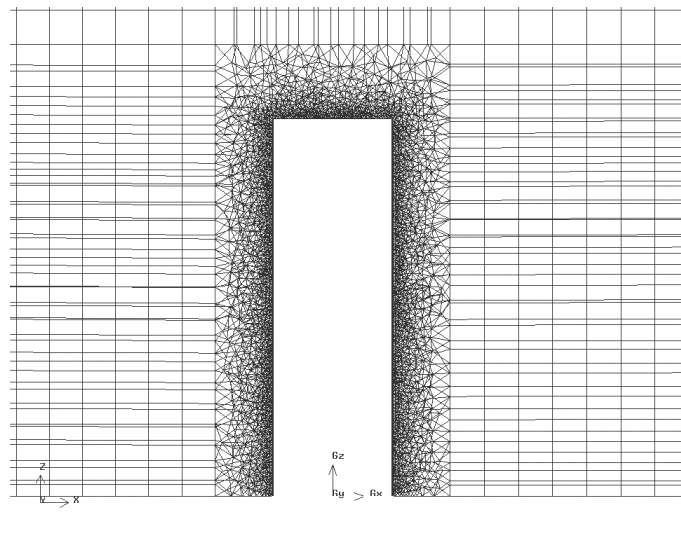
a) Overall grid distribution



b) Grid distribution in X-Y plan



c) Grid near the building surfaces (X-Y plane)



d) Grid near the building surfaces (X-Z plane)

**Figure 5.8 Grid generated for this study**

On the surfaces of the building model, a viscous boundary layer with 12 grid layers is generated. The resulted distribution of  $y^+$  on the building surfaces is shown in Figure 5.9 based on the preliminary computational results applying standard  $k-\varepsilon$  model. It can be seen that all the values of  $y^+$  on the 28 side surfaces are less than 4. Thus the enhanced wall treatment can be used.

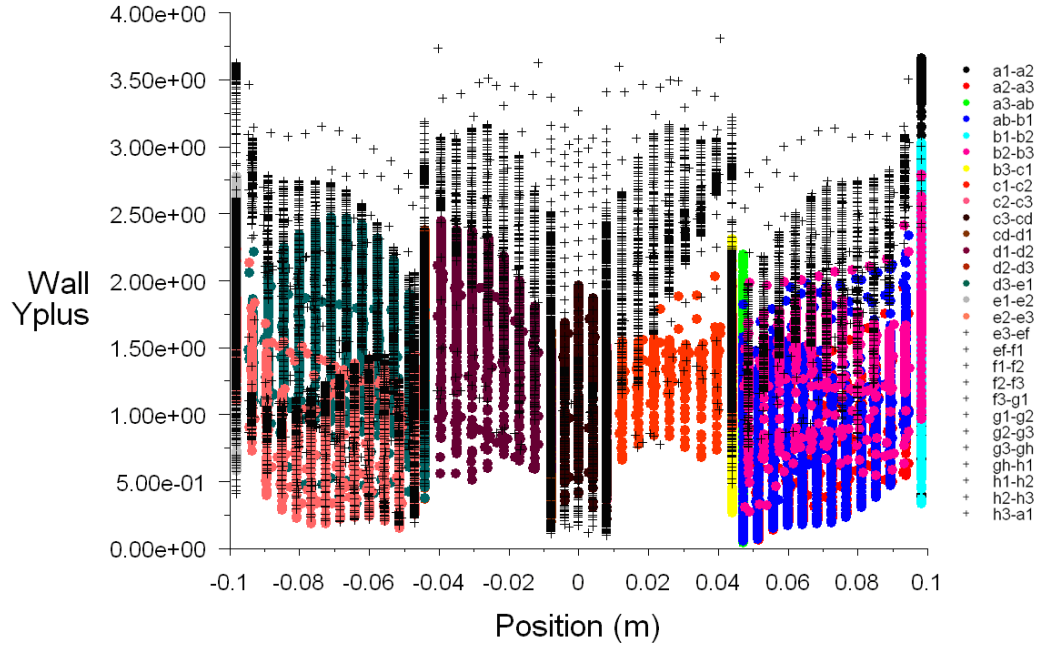


**Figure 5.9 wall unit distribution on the building surfaces**

#### 5.4.2 Turbulence Models and Numerical Methods

The boundary conditions considered in the present simulations are shown in Figure 5.7. In order to obtain better agreement between experimental and numerical results, boundary conditions adopted in the presented numerical simulations is about the same as those in the wind tunnel experiment. The velocity profile of the atmospheric boundary layer imposed in the domain inlet takes the power law with the exponent of the velocity profile equal to 0.2, as it was used in the wind tunnel. The kinetic energy of turbulence and its dissipation rate at the inlet section are calculated according to the following equations:

$$k = \frac{3}{2} (U_{avg} I)^2 \quad (5.1)$$

$$\varepsilon = C_{\mu}^{3/4} \frac{k^{3/2}}{l} \quad (5.2)$$

where  $U_{avg}$  is the mean velocity at inlet,  $I$  is the turbulence intensity, which is interpolated from the data obtained in the wind tunnel. Non-slip condition is employed in the building walls. At the top boundary and both sides of the domain, the slip type conditions are used.

The FLUENT code provides a variety of turbulence models to simulate turbulent flows. Standard  $k-\varepsilon$ , RNG  $k-\varepsilon$  and realizable  $k-\varepsilon$  models are selected in this study. These various kinds of  $k-\varepsilon$  models are commonly used in simulation of wind flows around bluff bodies. The performance of predicting wind-induced cross-contamination based on these turbulence models are evaluated during this study.

All the discretized equations are solved in a segregated manner with the SIMPLEC algorithm (Vandormaal and Raithby, 1984). The second order upwind scheme is used for spatial discretization.

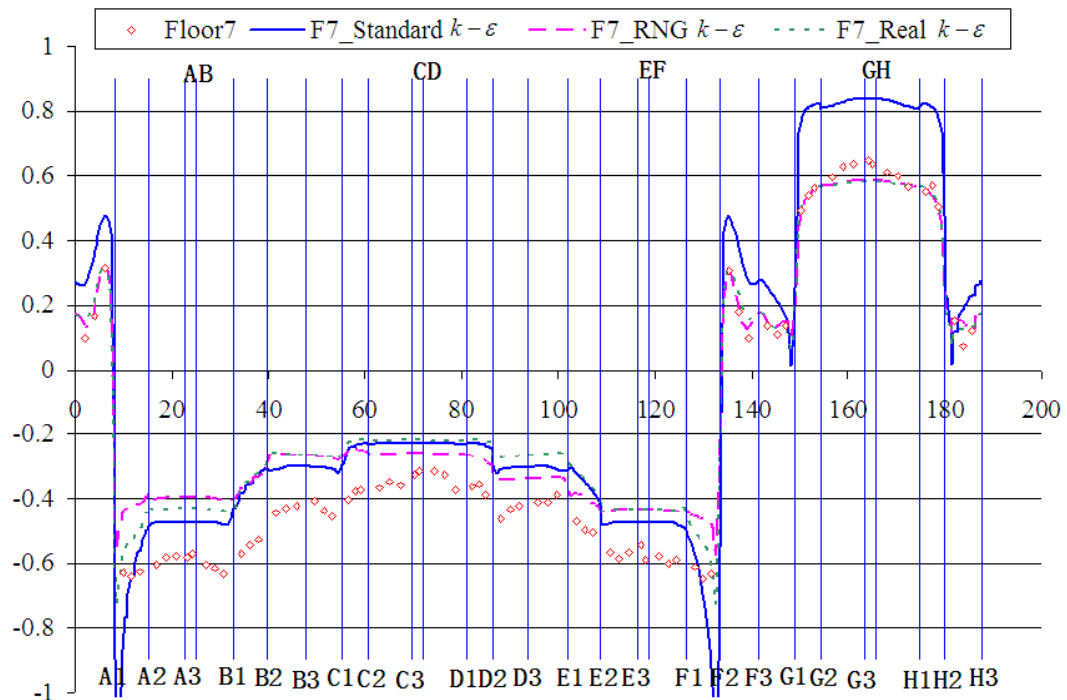
#### **5.4.5 Comparisons between CFD Results and Wind Tunnel Data**

The numerical study is considered for the cases at incident wind angle of  $0^\circ$  and  $45^\circ$ , respectively, using three kinds of  $k-\varepsilon$  turbulence models. The comparisons between simulated results and the measurements were first focused on the mean pressure coefficients along building surfaces. This is the first step to examine the accuracy of the present simulation results. Then the flow field simulated by CFD methods was

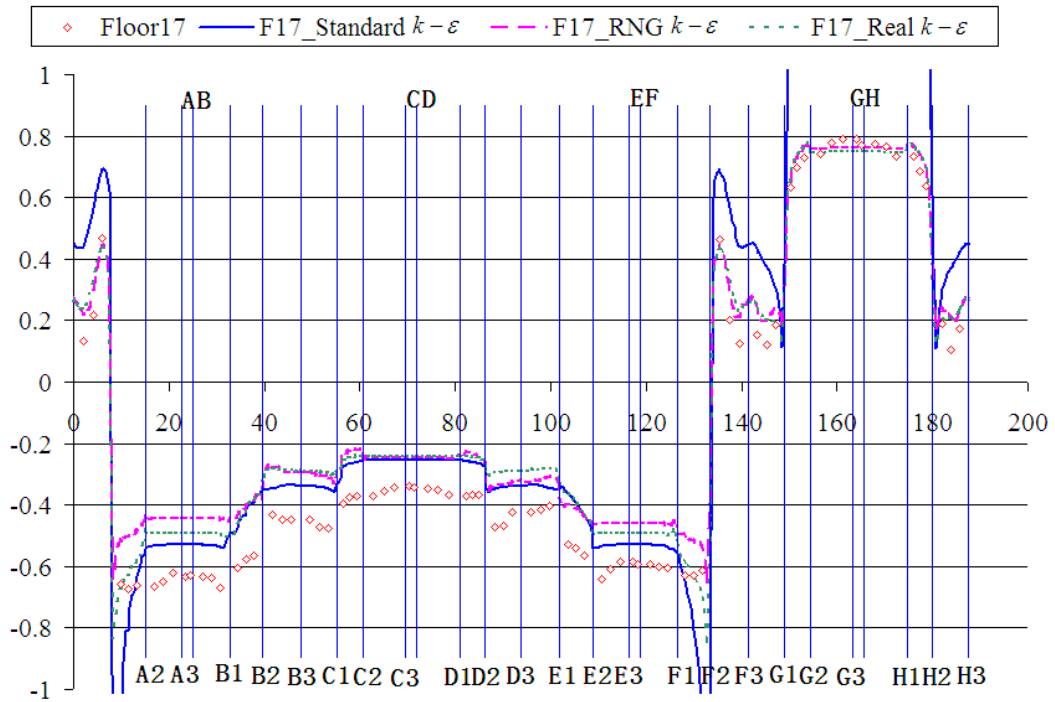
presented to reveal the detailed flow pattern around target building, benefiting from the advantages of numerical techniques. Finally the simulated concentration profiles were compared with experimental data and discussed.

### Mean Pressure Coefficients

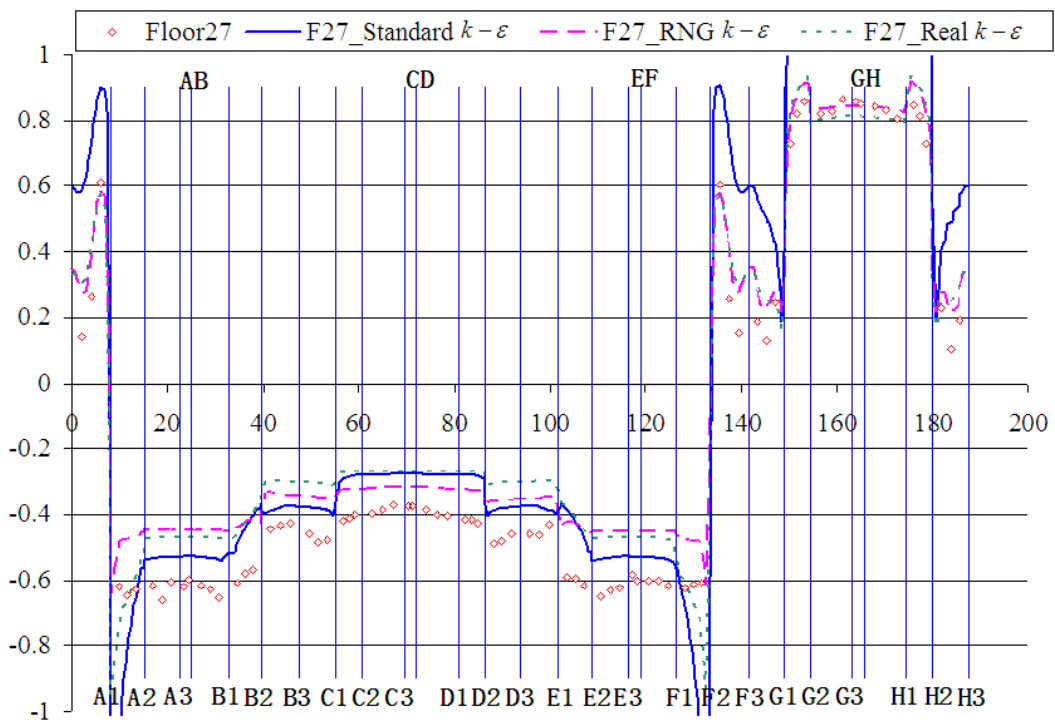
The comparisons between computed mean pressure coefficients and the experimental data under both normal and oblique wind directions were shown in Figure 5.10 and Figure 5.11, respectively, at different building heights. During the experiment, the pressure taps that were set up in the 7<sup>th</sup>, the 17<sup>th</sup> and the 27<sup>th</sup> floors were densely distributed, which also represented the lower part, the middle part and the higher part of the building. Therefore, the comparisons were made on the pressure coefficients obtained in these three floors.



a) at the 7<sup>th</sup> floor of the building

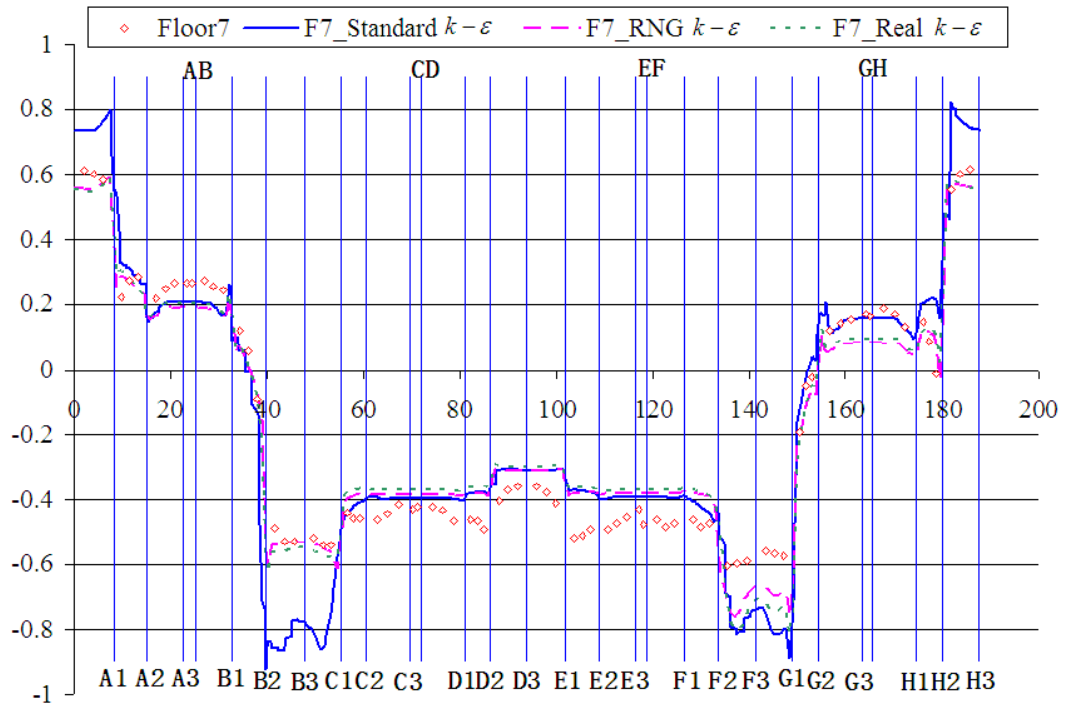


b) at the 17<sup>th</sup> floor of the building

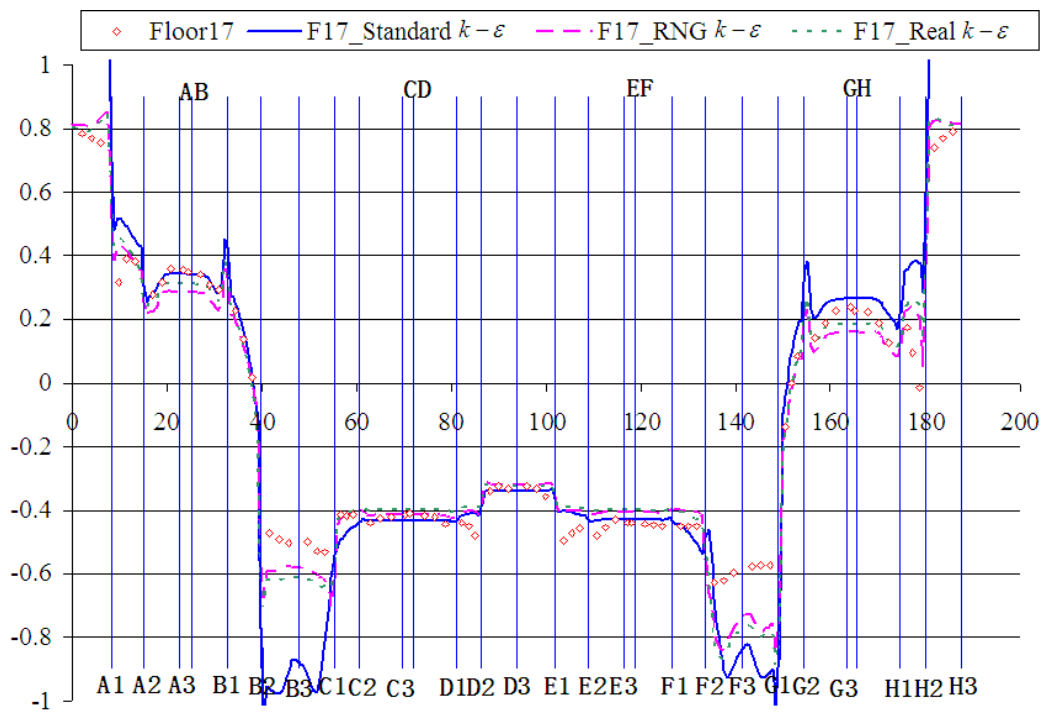


c) at the 27<sup>th</sup> floor of the building

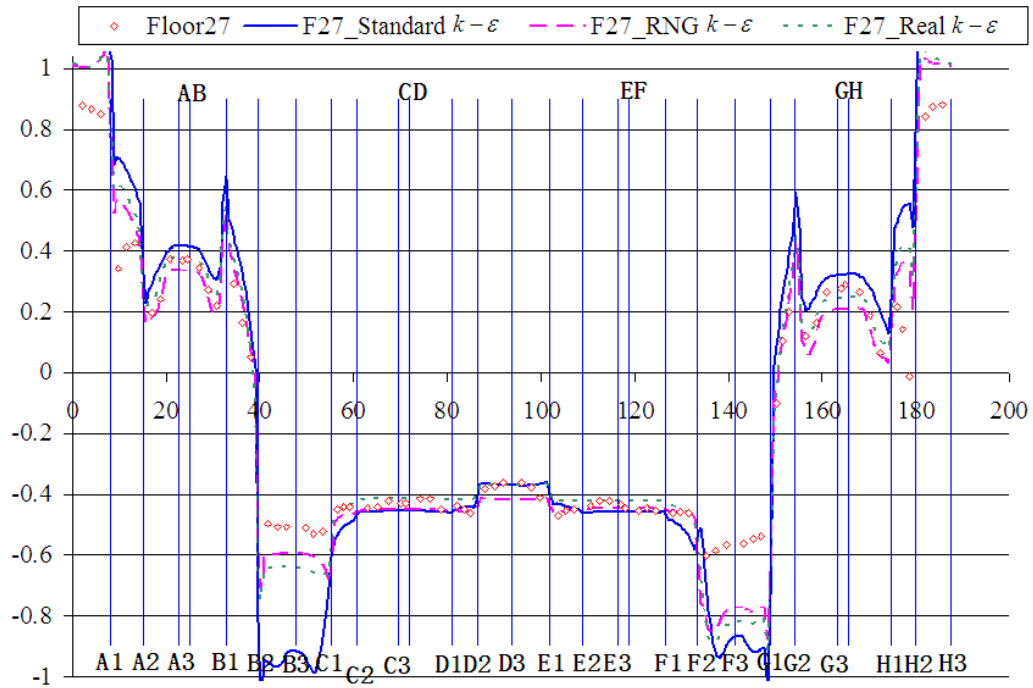
**Figure 5.10 Comparisons of mean pressure coefficients between CFD results and the wind tunnel measurements ( $\theta = 0^\circ$ ).**



a) at the 7<sup>th</sup> floor of the building



b) at the 17<sup>th</sup> floor of the building



c) at the 27<sup>th</sup> floor of the building

**Figure 5.11 Comparisons of mean pressure coefficients between CFD results and the wind tunnel measurements ( $\theta = 45^\circ$ ).**

Generally, it can be seen that the overall pressure distribution characteristics were revealed by the numerical results. The variation trend of surface pressure coefficient was illustrated from the simulated results. Different facades with either positive or negative  $C_p$  values were clearly distinguished. With regard to the performances of the three turbulence models, as shown in the figures, the standard  $k-\varepsilon$  model obviously over-predicts the pressure values. It is shown that the results obtained by both RNG  $k-\varepsilon$  and realizable  $k-\varepsilon$  models are in better agreement with the measurements under both normal and oblique wind directions, while noticeable discrepancies still exist in some particular regions.

Under normal wind direction, the simulated  $C_p$  from two revised  $k-\varepsilon$  models along the windward facades (from facade F2-F3 to facade H3-A1) at different floors is close to the measurement values. But in other facades with negative  $C_p$  values, the predicted results clearly differ from the experimental data, especially in the sideward facades (from facade A1-A2 to B1-B2, and from facade E1-E2 to F1-F2), indicating an unsatisfactory prediction performance in some particular regions where the airflow separates over building sharp edges. On the windward faces, it can be seen that the standard  $k-\varepsilon$  model tends to overestimate the pressure values on the windward faces, which is caused by the inexact prediction of turbulence energy  $k$  in the impinging region of the front face, as reported in previous studies (Huang et al., 2007). In some particular regions in the windward side (from facade G1-G2 to facade H1-H2), as shown in Figure 5.10b) and c), the  $C_p$  values predicted by standard  $k-\varepsilon$  model even greater than 1, which is evidently incorrect due to an unrealistic simulation of the normal turbulent stresses which contribute most to the turbulence production in such regions. It should be noted that the computed  $C_p$  from standard  $k-\varepsilon$  model along these facades seem to be more close to the experimental values. However, in consideration of the significantly over-predicted positive  $C_p$  values from standard  $k-\varepsilon$  model presented in the windward facades, it is reasonable to believe that the standard  $k-\varepsilon$  model over-predicted the  $C_p$  magnitude in both windward and leeward surfaces.

Under oblique wind direction, acceptable agreement was achieved between the simulated results obtained by all the three turbulence models against the experimental data, except for the surfaces where the flow separation occurs (façade

B2-B3, B3-C1, F2-F3 and F3-G1). Both revised  $k-\varepsilon$  models show better performances in predicting the pressure distribution in these areas. It is also shown that the computed  $C_p$  values from standard  $k-\varepsilon$  model in this case at different building floors are in better agreement with the experimental data than that of under  $0^\circ$  incident wind angle, except for facade H2-H3 and H3-A1, which directly face into the approaching wind. It can be explained by the less impinging effect occurred under oblique wind direction than that under normal wind direction.

The intention of this comparison is to preliminarily evaluate the accuracy of the presented numerical methods and validate the performance of the different  $k-\varepsilon$  turbulence models. As expected, both revised  $k-\varepsilon$  models improve the accuracy of predicting the mean pressure coefficient values, particularly in the windward surfaces. It should also be noted from the results that all the presented models still have their weakness in predicting the pressure distribution along side walls and back walls, and obviously discrepancies between the computed and experimental results could be found in the corner area of the building due to the complex flow in these regions, which was also reported in previous studies (Huang et al., 2007; Zhang and Gu, 2008). However, it is encouraging that the predicted results provided reasonable pressure distribution pattern compared with wind tunnel experiment data. Before performing comparisons about the tracer gas concentration field between the simulations and the measurements, the detailed flow field should be checked and analyzed. Taking the advantage of CFD techniques, the flow pattern around target building could be analyzed to further understand the complicated interactions between the approaching wind and the building with a complex shape.

## Flow Field Investigation

The predicted flow patterns under different wind incident angles are shown here. The locations of the selected sections are shown in Figure 5.12. Section 1 is the horizontal plane (X-Y Plane) at the height of the higher source (source located in the 26<sup>th</sup> floor), while Section 2 is the vertical plane (Y-Z Plane) that across the source's location. Figure 5.13a) and Figure 5.14 show the mean velocity contour distributions with 2D streamlines on Section 1, while Figure 5.13b) shows the mean velocity field with 2D streamlines on Section 2. The airflow pattern on the X-Z plane will be discussed in the next section combined with the concentration field.

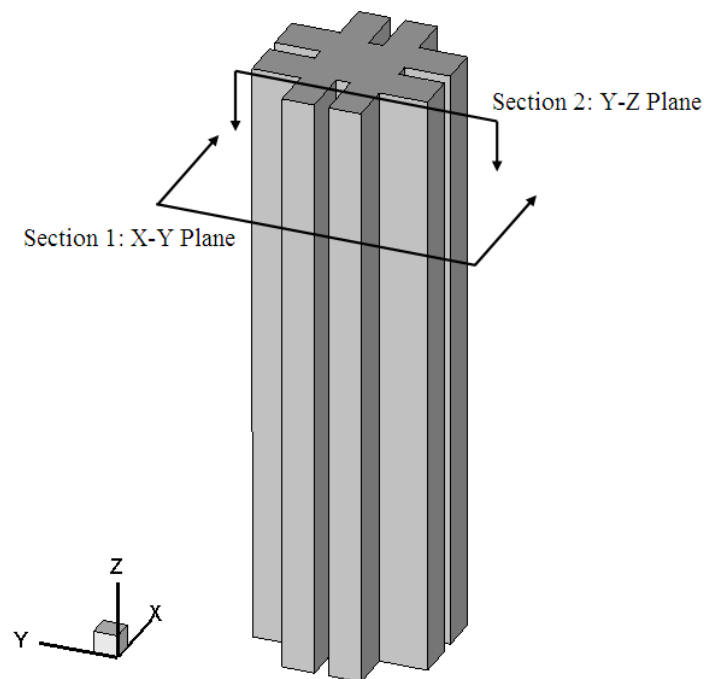
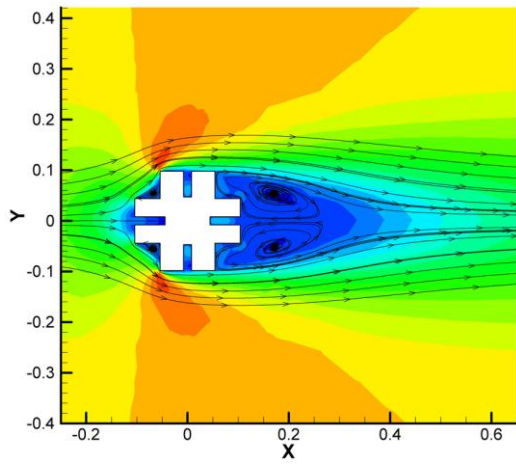
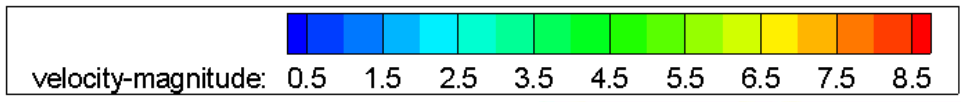
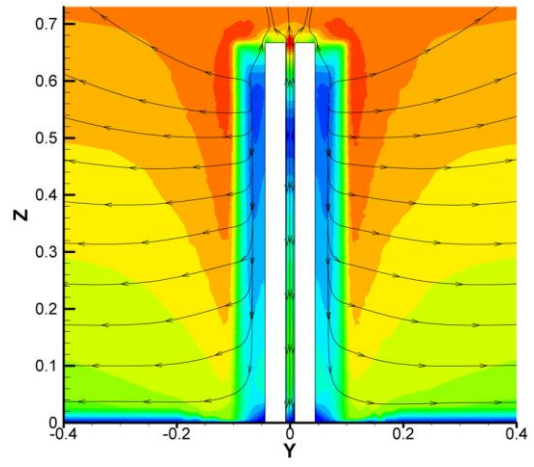


**Figure 5.12** Perspective view of the model and sections.

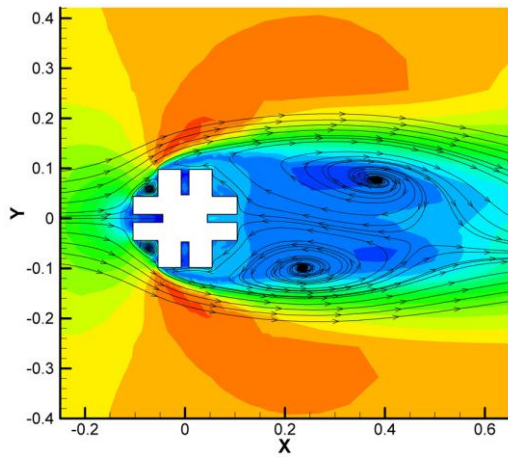
It can be seen from the results that the mean flow fields simulated by the three turbulence models were generally similar, and the typical flow field features were illustrated from the results. The oncoming wind impacts against the windward faces and produces a stagnation region in front of the building. A large recirculation region can be found behind the building and has a typical converging-diverging behavior. There are complicated vortex structures in the near wake of the building. A pair of vortices behind the building can be clearly seen. In general, the wake flow developing process is unsteady, but for the turbulent flow around target building, the  $k-\varepsilon$  models can merely present steady solutions. Thereafter, to explore the transient wake flow properties, more elaborate turbulent model should be applied, this, however, is beyond the scope of this study. The re-circulating region behind the building under oblique wind direction is relatively smaller than that of under normal wind direction. It should be noticed that due to the characteristics of the building shape, with eight wings extended from the center core of the building at different directions, the basic flow field is partly different from that of around a simple tall building with rectangular section. The airflow hits the windward wings and then separated over building sharp edges and bends around the building side wings into the wake. Also, the flow acceleration region is near to the leading edge of the side wings. Differing from the re-attachment phenomenon that can be observed on the side walls with relatively long and straight side faces under normal wind direction (Lakehal and Rodi, 1997), it was not obvious in the presented flow field around such building with two separate wings on each side.



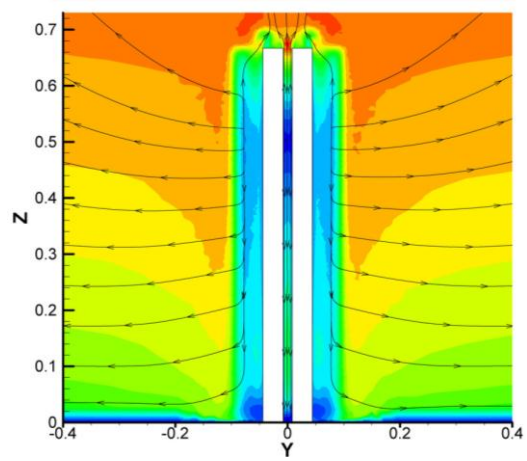
a1) Standard  $k-\varepsilon$



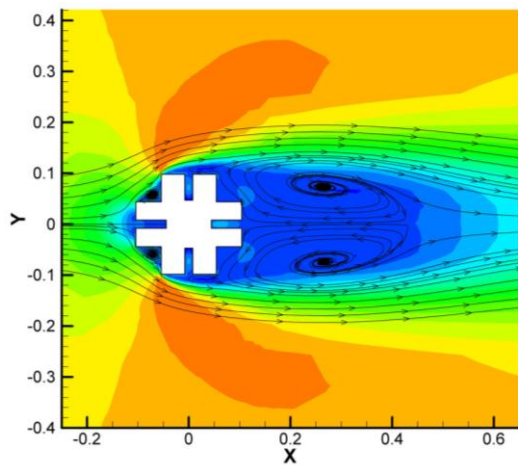
b1) Standard  $k-\varepsilon$



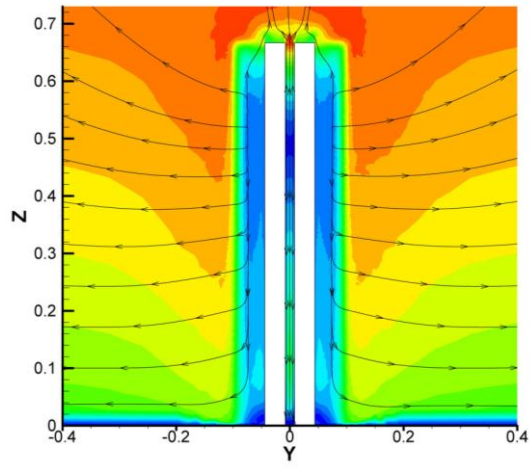
a2) RNG  $k-\varepsilon$



b2) RNG  $k-\varepsilon$



a3) Realizable  $k-\varepsilon$

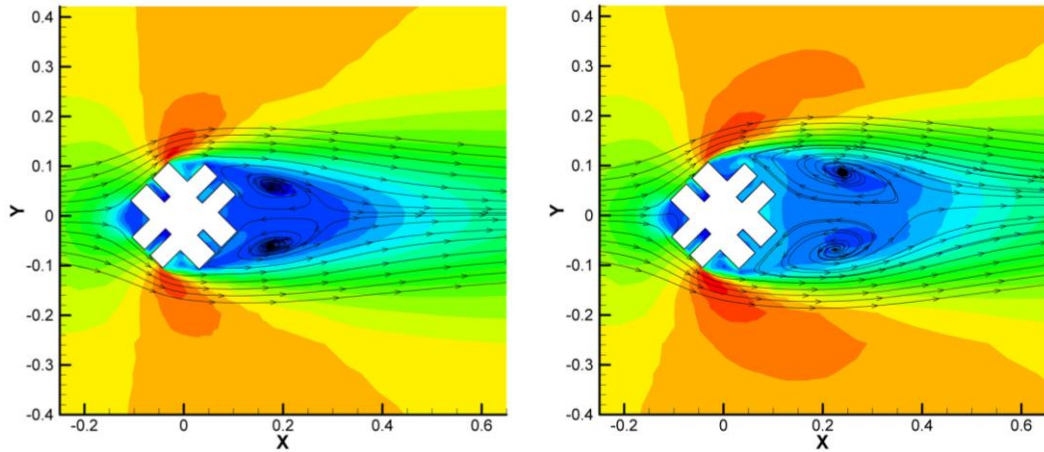


b3) Realizable  $k-\varepsilon$

**Figure 5.13 Mean velocity contour distributions with streamlines on: a) Section1;  
b) Section 2**

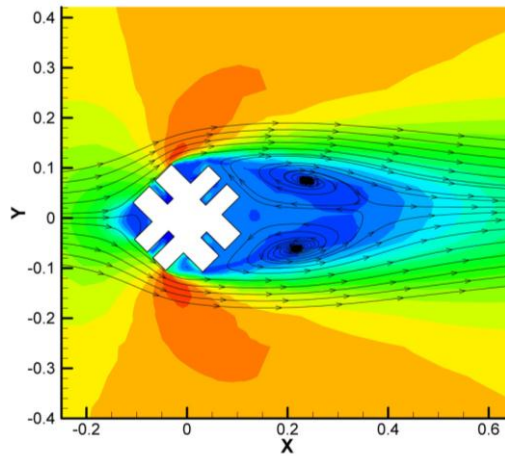
When compared the results from different  $k-\varepsilon$  models, the differences mainly lie in the features of the vortex in the wake region and the radius of curvature of the streamlines near to the building side wings. The locations of the vortex behind the building predicted by revised  $k-\varepsilon$  model are more downstream than that of predicted by standard  $k-\varepsilon$  model, and their shapes are also different. As for the second aspect, the results predicted by standard  $k-\varepsilon$  models show decreased radius of curvature, hence lead to lower pressures due to increased rate of entrainment of wake fluid into the more turbulent shear layer. This flow patterns can also explain that the larger magnitude of  $C_p$  values obtained by standard  $k-\varepsilon$  model at the back surfaces.

Focused on the flow field in the re-entrant space, the airflow velocity magnitude was comparatively small, indicating a relatively weak flow within the re-entrance space due to the restriction effect induced by nearby walls. However, it was also shown from Figure 5.13 b) (i.e., b1, b2, b3) that above approximately 2/3 of the building height, an upward stream can be found, while a downward airflow was found under this area.



a) Standard  $k - \varepsilon$

b) RNG  $k - \varepsilon$



c) Realizable  $k - \varepsilon$

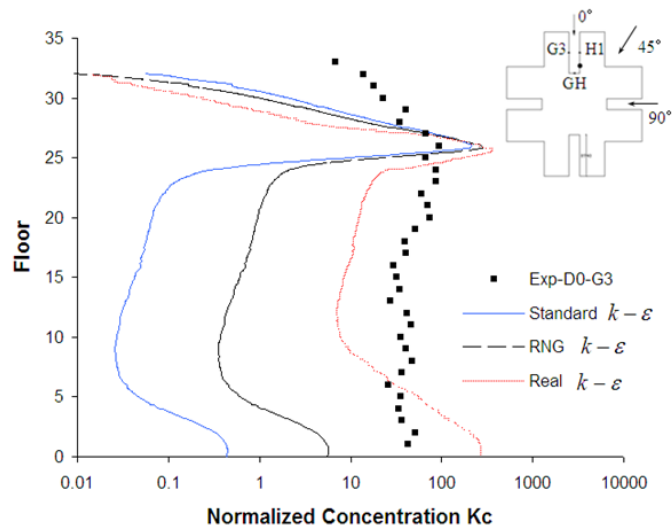
**Figure 5.14 Mean velocity contour distributions with streamlines on Section 1 under oblique wind direction.**

### Mean Concentration Profiles

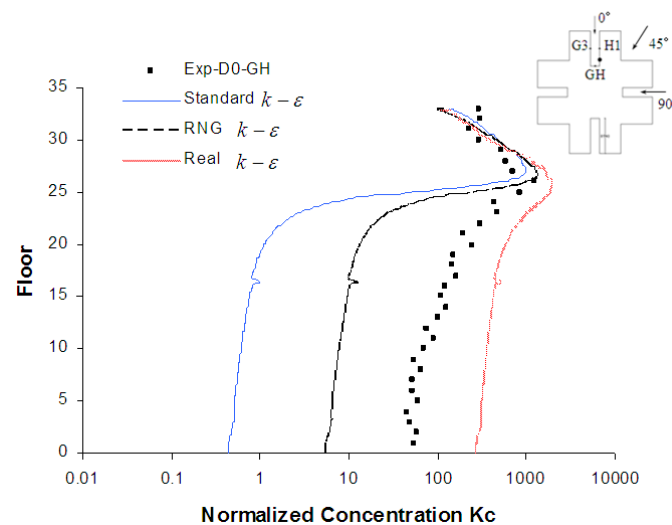
The former comparisons about mean pressure coefficient between simulated and experimental results partly proved the reliability of the numerical results. For further checking the accuracy of the numerical methods in predicting the pollutant

dispersion process within the re-entrant space, the computed normalized concentration values are compared with the wind tunnel measurement data.

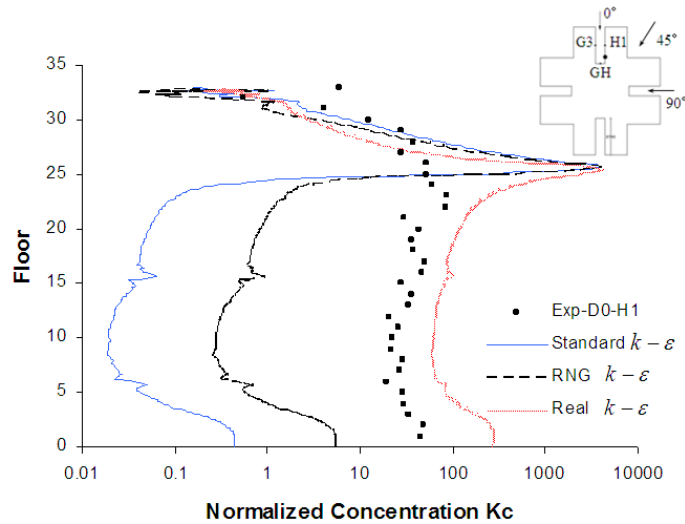
The predicted normalized concentration profile along the building height at G3\GH\H1 locations are compared with wind tunnel measurement results. Two cases are selected for the cross comparisons, with the source located in the 26<sup>th</sup> floor under  $\theta = 0^\circ$  and  $\theta = 45^\circ$ . Figure 5.15 is the normalized concentration values under normal wind direction.



a) Along the building height at point G3



b) Along the building height at point GH



c) Along the building height at point H1

**Figure 5.15 Comparisons of normalized concentration between CFD results with different turbulence models and wind tunnel measurement results ( $\theta = 0^\circ$ , the source was located in the 26<sup>th</sup> floor).**

Generally speaking, the dispersion features are partly illustrated by the simulation results. The concentration levels along each facade decrease with the distance from the source location. When the source gas was released from point H1, the tracer gas can be detected in point G3 and GH in both vertical directions under approaching wind effect. The prediction results of the concentration profile in the upper part of the building show acceptable agreement with the experimental data except in point G3, which basically reveal the upward dispersion under wind effect. For the downward dispersion, substantial discrepancies can be observed between predicted results and the measurement data. In the horizontal direction, it can be observed that the computed concentration values are relatively higher at point GH than that at point G3 and H1 in the floors below the source floor, which indicates the pollutant accumulation effect that happened in the deep side within this re-entrant space. At point G3 and H1, it is worth noting that the predicted concentration levels in the

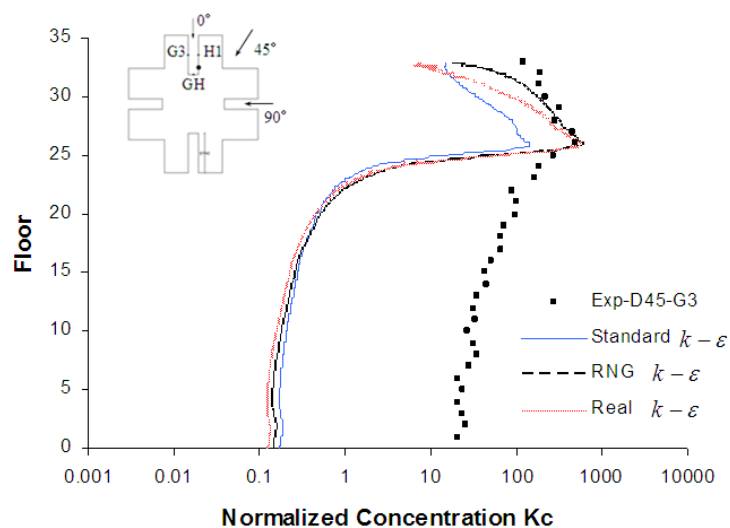
lower part of the building obviously increased, revealing a mixing effect due to the upwind vortex generated in front of the building in that region. However, compared with experimental data at point G3, similar concentration levels from the numerical results can be only detected in the vertical adjacent floors (i.e., the 25<sup>th</sup>, the 26<sup>th</sup> and the 27<sup>th</sup> floors), revealing an inadequate performance in predicting the pollutant dispersion in the horizontal direction.

For the predicted concentration level in the upper part of the building, the differences of the simulated results obtained from the three different models are not obvious. However, the downward dispersion is significantly underestimated by both standard and RNG  $k-\varepsilon$  models, and the simulated concentration values in the vertical adjacent lower floors quickly reduced to a negligible level. It appears that the results obtained by realizable  $k-\varepsilon$  model are more close to the measurements, which is approximately no more than seven times of the measurement values in point GH and H1, except at the source floor in point H1. In point H3, from the results computed by realizable  $k-\varepsilon$  model, it is shown that the concentration level rapidly reduced to a significantly low level in the vertical adjacent floor. The upward dispersion at that point can not be correctly simulated by all the three models. However, in the downward direction at that point, the results from realizable  $k-\varepsilon$  model show acceptable agreement with the experimental data.

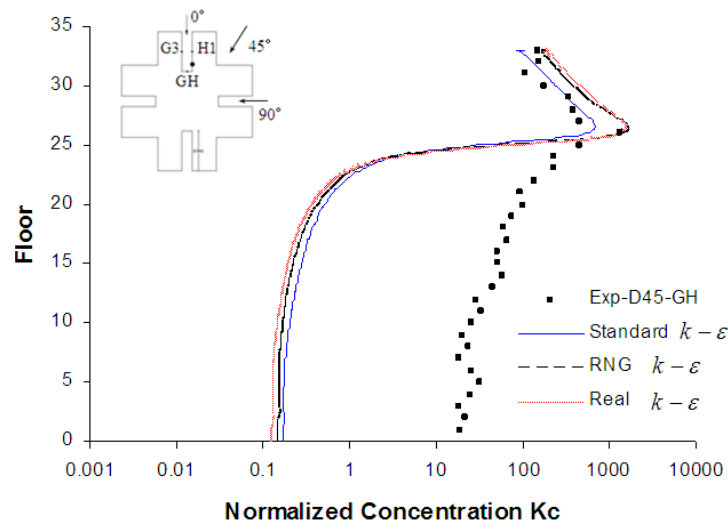
The dispersion characteristics under oblique wind condition ( $\theta = 45^\circ$ ) are also simulated by rotating the building in the domain. The boundary conditions and grid generation style are the same as that used in normal wind direction. Figure 5.16

illustrates the comparisons between CFD results and wind tunnel data under oblique wind direction.

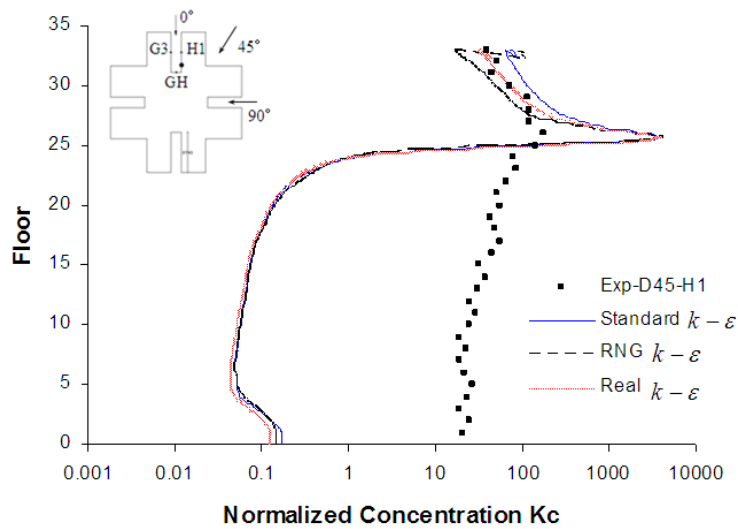
It can be seen from the results that the predicted concentration profiles have the same trend as that of under normal wind condition. In the upper part of the building with a higher concentration level, the predicted results are generally acceptable compared with experimental data, which illustrates the upward vertical dispersion characteristics. However, in the lower part of the building, the concentration profiles predicted by the three different turbulence models have no noticeable difference. The computed normalized concentration values still have over two orders of magnitude differences compared with the experimental data, which presents an unsatisfied performance in predicting downward vertical dispersion under oblique wind condition.



a) Along the building height at point G3



b) Along the building height at point GH



c) Along the building height at point H1

**Figure 5.16 Comparisons of normalized concentration between CFD results with different turbulence models and wind tunnel measurement results ( $\theta = 45^\circ$ , the source was located in the 26<sup>th</sup> floor)**

Based on the direct comparisons about normalized concentration profiles, it is shown that the CFD method with the presented  $k-\varepsilon$  turbulence models can provide

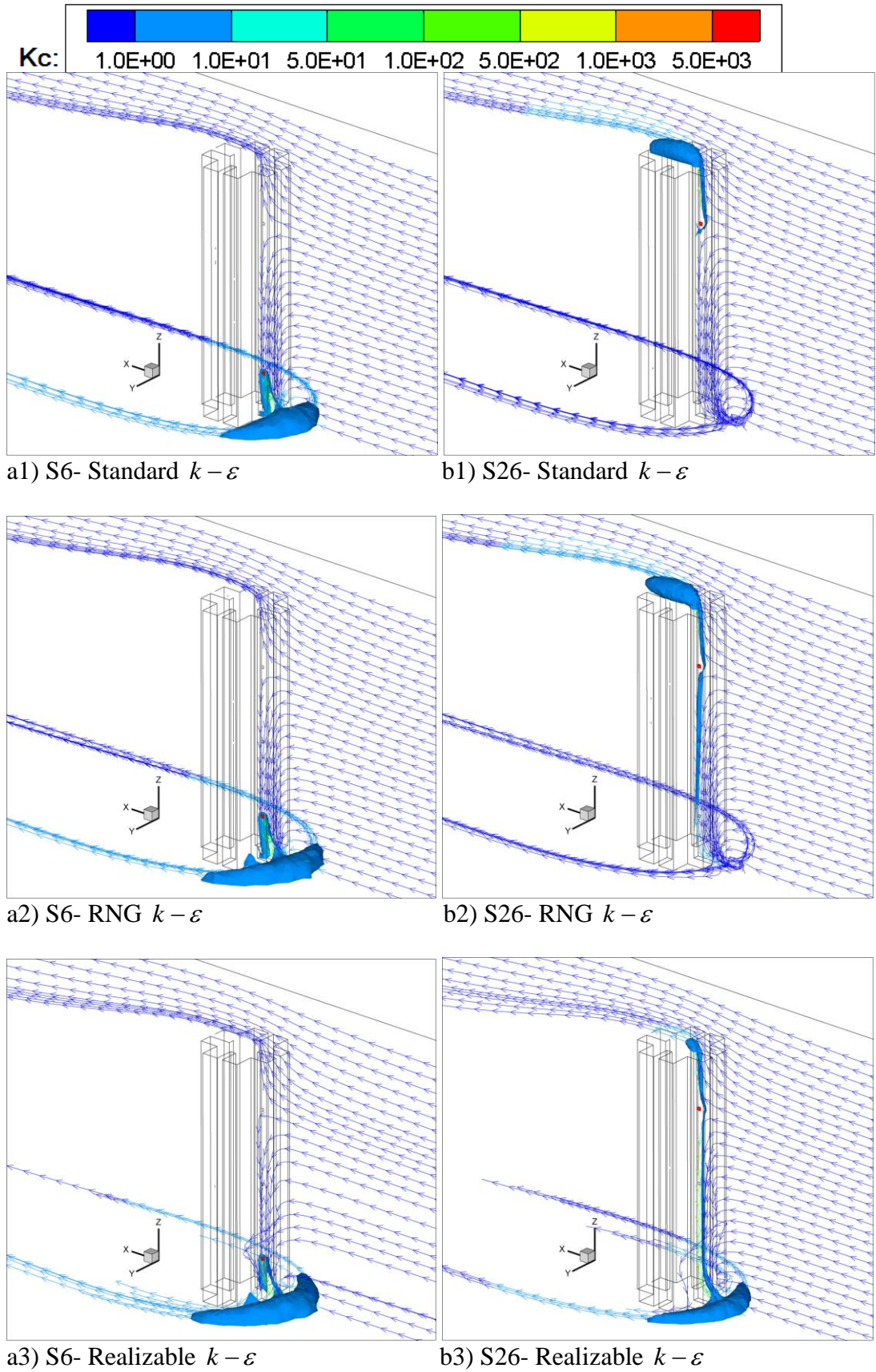
qualitative information about wind-induced cross-contamination. Benefiting from the advantages of CFD method, the detailed dispersion routes predicted by the three  $k-\varepsilon$  turbulence models under different circumstances are presented below. It is helpful to further analyze the differences among the presented  $k-\varepsilon$  models, and gives more direct information on the features of wind-induced cross-contamination.

Figure 5.17 and Figure 5.18 are the time-averaged three-dimensional (3D) streamtraces colored by the normalized concentration magnitude with various initial locations. An iso-surface where the computed concentration values equal to 1/1000 of the source strength is also presented in the figures. Total 12 cases are presented here, with different source locations under both normal and oblique wind conditions. Both the 3D streamlines colored by  $K_c$  values and the iso-surface are useful in visualizing the predicted dispersion route under wind effect.

Firstly, the streamlines illustrate the airflow pattern under different wind directions, as was introduced in the last section. Also, these colored 3D streamlines clearly show how the tracer gas travels with the ambient airflow after it was released from the source. Under normal wind direction, when the source was located in the lower part of the building, the tracer gas moves downward within the re-entrant space, accumulated in the lower part of windward areas. Then it goes around the building at the junction of the building and the ground, and moves toward the wake region. When the source was located in the upper part of the building, pollutant can be found in both vertical sides. Under oblique wind direction, it can be seen that part of the airflow passes over the opening of the re-entrant space around one side of the

building, while some of the approaching wind enters into the re-entrant space. Secondly, the regions where the computed concentration values lower than 1/1000 of the source concentration can be considered as “insignificant”. The 3D iso-surface of 0.1% source concentration indicates the maximum influenced region under wind effect. Thus, the possible areas that have the potential risks of cross-contamination can be directly addressed by the predicted results. However, in view of the significantly underestimation of concentration level in the downward direction, as that shown in Figure 5.16, the downward dispersion under oblique wind condition still could not be overlooked.

All the three different  $k-\varepsilon$  models computed similar  $K_c$  profiles under oblique wind direction with different source locations. Under normal wind direction, when the source was located in the upper part of the building, the dispersion in both vertical directions can be observed from the predicted results by the standard  $k-\varepsilon$  model. The results obtained by RNG  $k-\varepsilon$  model clearly revealed the upward dispersion, while the results from realizable  $k-\varepsilon$  model emphasize the downward dispersion.



**Figure 5.17 Streamlines colored by  $K_c$  values and the iso-surface under normal wind direction: a) Source at the 6<sup>th</sup> floor; b) Source at the 26<sup>th</sup> floor**

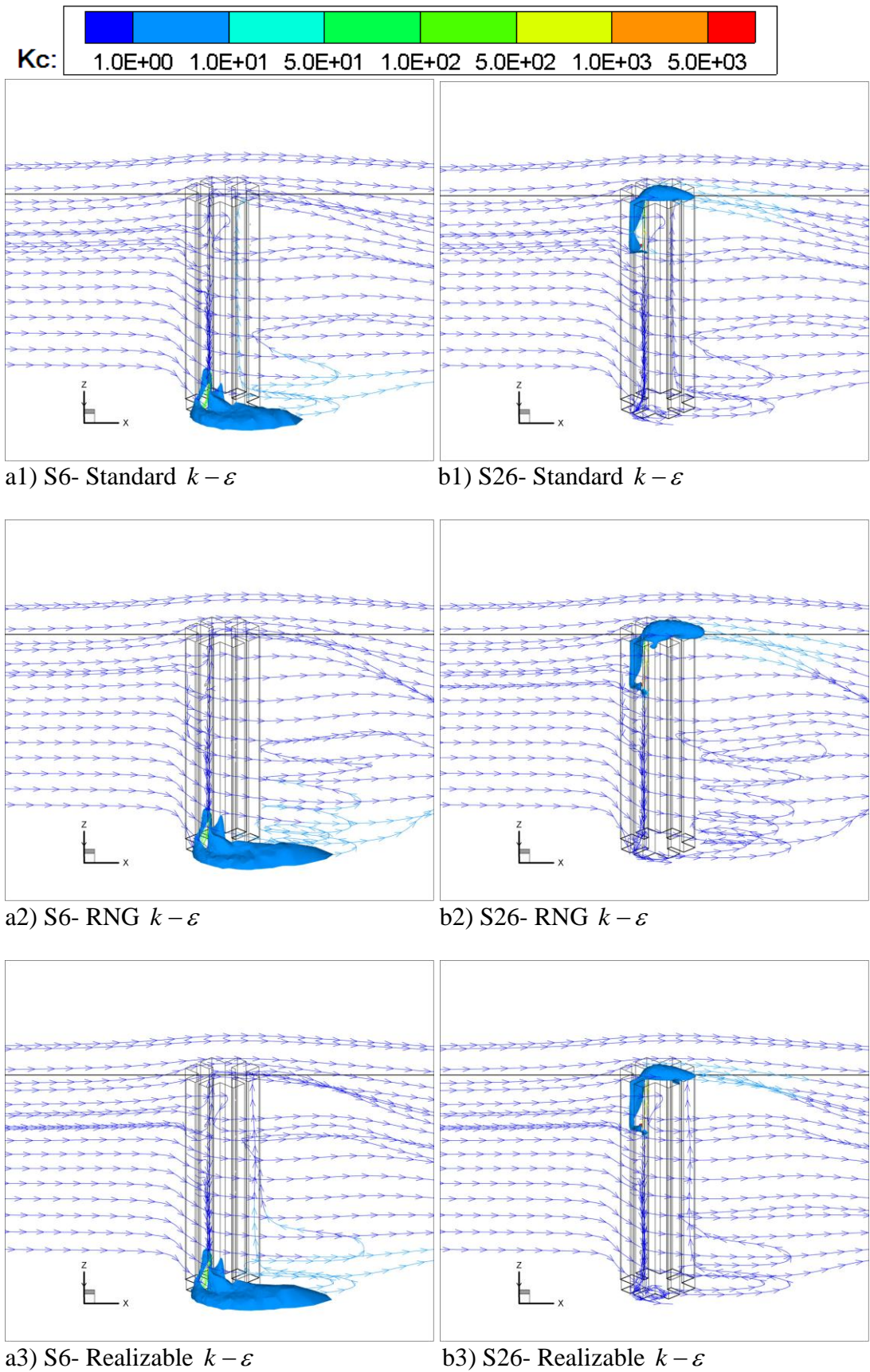


**Figure 5.18 Streamlines colored by  $K_c$  values and the iso-surface under oblique wind direction: a) Source at the 6<sup>th</sup> floor; b) Source at the 26<sup>th</sup> floor**

#### 5.4.4 Further Discussions

RANS turbulence models have been employed to simulate the cross-contamination around a HRR building with a complex geometry. The reliability of numerical results was analyzed here step by step. It was shown that the predicted pressure distributions were generally acceptable, when compared with the wind tunnel measurements. With regard to tracer gas concentration prediction, the main observation from all the cases is that the numerical simulations basically illustrate the dispersion characteristics under approaching wind effect. The simulated concentration levels are within a factor of seven times of the wind tunnel data under normal wind direction, while two orders of magnitude discrepancies under oblique wind direction could be found through the comparisons between simulated concentration level and experimental data. It can be concluded that, for the cross-contamination study around such a building with complex building shape, CFD method with the three  $k-\varepsilon$  turbulence models can only be used for qualitative research.

For the flow field and dispersion process under normal wind condition, the realizable  $k-\varepsilon$  model showed the closest agreement with the experimental data. For oblique wind direction, the computed results from all the three models are generally similar. Considering about the severe underestimation of the concentration level by all the models in the downward direction, it is hard to judge which model is better. In view of the unsatisfactory performance in predicting wind-induced cross-contamination, CFD methods with the presented  $k-\varepsilon$  turbulence models are not recommended for further and detailed studies.

## 5.5 Summary

The wind tunnel experimental results presented in this chapter provide fundamental information on the flow and dispersion field associated with various arrangements of incoming wind directions and source locations. It can be found that the characteristics of pollutant dispersion around HRR building with cross building shape under wind effect are quite different from that of around slab-shaped building dominated by buoyancy effect. In the mean time, the wind tunnel test data provided in this chapter serves to validate the numerical methods in order to perform detailed investigation on pollutant dispersion around HRR building. The performance of employing CFD simulation method in wind-induced cross-contamination study were discussed and analyzed here.

Analysis of flow and dispersion around complex-shaped building by CFD method is a very difficult task. The complicated interaction between building and boundary layer flow is hard to be simulated by numerical method. As for the target building during this study, which has many sharp edges at their corners, it requires very fine grid discretization to analyze such flow fields with high precision. The accuracy of the numerical approaches has been assessed by the validation efforts made above, through the comparative exercises provided during this study. The effectiveness of the turbulence models and numerical treatments for solving the presented problem were investigated in detail.

In general, it is encouraging to obtain results comparable with the wind-tunnel measurements by CFD method. It is concluded that the basic features in both flow

and concentration fields can be well reproduced by the predicted results. However, it should be noticed that obvious discrepancies were found during the comparisons between numerical results and experimental data. Further improvements are needed for CFD applications in wind engineering and pollutant dispersion around such complex building, including grid generation strategies for complex solution domain, more reliable turbulence models, more accurate and realistic boundary conditions and the application of higher order of numerical schemes for space and time discretization, etc. At present, a wind tunnel test with careful design and considerations that can provide high resolution experimental results is still indispensable for wind-induced cross-contamination studies.

## **Chapter 6**

# **Experimental Study on Large Scale Building Model with Openable Windows**

### **6.1 Introduction**

In Chapter 5, the basic characteristics of wind-induced cross-contamination around a 30-story sealed building were presented. The performance of using CFD techniques to predict wind effects on the pollutant dispersion around complex-shaped building was evaluated and discussed. It was found that CFD method is capable of revealing basic features of such problem, while large differences still exist during the comparisons between prediction results and experimental data.

In order to further investigate the wind effect on the pollutant dispersion around a typical HRR building with building shape II, another series of experiments were designed and performed in the low-speed section of CLP Power Wind/Wave Tunnel. This stage of experiment was conducted under model B with larger geometry scale that can allow greater spatial resolution of concentration data. The wind-induced pressure and contaminant concentration distributions were used in complements for evaluating the possibility of discharged indoor air pollutants re-entering adjacent indoor environments in the same building. The experiments were designed under both open-window and no-window conditions to compare the differences between these two configurations. Mean concentrations and concentration fluctuations at different positions were measured and analyzed to further reveal the air pollutant dispersion mechanisms under wind effect.

## 6.2 Experiment Setup

A 1:30 model was constructed for this stage of experiment, and the blockage ratio in the wind tunnel is controlled at approximately 5%. The model represents a 10 stories HRR building of 30m height in prototype. Figure 6.1 is the photo of the experiment configuration.



**Figure 6.1 The photo of the experiment configuration.**

### 6.2.1 Concentration Measurement Setup

Total 24 cases were conducted for the concentration measurement. Firstly, under closed-window condition, as summarized in Table 6.1, 6.2, a series of testing cases were designed with different source positions and upcoming wind directions. The

wind direction was represented by  $\theta$ , defined as the angle between the wind direction and the symmetry axis Y of the building plan, as shown in Figure 6.2. Our experiment design was planned to investigate the features of air pollutant dispersion under both normal and oblique wind directions. The situations under the prevailing wind direction,  $\theta = 0^\circ$ , were studied in detail by examining both the concentration and pressure distributions, and the concentration profiles under other wind directions ( $\theta = 45^\circ, \theta = 90^\circ$ ) were also presented for the comparison of pollutant transport process under different wind directions, in view of the non-symmetry geometry of the building. The tracer gas concentration profiles can reveal pollutant transmission route under wind effect, while the potential ventilation and possible airflow pattern could be evaluated by examining pressure coefficient distribution.

**Table 6.1 The configuration of each case under prevailing wind condition  
(Closed-Window)**

Case No.	E1	E2	E3	E4	E5	E6
Source	3 <sup>rd</sup>	3 <sup>rd</sup>	6 <sup>th</sup>	6 <sup>th</sup>	9 <sup>th</sup>	9 <sup>th</sup>
Location	Floor	Floor	Floor	Floor	Floor	Floor
Orientation	Wind-ward	Lee-ward	Wind-ward	Lee-ward	Wind-ward	Lee-ward
Measurement Points	P1 to P4	P5 to P8	P1 to P4	P5 to P8	P1 to P4	P5 to P8

**Table 6.2 The configuration of each case under other wind conditions (Closed-Window)**

Case No.	E7	E8	E9	E10	E11	E12
Source Location	3rd Floor	6th Floor	9th Floor	3rd Floor	6th Floor	9th Floor
Orientation	90°	90°	90°	45°	45°	45°
Measurement Points	P1 to P4					

Secondly, all the experimental cases were repeated under open-window conditions. In the building model, 4 of 8 units in each floor have been designed to have openable windows with effective open area equal to 50% of the real window size. According to the relevant building regulations in Hong Kong (CAP 123F) (Anonymous, 1997), the window's area should be at least equal to 1/16<sup>th</sup> of the floor area of the room for the purpose of natural ventilation. Also, in Chinese Standard (Residential Building Code) (GB50368-2005, 2005), it is said that for each dwelling, the window's area should be no less than 1/20<sup>th</sup> of the floor area of the dwelling. Therefore, the window-to-floor area ratio for the present model is controlled at approximately 7.4%. The window's location and its size are shown in Figure 6.5, while the height of all the windows is 900mm (in prototype).

The tracer gas used is air with a 99000ppm propane concentration. The tracer gas was released through a flow-meter at a constant flow rate of 58.5ml/s, and this flow rate was low enough to ensure that source momentum effects were not significant. At each wind direction, the tracer gas was released at three different floors in one of the re-entrant spaces, respectively at the 3<sup>rd</sup> floor, the 6<sup>th</sup> floor and the 9<sup>th</sup> floor on façade A1-A2, at a point representing the normal position of toilet exhaust air, and the

nozzle exit was flush with the building surface. The concentration measurements were taken at four points each floor on the same side where the source was active at one of the three floors. The four locations at each floor height represent where windows are usually located. The detailed arrangement of measurement locations is shown in both Figure 6.2 and Figure 6.3. At each measurement position, sample air was collected over a period of 120s at a data-acquisition rate of 150 Hz to avoid aliasing errors (the Nyquist criterion). This sampling time of concentration measurements was also suggested by Mfula et al. (2003). The measurements correspond to full-scale concentrations obtained over a 1hr period.

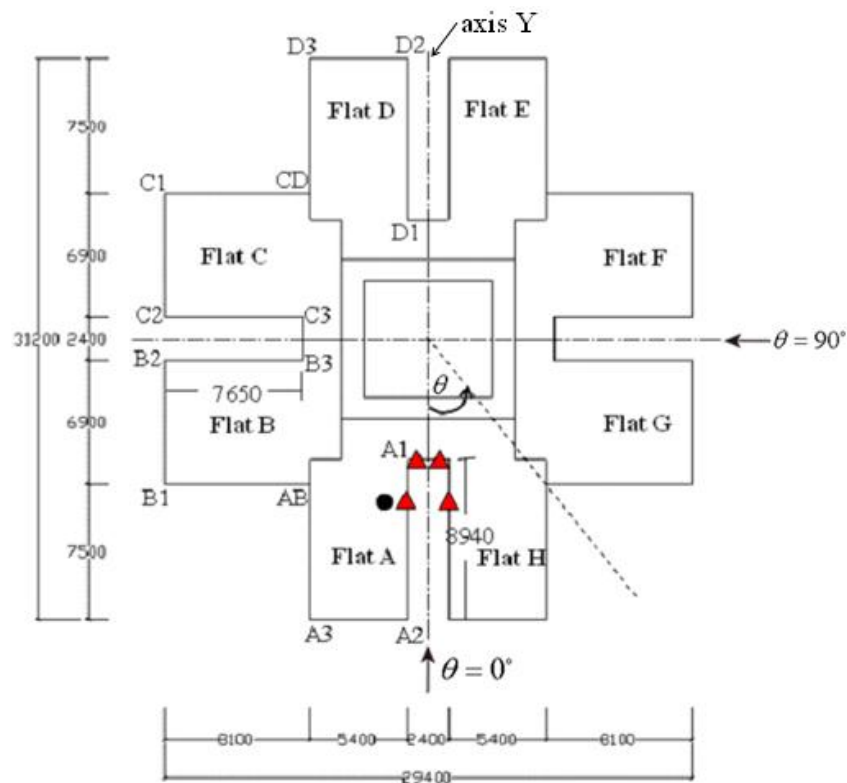


**Figure 6.2 Plan view of the experiment model**

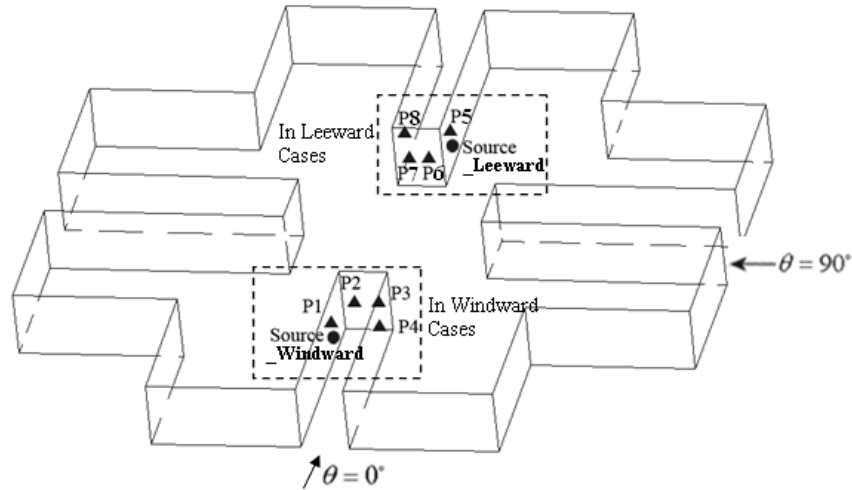


**Figure 6.3 Detailed positions of tracer gas concentration measurement points and source location in one single floor.**

### 6.2.2 Quality Assurance of Statistical Results

For statistical analysis of the concentration data, Aubrun and Leitl (2004) have evaluated the influence of the averaging time on the statistical results through the comparisons between wind tunnel experimental data and field measurement results. A dimensionless averaging time  $T_a^* = T_a / (L_{ref} / U_{ref})$  was used, where  $T_a$  is the absolute averaging time,  $L_{ref}$  and  $U_{ref}$  are the reference length and wind velocity, respectively. Compared to fully converged statistical results ( $T_a^* = 36000$ ), it was found that when the averaging time satisfied  $200 < T_a^* < 400$ , the experimental relative error for statistical results was acceptable. With regard to the present experiment, the  $T_a^*$  calculated based on 120s averaging time is approximately 390, which falls in that range.

To further check the reliability of the results, a beforehand analysis was performed to estimate of the minimum sampling time from specific tests. The minimum averaging time to reach a converged (i.e. representative) standard deviation is roughly 60s and 90s in selected key measurement points under close and open window conditions, respectively, as shown in Figure 6.4. The abbreviation “D”, “S”, “F” and “P” represent the wind incident angle, source location, measurement floor and measurement point, respectively. Therefore, 120s sampling/averaging time additionally ensured an acceptable repeatability in the fluctuation results.

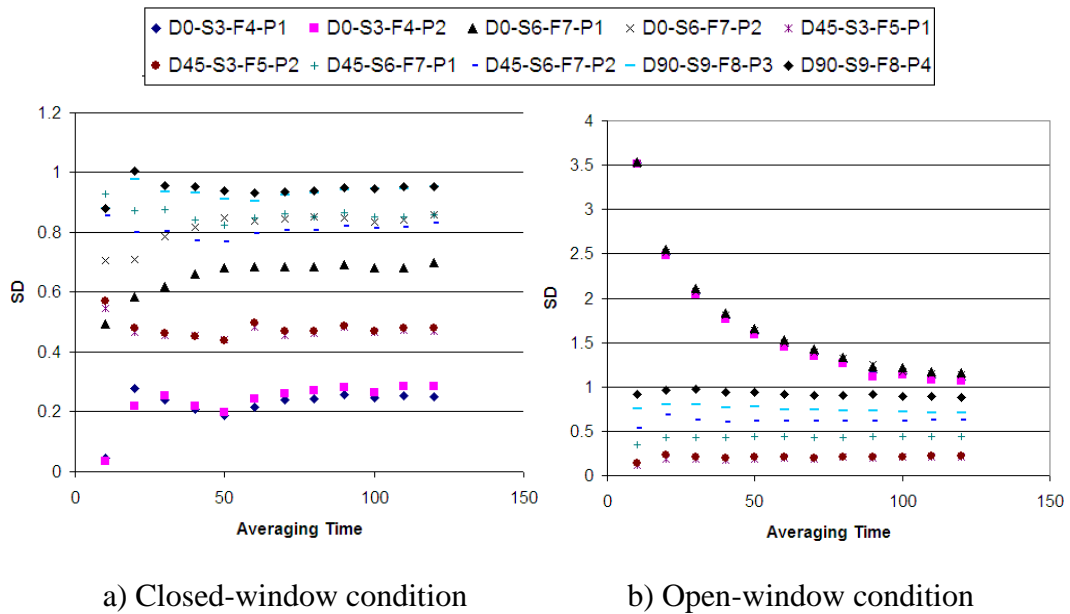


**Figure 6.4 Standard deviation versus averaging time**

### 6.2.3 Pressure Measurement Setup

Surface pressures were measured simultaneously by 230 pressure taps under closed-window condition. The pressure measurement points were arranged along the exteriors of two units of the building, as shown in Figure 6.5, thus the pressure



**Figure 6.5 Pressure Measurement Points and Window's Locations**

### 6.2.4 Simulated Wind Profile in Low Speed Wind Tunnel

In this study, the approach velocity measured in the wind tunnel at building height (1m at model scale) was 3.27m/s, so that the building Reynolds number exceeds the value of 15000 to ensure that the measurement results were independent of Reynolds number. The designed and measured mean velocity and turbulence intensity profile are shown in Figure 6.6.

The normalized mean concentrations less than  $10^0$  are approximately lower by over two orders of magnitude than the highest mean concentrations detected in the experiments, which could be considered as “insignificant” compared with other floors. Besides, the results higher than  $10^0$  have a higher accuracy and confidence based on the calibration process and error analysis. Therefore, the following analysis is mainly focused on the floors and situations in which the non-dimensional concentration is higher than  $10^0$ .

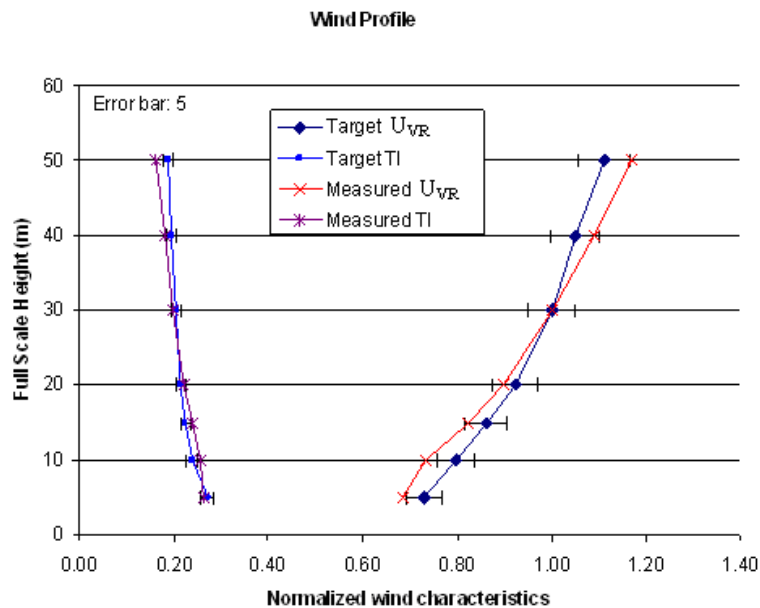
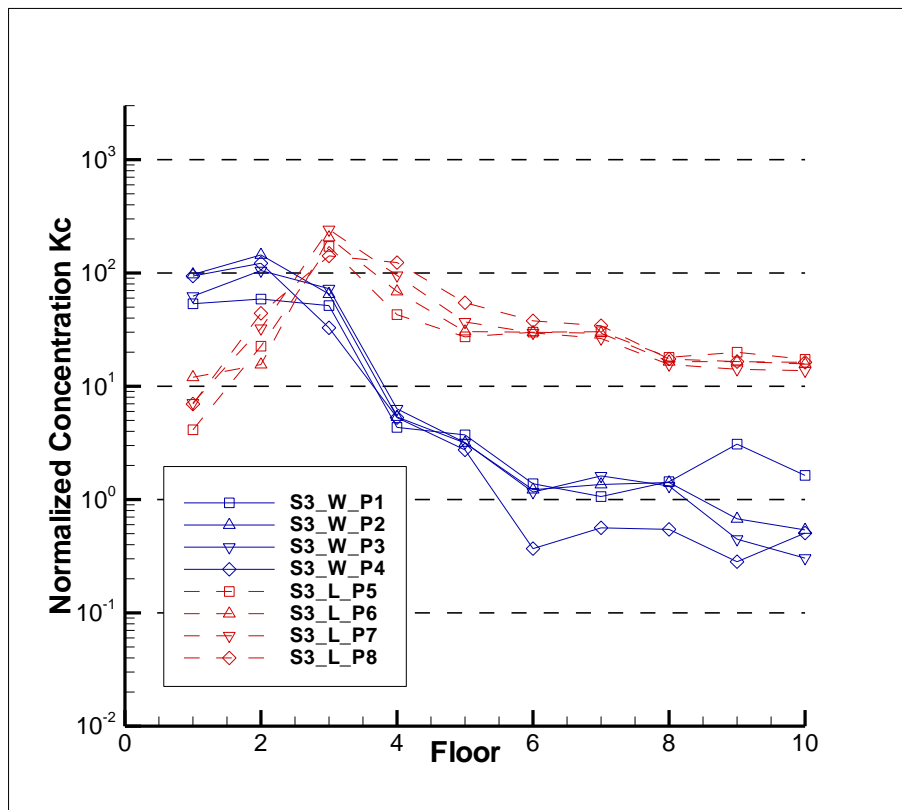


**Figure 6.6 Normalized wind profile of the approaching wind.**

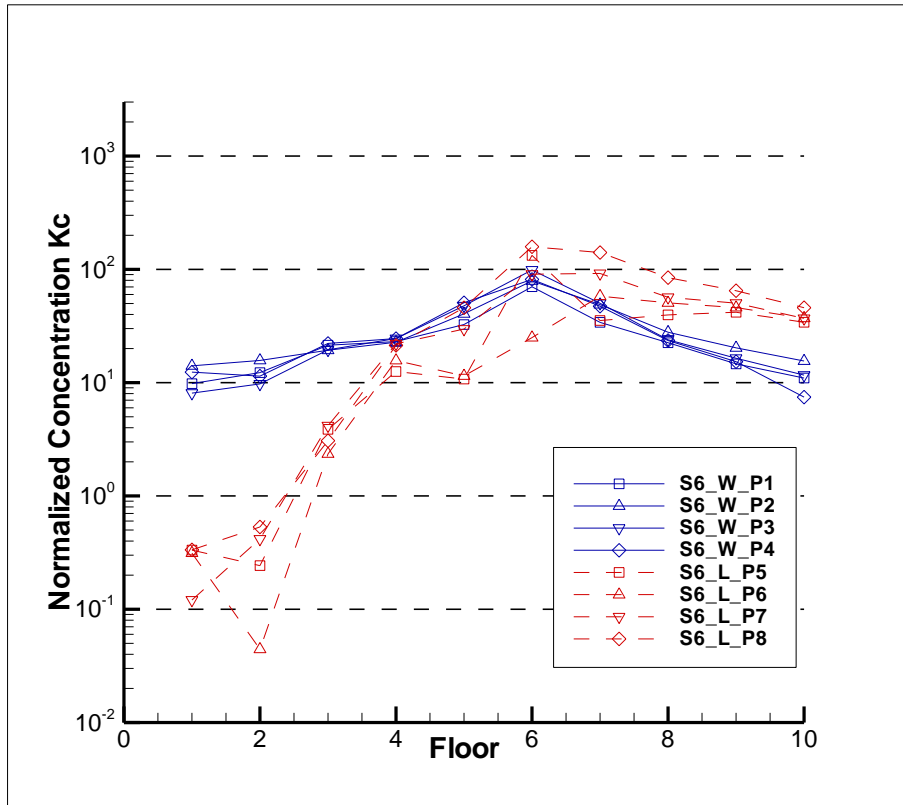
### 6.3 Mean Pressure Distribution and Mean Concentration Profile

#### 6.3.1 Results under Prevailing Wind Direction with Closed-window

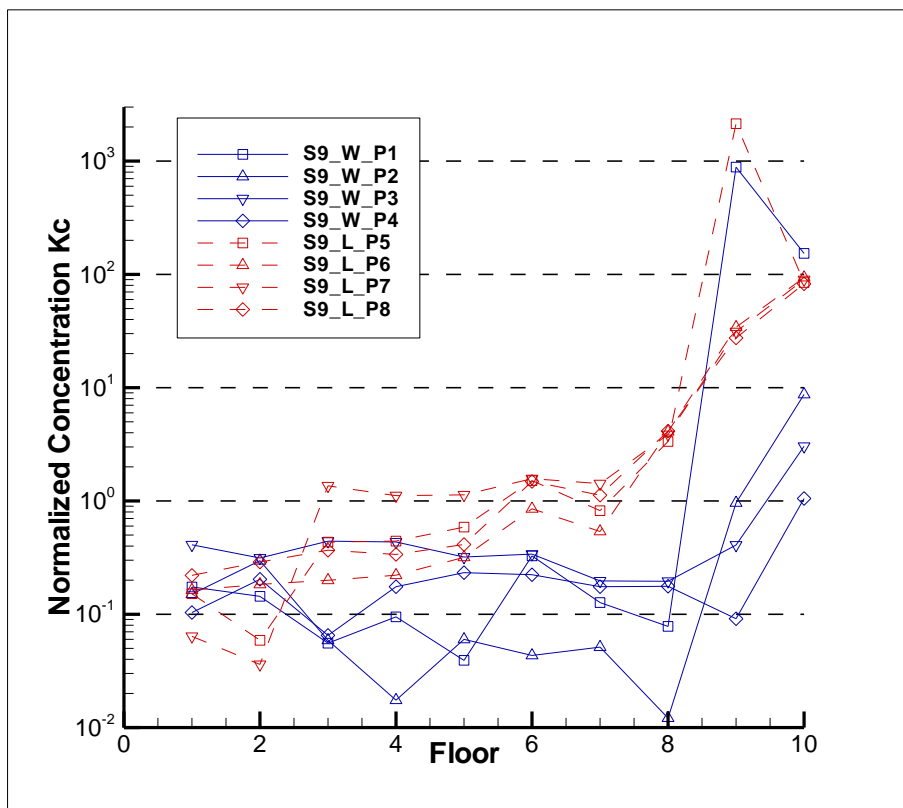
The situation under the prevailing wind condition was particularly studied in the present work, with the normalized concentration distributions in the two re-entrant spaces, respectively windward and leeward, closely examined.



a)



b)



c)

**Figure 6.7 Normalized concentration distributions within the windward (W) and leeward (L) re-entrant spaces under prevailing wind condition with closed-window, when tracer released at a) the 3<sup>rd</sup> floor; b) the 6<sup>th</sup> floor; c) the 9<sup>th</sup> floor. (The abbreviation “S\_W” and “S\_L” represent if the source located windward or leeward was active, respectively.)**

Figure 6.7 shows the normalized concentration at each floor under one prevailing wind direction when the tracer gas was released at three different floors. The tracer gas concentrations were found to be variable with the positions of each measurement points on the test building surface, indicating the pollutant dispersion route within the re-entrant space under wind effects. The highest values mostly appeared at the floors where the tracer was released, and the concentrations at other floors generally decreased with distance from the source floor at both vertical directions. But the highest concentrations were found at the 10<sup>th</sup> floor when the tracer was released at the 9<sup>th</sup> floor (Figure 6.7c). Besides, the tracer gas was also detected in the points which located in other facades besides A1-A2, demonstrating that dispersion also happened in horizontal direction due to wind effect.

In Figure 6.7a, when the tracer source was located in the 3<sup>rd</sup> floor, a rapid decay occurred in the upward direction in the windward case, while in the leeward case, the rapid decay occurred in the downward direction. It was observed that the concentrations in the floors lower than the source floor were almost equal to that in the source floor in Case E1, but those above the source 3<sup>rd</sup> floor decreased rapidly. In the adjacent upper floor, the concentration decreased almost by one order of magnitude compared with the source floor. This implies that the tracer gas is more

likely to be transported to the lower floors when the re-entrant space was facing to the coming wind. In Case E2, it was revealed that the tracer gas concentration descended slowly above the source floor, and remarkable concentrations were obviously detected in the upper floors. The results show that the tracer gas has a trend to move upward in the leeward condition, leading to a higher risk of being contaminated in the upper floors. Figure 6.7b shows the result obtained when the source was located at the 6<sup>th</sup> floor. It was found that the concentration distributions in the vertical direction were basically symmetrical from the source floor in Case E3, and the concentration values decreased smoothly with the distance from source floor. It suggested that the contamination may spread similarly in both vertical directions when it was released in the middle part a windward re-entrant space of a 10-story building. However, under leeward condition, the concentrations measured in the upper floors were relatively higher than that in the lower floors. It was evidently clear that only small part of the tracer gas was transmitted to lower part of the building, while most of it was carried upward to the higher floors. Figure 6.7c illustrates the concentration distribution when the source was located in the top floors of the building, the 9<sup>th</sup> floor. Apparently low concentrations were monitored at all the measurement points below the source floor in both windward and leeward configurations. Even for the adjacent lower floor, it was shown that the concentrations measured at different facades significantly decreased to a negligible level. However, it should be noticed that relatively high concentrations were detected in the adjacent upper floor except in the source facade A1-A2.

In general, overall higher pollutant concentrations were found in the leeward side than in the windward side. Tracer gas released at the middle floors tended to generate

an overall higher concentration in the re-entrant space in both leeward and windward conditions.

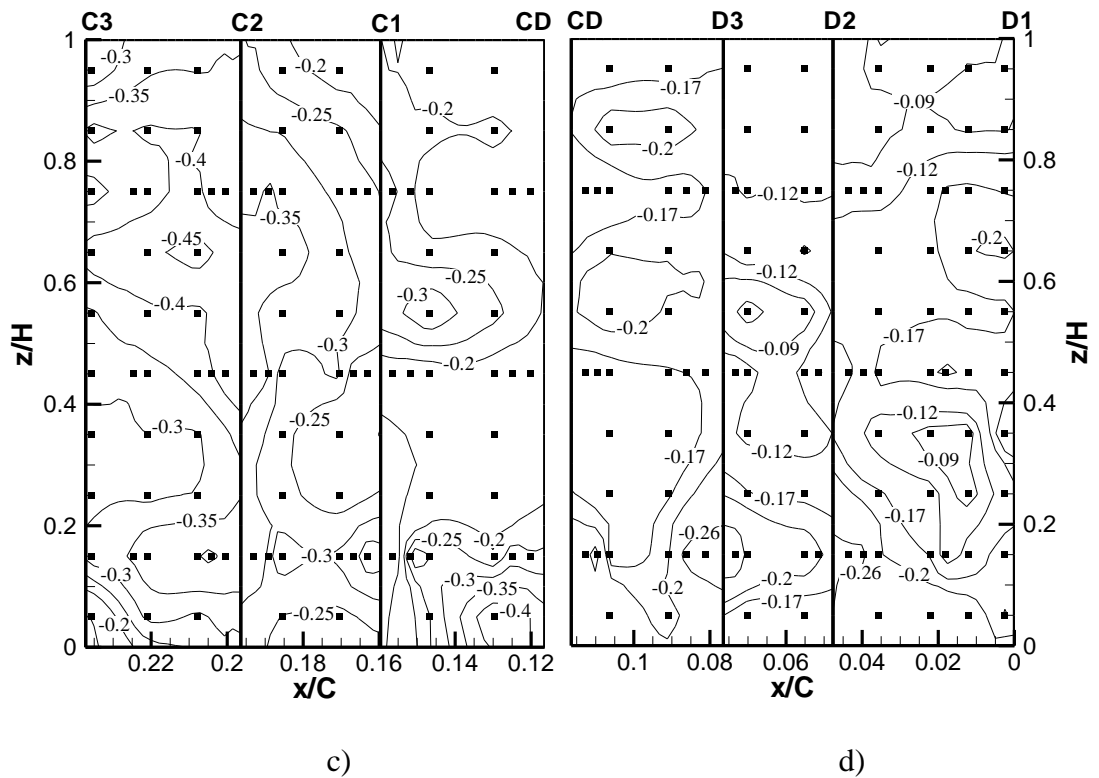
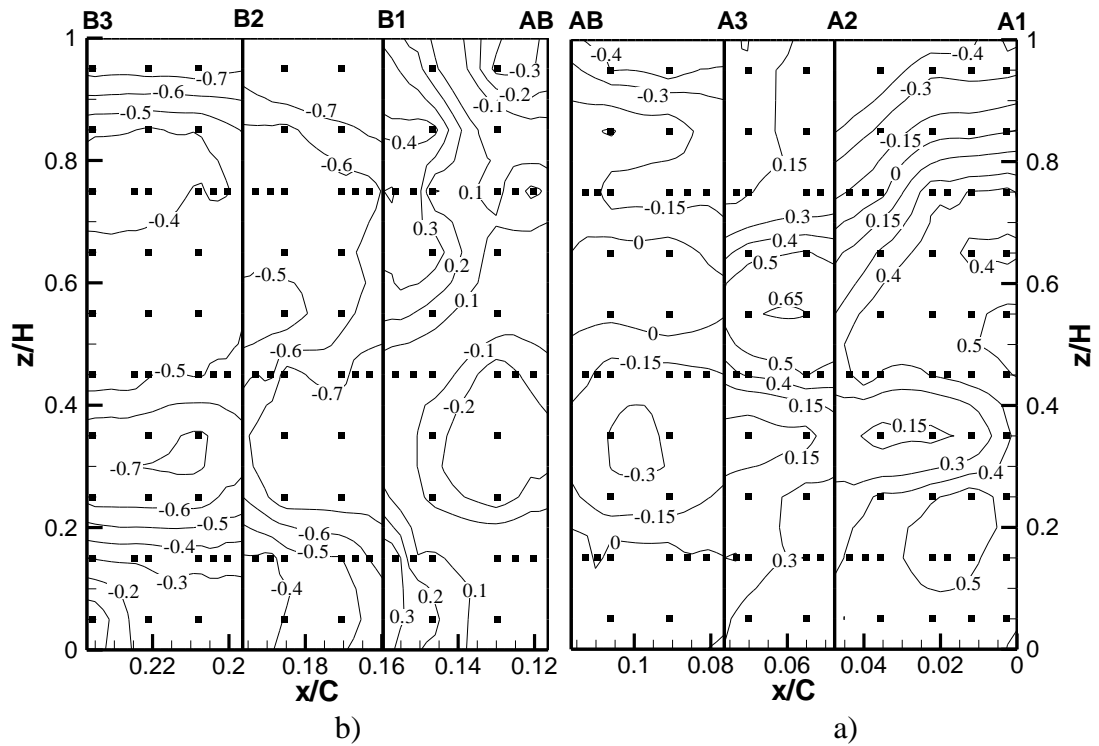


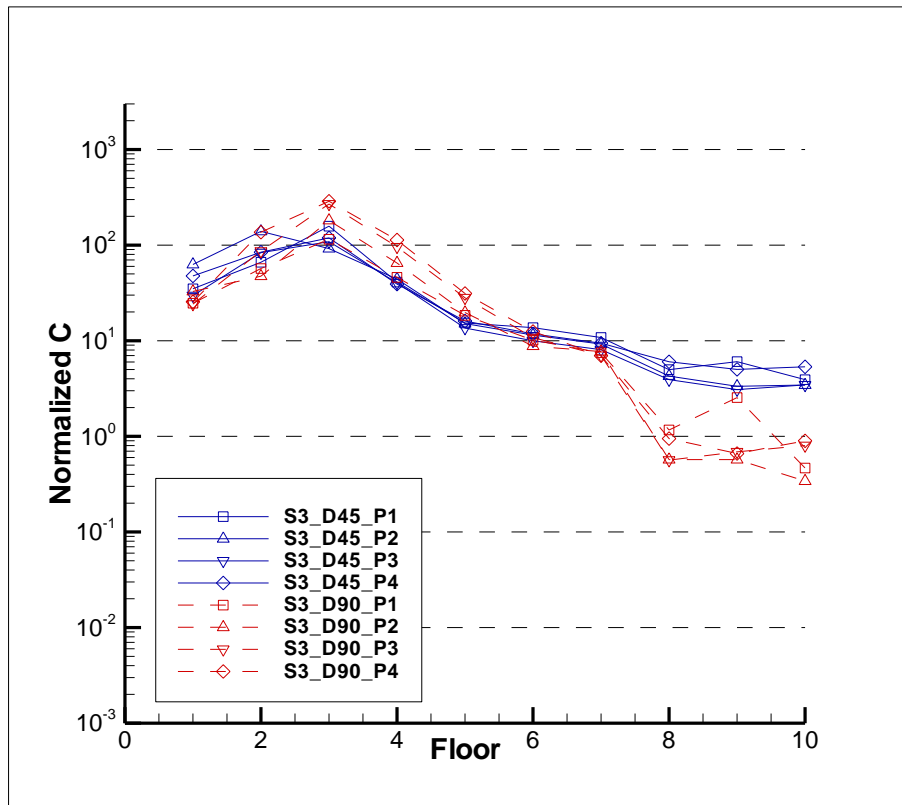
**Figure 6.8 Contour lines of the mean pressure coefficient on the building envelopes of different flats under prevailing wind direction ( $\theta = 0^\circ$ ): a) Flat A; b) Flat B; c) Flat C; d) Flat D. (The black points “■” shown in the figure are original measurement points)**

The mean pressure coefficient distributions along different building façades under the prevailing wind direction are shown in Figure 6.8. The measured pressure coefficients obtained by wind tunnel method could also be used to reveal the air flow pattern around the building. The X coordinate is the horizontal distance from point A1 (in Figure 6.8a, 6.8b) or D1 (in Figure 6.8c, 6.8d), normalized by the building perimeter (C), while the Y coordinate is the vertical distance normalized by the building height. This figure shows only half part of the whole building with 4 units due to the symmetric feature. The pressure coefficients along the exteriors of each unit are presented in contour lines, which were generated from the measurement point data. The black points (■) shown in the figures are the original measurement points. They were distributed in 10 rows, with each row located in the middle height of each floor. Apparently, the pressure distributions are quite complicated due to the interaction between the wind and the complex building shape. The distribution along each facade was different due to their particular orientations. Positive  $C_p$  values were found in the windward wall, along façade A2-A3 with a peak value up to 0.7 presented at the 6<sup>th</sup> floor, as shown in Figure 6.8b. In most of the other façades  $C_p$  values were generally negative, while in façade A1-A2, A3-AB and AB-B1,  $C_p$  values varied from positive to negative. From the results the peak negative  $C_p$  value

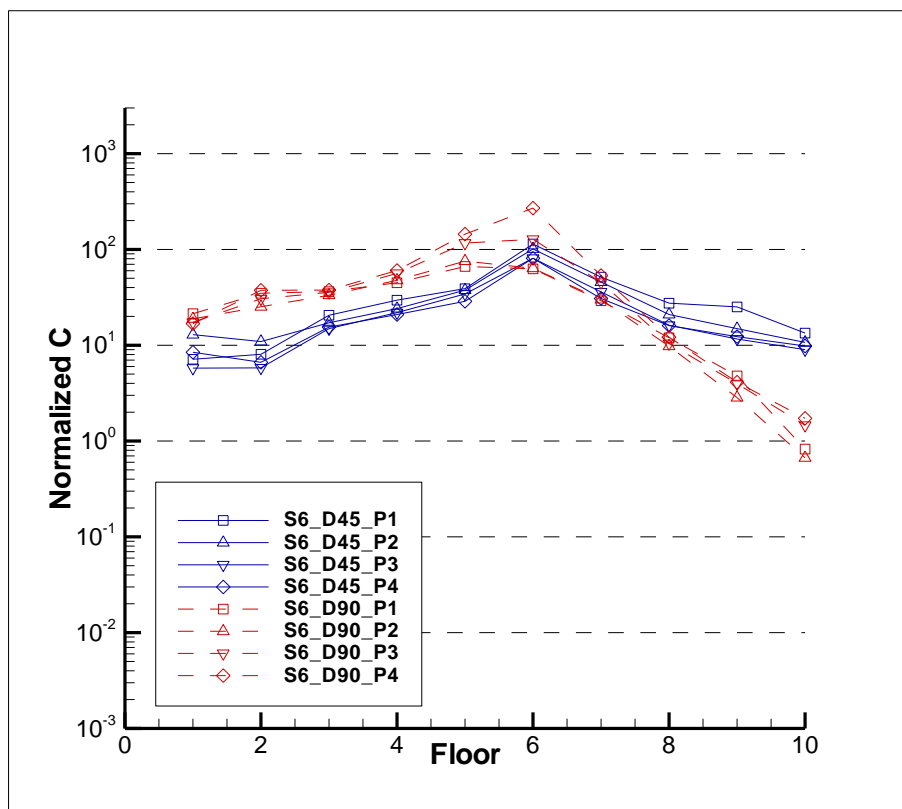
is found at façade B1-B2, probably caused by the effect of separation flow occurring over the leading edge B1.

Furthermore, the pressure distributions presented here play important roles in the following two aspects. a). It could be used to examine the pollutant dispersion route from another point of view. The likely surface flow directions along different façades, which are strongly related to the concentration fields, could be revealed from the pressure distributions on each surface. For façades A1-A2 and D1-D2, each of them is one of the external walls that form the re-entrant spaces in windward and leeward directions, respectively. As shown in Figure 6.8b, the  $C_p$  values decreased from A1 to A2, especially in the higher part of the surface, indicating a possible surface flow direction from inside to outside in the re-entrant space. While in façade D1-D2, the pressure difference was relatively small. This probably resulted in the pollutant being more difficult to be carried out of the re-entrant space in the leeward side. Consequently, the concentration level in the leeward was generally higher than that of windward cases, especially in the upper part of the building. b). The pressure difference between adjacent façades indicates the possible window-gap ventilation for each flat. For example, examining the  $C_p$  values at all the envelope surfaces of Flat A, it can be deduced that possible infiltration or cross-ventilation air flow could happen from facade A1-A2 toward A3-AB. Therefore, once pollutant was accumulated in the surface A1-A2, Flat A should be assumed to have the risk of cross-contamination under wind effect.

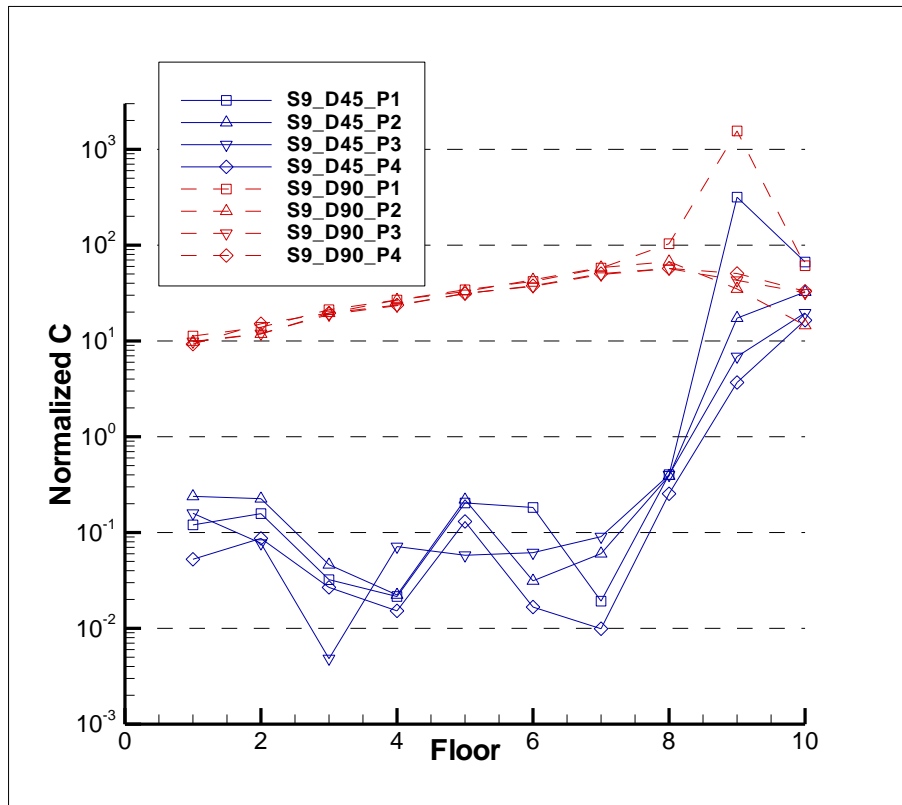
### 6.3.2 Results under Other Wind Directions with Closed-window



a)



b)



c)

**Figure 6.9 Normalized concentration distributions under other wind directions (The abbreviation “D45” and “D90” represent the wind direction is  $\theta = 45^\circ$  or  $\theta = 90^\circ$ , respectively) with closed-window, when tracer released at a) the 3<sup>rd</sup> floor; b) the 6<sup>th</sup> floor; c) the 9<sup>th</sup> floor.**

Figure 6.9 shows the normalized tracer concentration distributions under other approaching wind directions ( $\theta = 45^\circ$ ,  $\theta = 90^\circ$ ), with different source locations. Basically, the concentration values measured under these two wind directions were relatively high, especially when  $\theta = 90^\circ$  and the tracer gas was released at the 9<sup>th</sup> floor, which means the air pollutant exhausted from the index floor would not be easily vented out of the re-entrant space under this sideward condition. As shown in

Fig 6.8a, when the source gas was released at the 3<sup>rd</sup> floor, it can be spread equally in both vertical directions, and the concentration reduced by one order of magnitude after 3 floors in the upward direction. In particular, it should be noticed that when  $\theta = 90^\circ$  and the source was located in the 9<sup>th</sup> floor, the concentration levels detected in other floors were almost of the same magnitude. The decline of concentration was the slowest comparing with the results obtained from other tests during the experiment, which suggested that the most serious cross-contamination would probably happen when the approaching wind incident angle was  $90^\circ$  and the source was located in the top few floors of the building. The concentrations detected at the greatest distance from the source still remained in a high level. Generally speaking, the risk of cross-contamination was relatively high when the wind direction was  $90^\circ$ , which confirmed a similar result reported in a previous CFD study (HKSAR Planning Department, 2005) in the case of a building cluster. It was probably due to the “air curtain” effect caused by the air movement across the opening of the re-entrant space. Air inside the re-entrant space moved quite slow and almost has no exchange with outside. As a result, the air pollutant was difficult to be exhausted.

Furthermore, it can be observed that under oblique wind condition, the concentration profiles were similar to that of windward case when  $\theta = 0^\circ$ . Under oblique wind direction, the upcoming airflow will be first impinging on façade A1-A2, and then flow to the deep side of the re-entrant space restricted by the wall. Due to the complex building shape, such block effect induced by the wall leads to similar consequences when the approaching incident angle was  $\theta = 0^\circ$  and  $\theta = 45^\circ$ . Also, complicated vortex could be generated in the building roof under oblique wind direction. Probably the pollutant exited from higher part of the building could be

easily entrained out from the re-entrant space when  $\theta = 45^\circ$ , while accumulated in the space when the pollutant was originating from lower floors.

### **6.3.3 Further Discussions**

#### **Vertical dispersion**

The effect of pollutant dispersion in the vertical direction could be explained by the wind induced surface flow pattern along the building surface (ASHRAE, 2007). 1). For the re-entrance at the windward, as shown in Fig 6.7a, in the lower part of the building, upwind vortex could be generated and thus the pollutant emitted from the 3<sup>rd</sup> floor could be transported in the downward direction. Moreover, the wind flow comes to the windward wall and rests at the buildings to form a front stagnation region, which resulted in the symmetrical concentration distribution in the vertical direction as illustrated by Fig 6.7b. When the source was located at the 9<sup>th</sup> floor, the wind flow passes the upper part of the building and then most of the tracer gas could be exhausted upward over the building roof, and low concentrations were detected below the source floor, as shown in Fig 6.7c. 2). As to re-entrance at the leeward, all the results indicated that the tracer gas was likely to move upward in the vertical direction near the wall. This is probably contributed by the vertical vortices generated at leeward wall, with flow direction from bottom to top. Mavroidis et al. (2003) also presented similar results in the case of plume dispersion around one simple tall obstacle. The tracer gas released from the source could be entrained and mixed vertically up to the top of the building, which led to higher possibility of being contaminated in the upper floors.

Besides the pollutant transmission direction discussed above, the dilution degree should also be paid attention to. It can be observed from the results that the concentration levels can be of the same magnitude in several floors away from the source. In some particular cases, such as Case E1 and Case E4, the concentration values measured in the immediate vertical adjacent floor could even be equal to the concentration detected in source floor.

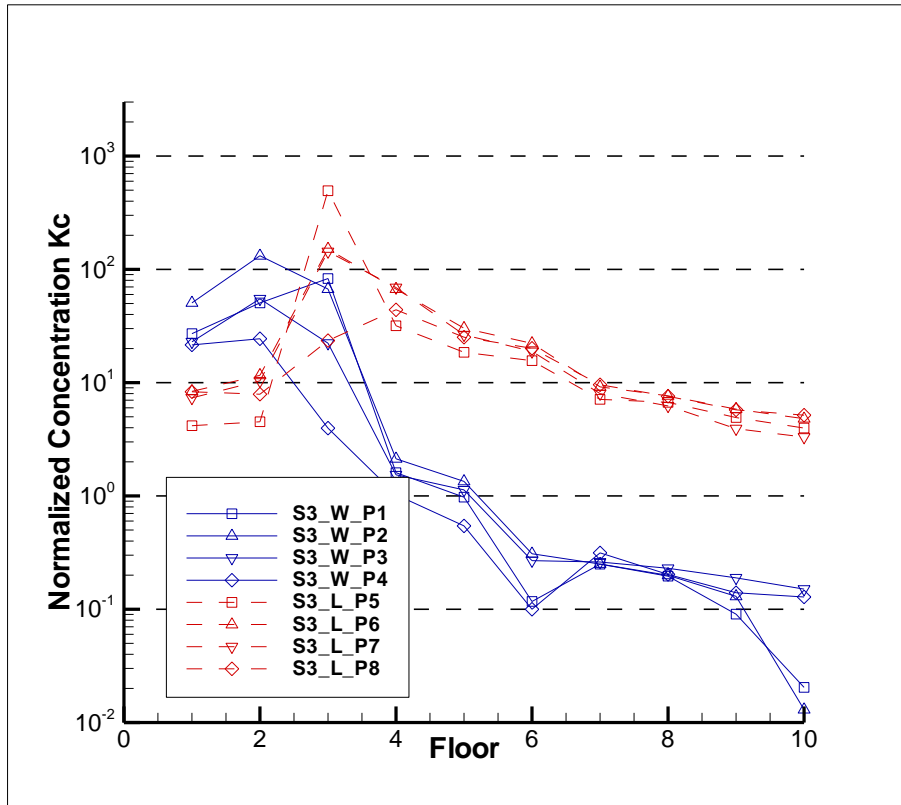
### **Horizontal dispersion**

The concentration distributions along different façades illustrated the horizontal transmission route under wind effect. It can be clearly seen that the tracer gas was not only detected along the source façade, but also along other façades. The concentration values measured at different facades with the same height were generally uniform. As shown in the results of Case E1, Case E3 and Case E9, the concentration values measured in different facades at several floors were almost equal, which means the pollutant could be accumulated along the deep side in the re-entrant space and spread in the horizontal direction. This can be explained by the block effect induced by adjacent walls, the pollutant can not be easily transported out of the re-entrant space in the horizontal direction. Further, through examining the pressure coefficient variations along facade A1-A2, for Flats A&H in the windward side, the direction of airflow would be from the re-entrance depth to the external, i.e., from point A1 to point A2, bringing accumulated pollutants, typically the kitchen exhaust located around point A1 in reality, into the units through any other openings. In particular, the pressure distributions shown in Fig 6.8 also revealed another possible horizontal transmission path under wind effect. By examining the  $C_p$  values at all the envelope surfaces of the two sides of each flat, the possible infiltration

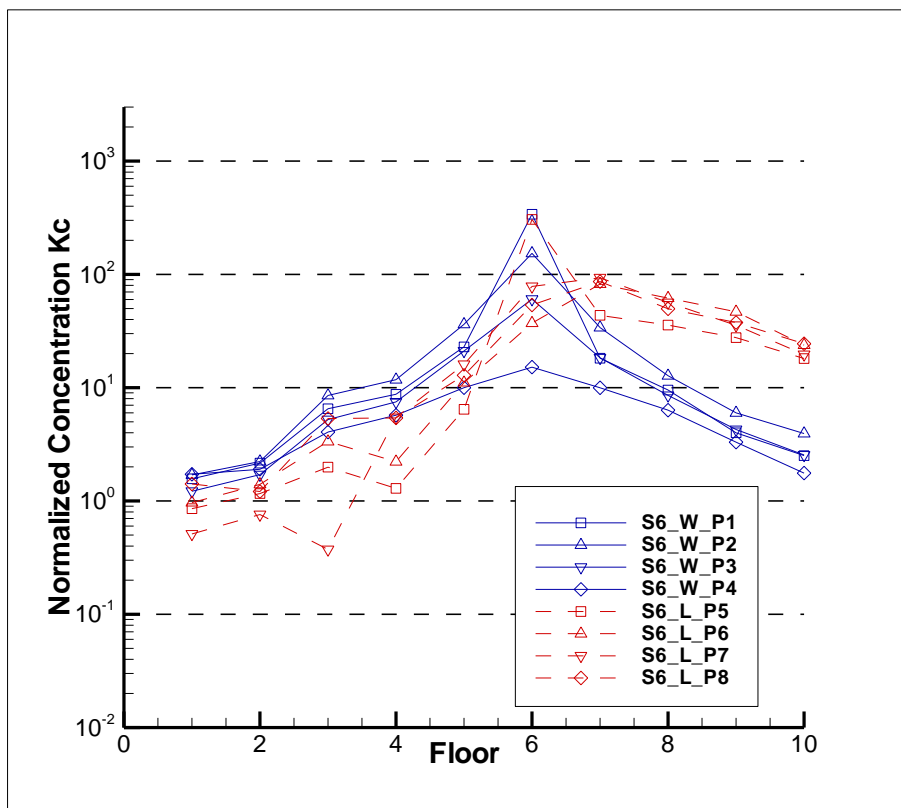
airflow direction could be observed in the horizontal direction. For the residential units Flats D&E in leeward side, the surface pressure differences between facade D1-D2 and CD-D3 are small ( $\Delta C_p = 0.08$ ), indicating relatively low cross-ventilation driving force. On the other hand, the pressure difference would avoid the infiltration of the accumulated air pollutant in the re-entrance into the units. For Flats A&H, it appears that the walls facing re-entrant space have higher pressures, and the pressure differences between facade A1-A2 and A3-AB are generally high ( $\Delta C_p = 0.4$ ), implying the possible infiltration of the air pollutant in the re-entrant space, coupled with the surface flow direction from A1 to A2 as mentioned above. However, since the re-entrance is located windward, it has been observed that pollutant concentration in most of the measurements points is low, except for some points that are located in the deep side of the re-entrance space. Comparatively, Flats B&G have desirable pressure distributions, favor cross-ventilation from B1-AB toward B2-B3 ( $\Delta C_p = 0.7$ ), yet avoiding infiltration from the re-entrant space.

#### **6.3.4 Results under Prevailing Wind Directions with Open-window**

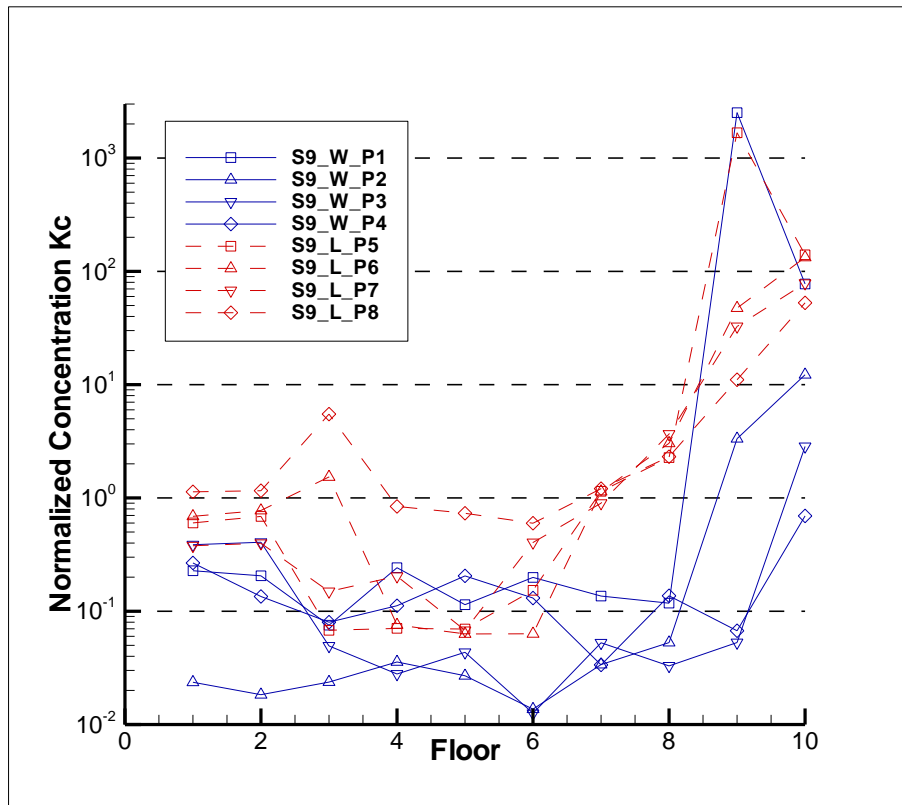
All the cases shown in Table 6.1 and Table 6.2 were repeated under open-window condition to evaluate the effect induced by the residents' behavior of window opening. In this series of experiments, the differences of wind-induced cross-contamination between closed-window and open-window condition were revealed. The concentration measurement locations and method were the same of that under closed-window condition. The mean concentration profiles under the prevailing wind direction are shown in Figure 6.10.



a)



b)



c)

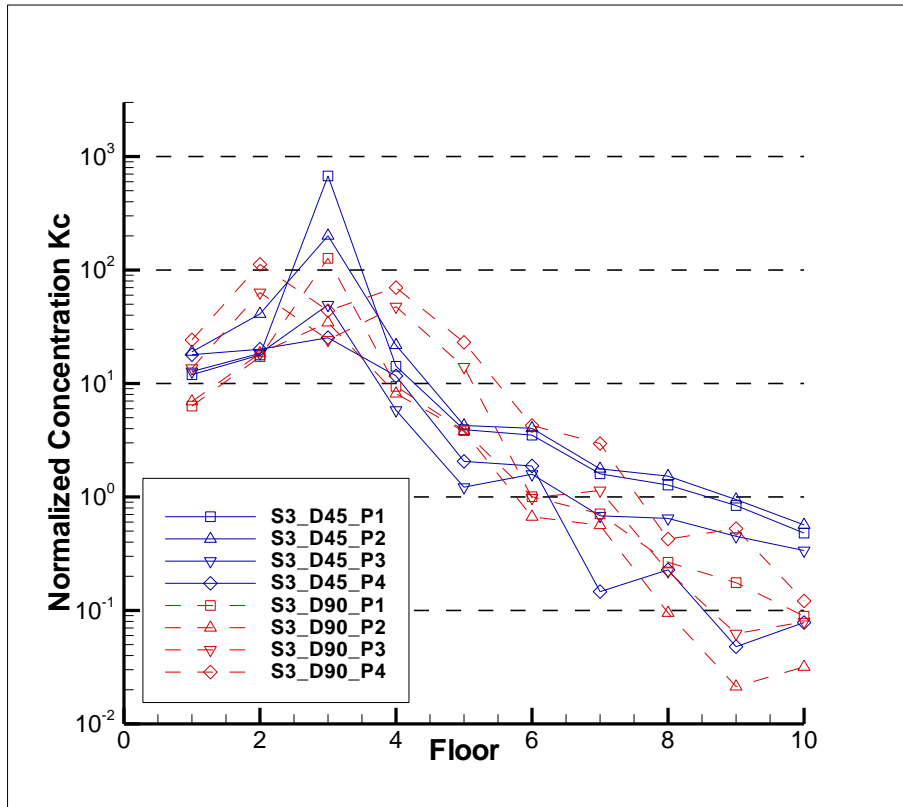
**Figure 6.10 Normalized concentration distributions within the windward (W) and leeward (L) re-entrant spaces under prevailing wind condition with open-window, when tracer released at a) the 3<sup>rd</sup> floor; b) the 6<sup>th</sup> floor; c) the 9<sup>th</sup> floor.**

It can be observed that the pollutant dispersion characteristics within the re-entrant space is similar to that of shown in Figure 6.7, while the concentration level in each measurement point was relatively lower than that of under closed-window condition. The highest concentration still presented in the source floor, and the concentrations at other floors generally decreased with distance from the source floor, both upward and downward, while the concentration level reduced more rapidly than that of shown in Figure 6.7. The largest discrepancy in concentration magnitude was found in case E3, when the source was located in the 6<sup>th</sup> floor, the concentration values obtained in windward re-entrant space under closed-window condition were about 4

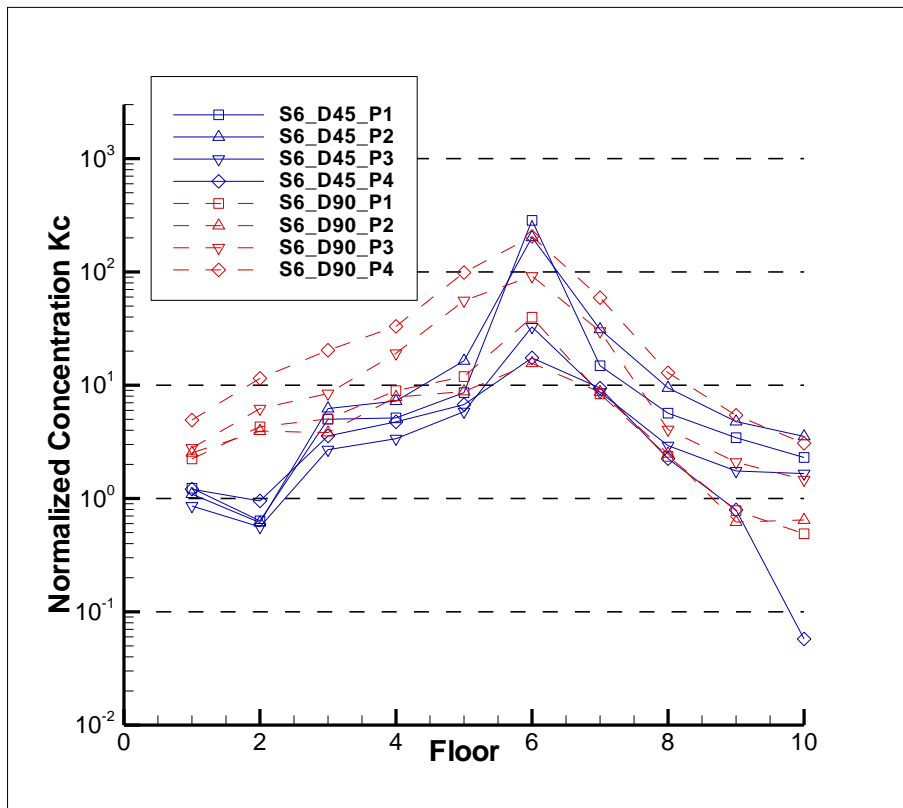
times (averaged from all the measurement points) larger than those obtained under open-window condition.

### 6.3.5 Results under Other Wind Directions with Open-window

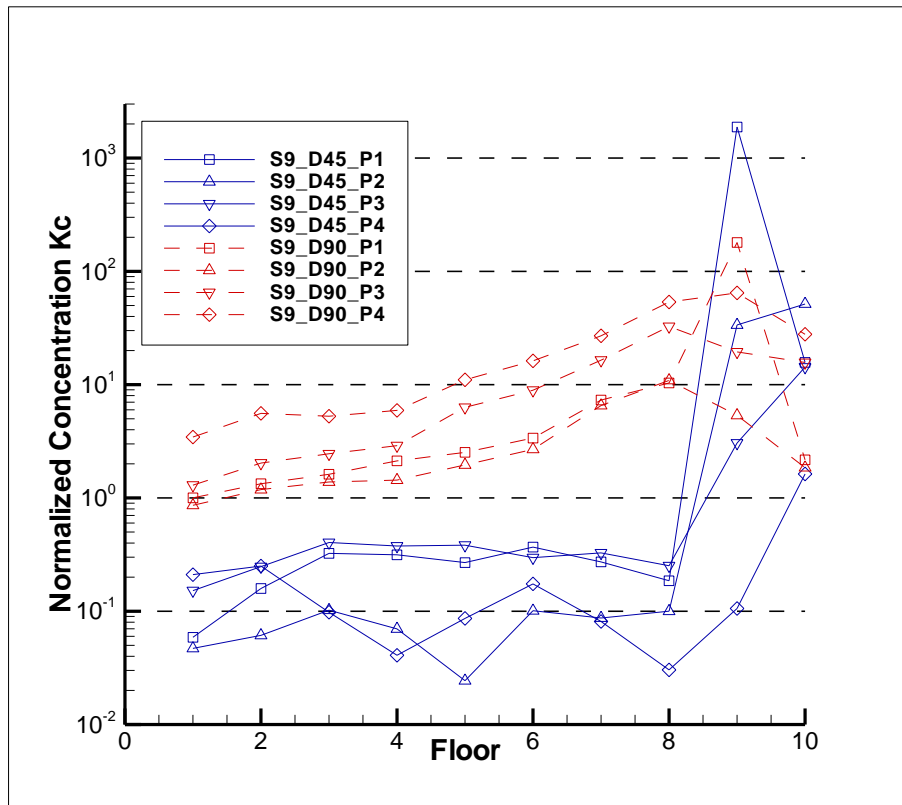
Figure 6.11 shows the mean concentration profiles with open-window under other wind directions ( $\theta = 45^\circ$ ,  $\theta = 90^\circ$ ). Compared with Figure 6.9, it also can be seen that the overall concentration level was obviously lower when there are openings along building facades. The dilution effect induced by cross-ventilation under these two wind directions is relatively stronger than that of under prevailing wind directions. Taking no account of the extremely low concentration values, for each pair of cases with the same wind direction and the source location, the averaged  $K_c(close)/K_c(open)$  ratio were from 4 to 7. For each individual measurement point, the ratio is ranged from about 1 to 12. In Figure 6.11b, when the source was located in the middle height of the building, the concentration values measured in two floors away from the source floor were clearly reduced, while in Figure 6.9b, the concentration level can be of the same magnitude as that of the source floor. Comparing Figure 6.9c and Figure 6.11c, when the incident angle is  $90^\circ$ , the tracer gas concentrations detected in other floors were clearly lower under open window condition, while that under closed window condition remain in almost the same magnitude.



a)



b)



c)

**Figure 6.11 Normalized concentration distributions under other wind directions ( $\theta = 45^\circ$ ,  $\theta = 90^\circ$ ) with open-window, when tracer released at a) the 3<sup>rd</sup> floor; b) the 6<sup>th</sup> floor; c) the 9<sup>th</sup> floor.**

It can be concluded that under the current configurations, when the window-to-floor area ratio is approximately 7.4%, the key features of wind-induced cross-contamination are similar between open-window and closed-window situations. The tracer gas dispersion trends are about the same. The obvious differences of mean concentration profiles only exist in the concentration magnitudes, the concentrations measured under open-window condition are generally within one order of magnitude less than those under closed-window condition.

## **6.4 Concentration Fluctuation Characteristics**

The mean concentration distributions were thoroughly studied in the above sections, which revealed the detailed features of mean concentration fields around HRR building under various situations. On the other hand, accidental release of highly toxic pollutant may occur sometimes, such as highly infectious disease outbreak or flammable gas leakage. Thus, it is necessary to estimate not only the mean concentration but also the concentration fluctuations. In this section, the features of concentration fluctuations are examined from the following two points of view. The first is to check the turbulent fluctuation characteristics of wind-induced cross-contamination. For this purpose, it is important to analyze concentration fluctuation values in relation to the levels of the mean concentration. The concentration fluctuation intensities together with cumulative distribution functions of concentration data are presented and discussed. The second is from a practical point of view. As for this aspect, the original data-acquisition rate of 150 Hz is not required. For example, to study the odour dispersion process, the important parameter which can lead to an experience of annoyance depends upon the “instantaneous” concentration level with a time scale related to humans’ breath period. Moreover, for the prevention of highly infectious disease, the temporal behavior of the dispersion process must be captured and analyzed with a time scale as small as one inhalation period of humans (between 1 and 2s). Therefore, the 90-percentile, the instantaneous infection risk was calculated using the 2s-averaged (in prototype) data.

### **6.4.1 Concentration Fluctuation Intensity**

Concentration fluctuation intensity is defined as

$$i = \frac{\sigma_c}{C_{mean}} \quad (6.1)$$

where  $\sigma_c$  is the standard deviation, and  $C_{mean}$  is the mean concentration. After examining the mean concentration data, in general, when the source was located in the 3<sup>rd</sup> floor, the vertical adjacent two units are the most significant influenced floors. Also, when the source was located in the 6<sup>th</sup> floor, the influence region could be extended to three vertical adjacent floors. Therefore, the concentration fluctuation intensities of the adjacent two floors were presented (Figure 6.12) when the source was located in the 3<sup>rd</sup> floor, while that of the adjacent three floors were presented when the source was located in the 6<sup>th</sup> floor (Figure 6.13).

First of all, it should be noted that, for most of the points, the values of the concentration fluctuation intensity are greater than one, suggesting the fluctuations in instantaneous concentration are at least of the same values as the actual mean concentrations. Combined the results with the mean concentration distributions, it can be found that the fluctuation intensities gradually increase towards the edges of the plume, where the mean values are relatively low. Examining the window's effect, the fluctuation intensity is generally larger at each measurement point under open window condition than that of under closed-window condition. Furthermore, the concentration fluctuation intensity is nearly uniform on each of the building facades at the same floor when the window is closed, while it can be different from each other under open-window condition. These results indicate that the flow is more complex and more turbulent under open-window condition due to the stronger mixing effect introduced by cross-ventilation. These Figures also reveal that the

distributions of concentration fluctuation under different window opening conditions are relatively similar. This is consistent with the turbulence scales generated by the interaction of building with the flow, which is mainly dominated by the building structure.

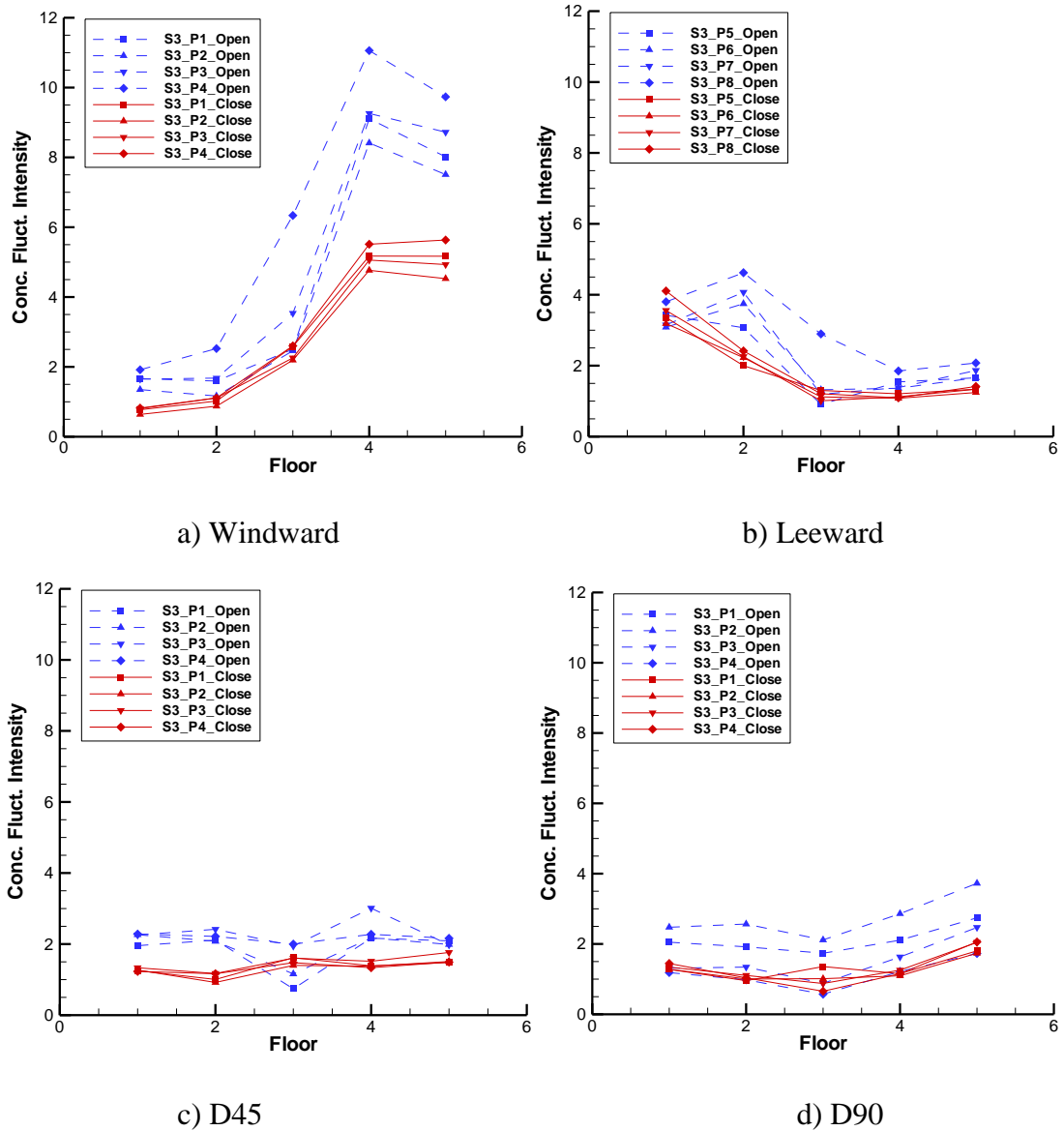
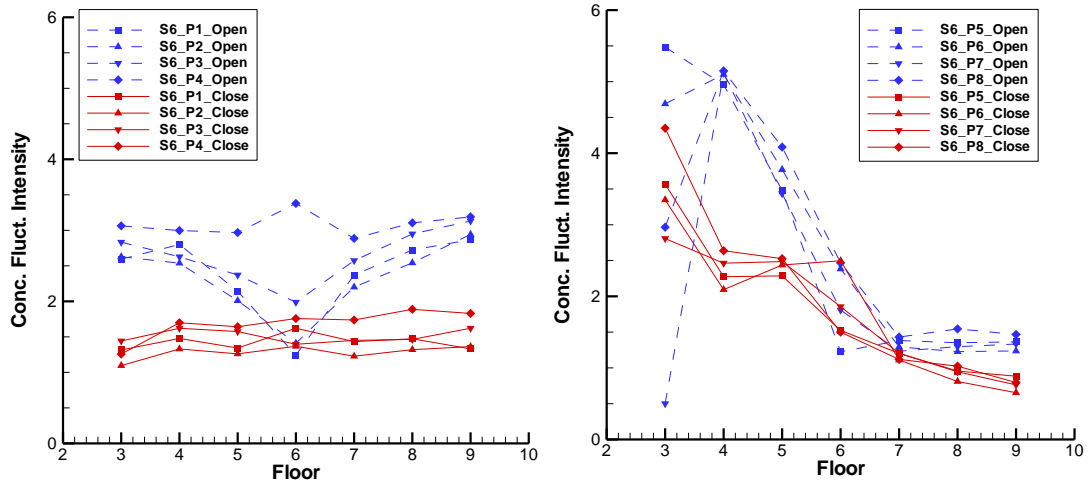
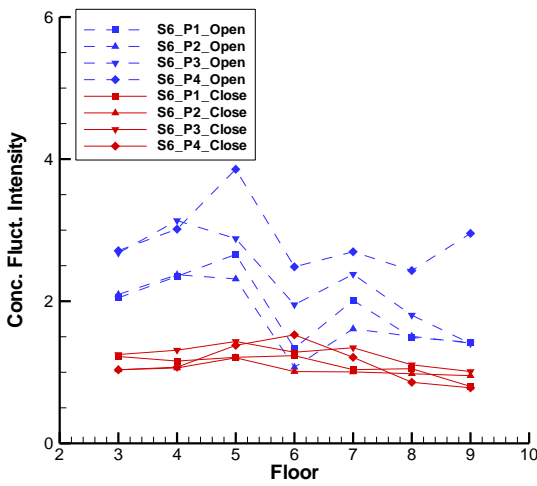


**Figure 6.12 Concentration fluctuation intensity when source was located in the 3<sup>rd</sup> floor**

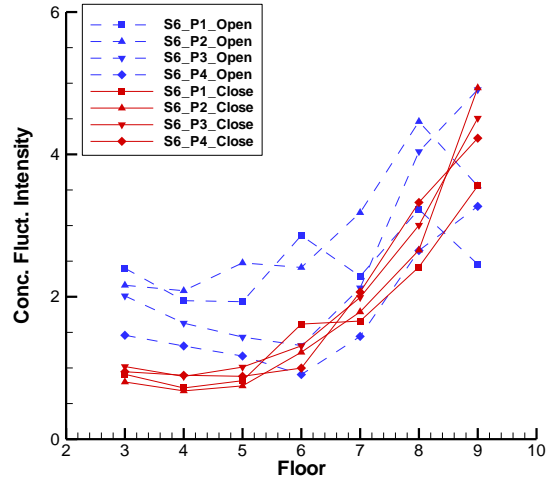


a) Windward

b) Leeward



c) D45



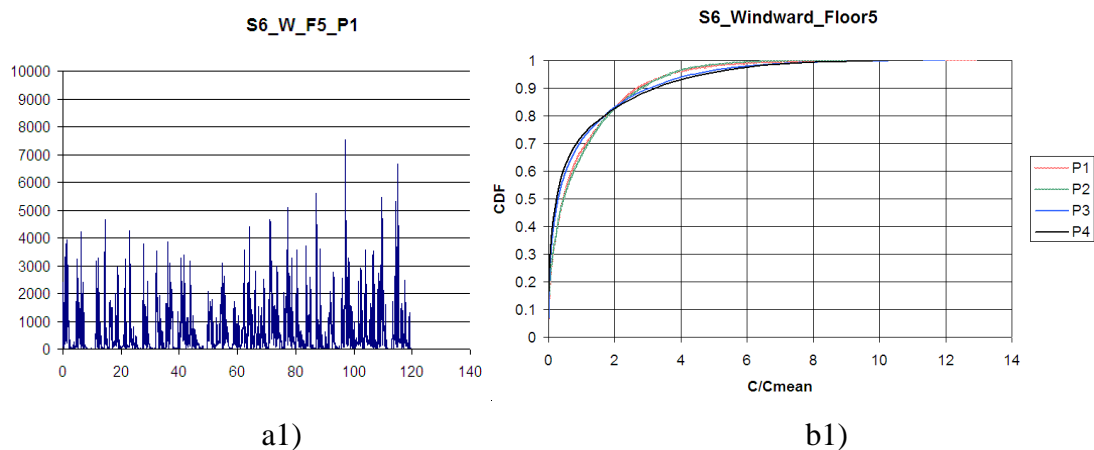
d) D90

**Figure 6.13 Concentration fluctuation intensity when source was located in the 6<sup>th</sup> floor**

### 6.4.2 Cumulative Distribution Function

Another important parameter presented here is the cumulative distribution function (CDF) of each concentration time series. The CDF gives the proportion of concentration readings which are below a given concentration. It is expressed as the

ratio between the instantaneous and mean concentration values. The CDF provides the following information: a) the concentration fluctuation intensity which is indicated by the slope of the central part of the curve (the lower the intensity the steeper the gradient); b) intermittency, which is indicated by the intercept on the vertical axis; c) the ratio between peak and mean obtained from the value where CDF reaches 1. The definition of intermittency is the proportion of the concentration time series for which the concentration is at or below a threshold value, which in this case is the zero concentration. It should be pointed out that a significantly large amount of data has been obtained during the experiment, which can be used for this analysis. However, when the source is located in the middle height of the building, the contaminated degree is relatively higher compared with the results under other source locations, which deserves further analysis. Therefore, the following results presented here are firstly derived from the data when the source is located in the 6<sup>th</sup> floor, under prevailing wind direction, followed by a direct comparison between the other two wind directions.



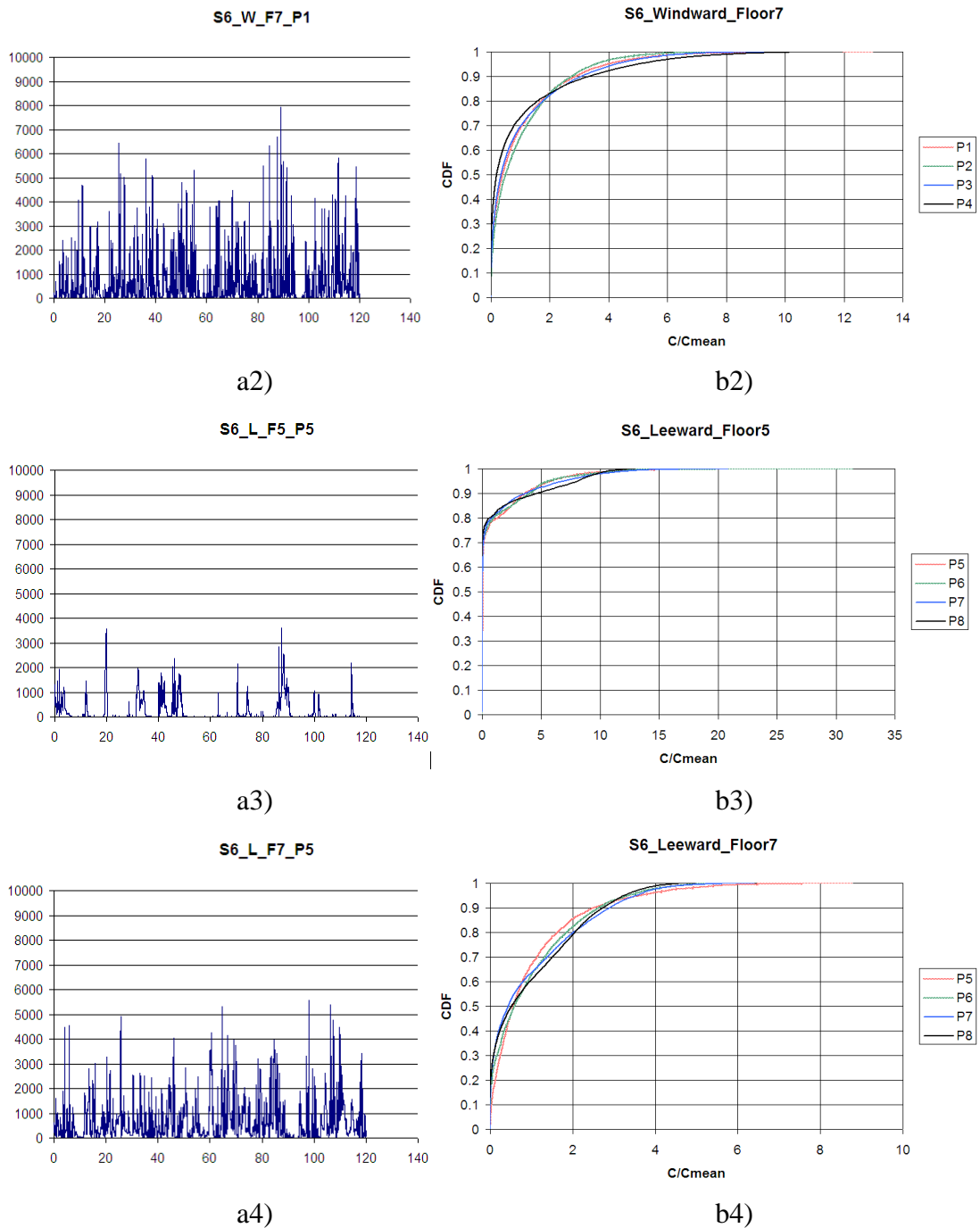


**Figure 6.14 Time series for point P1 (in windward cases) or P5 (in leeward cases) and CDF shapes at vertical adjacent floors with closed-window condition. (The abbreviation F5 and F7 represent the 5<sup>th</sup> floor or the 7<sup>th</sup> floor, respectively; W and L represent in windward or leeward condition, respectively.)**

Figure 6.14b presents the progression of the CDF shapes at the vertical adjacent floors, when the source is located in the 6<sup>th</sup> floor under closed-window condition.

The time series for one of the selected points are also presented in Figure 6.14a for the comparison purpose. Firstly, it can be seen that the basic fluctuation feature at each measurement point is clearly revealed through the CDF shape. For example, as shown in Figure 6.14 b3, the intermittency factors for the points located in the 5<sup>th</sup> floor under leeward condition are greater than 0.7, while they are about 0.2 in other positions (as shown in Figure 6.14 b1, b2 and b4). This is also reflected by the concentration time series data presented in the figures, for the points in the 5<sup>th</sup> floor under leeward condition, the concentration value is nearly zero in about 70% of the sampling period. Besides, it is shown that both the fluctuation intensity and the peak to mean ratio at these points are relatively large, due to the comparatively low value of the mean concentration obtained at that floor.

Secondly, comparing with the CDF shapes presented in the figures, with regard to the different measurement points at the same floor, the CDF shapes are very close to each other, indicating a similar feature of concentration fluctuation characteristics at the same floor. With regard to the different floors, comparing Figure 6.14 b1 and b2, the CDF shapes are much alike in the vertical upper and lower floors. This suggests that the cumulative distribution frequencies of concentration fluctuation in the vertical direction are basically symmetrical from the source floor under windward condition. Combined with the mean concentration distribution revealed in Figure 6.7b, both mean concentration and concentration fluctuation have similar symmetric feature in the vertical direction under this scenario. As to the different building orientations, from the comparisons between b1 and b3, b2 and b4, it can be seen that the shapes of CDF are similar in the vertical adjacent upper floor under windward and leeward cases, while obvious differences exist in the adjacent lower floor.

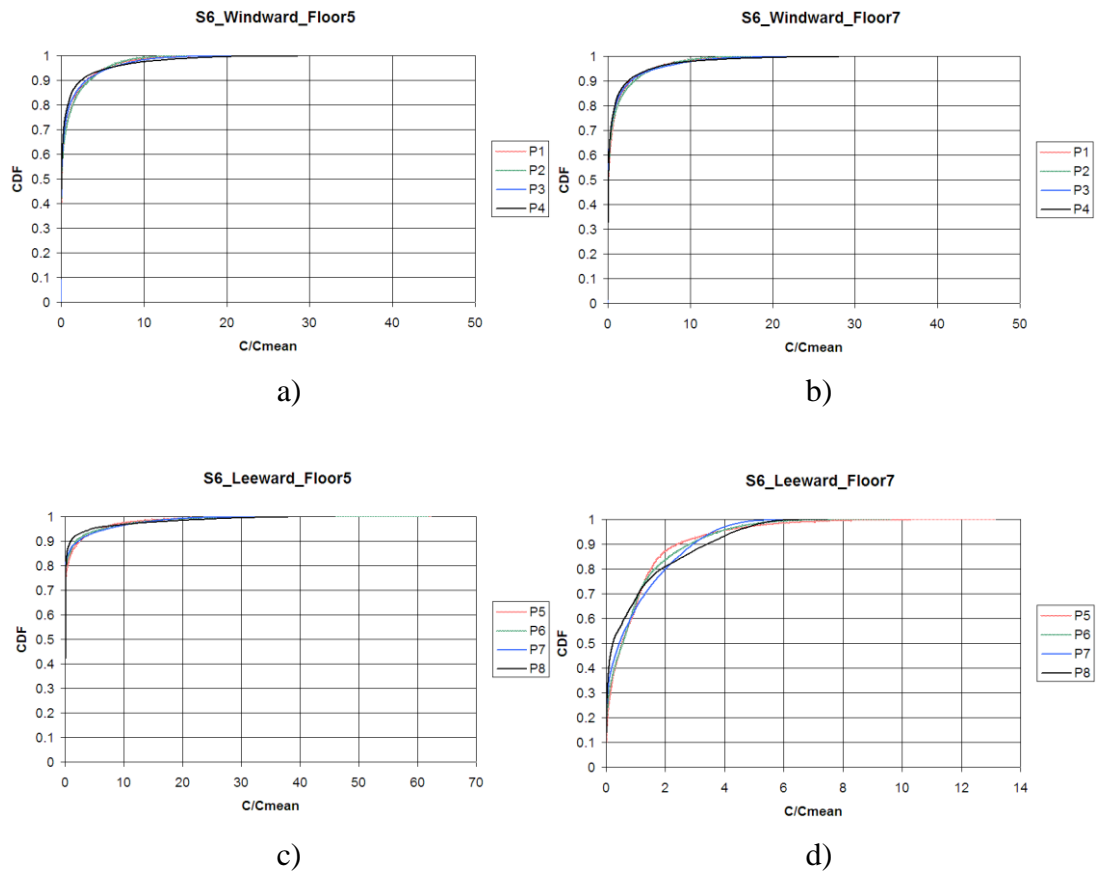
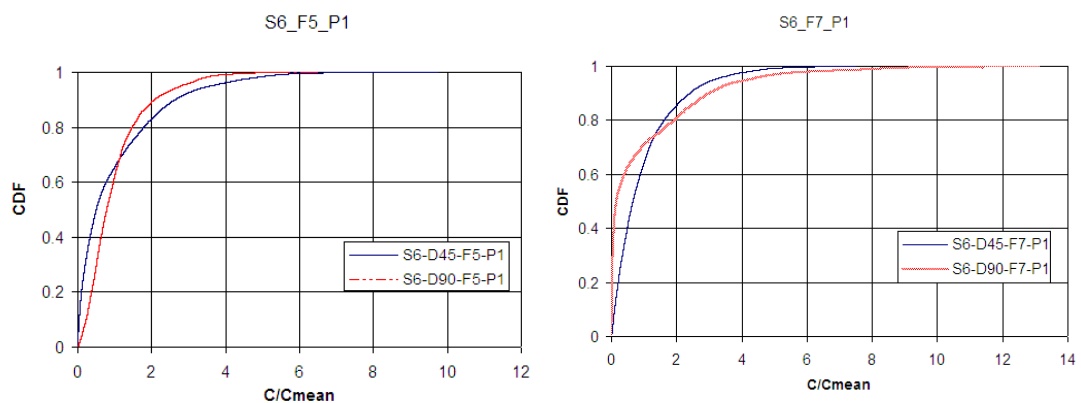


**Figure 6.15 CDF shapes at vertical adjacent floors with open-window condition. (The abbreviation F5 and F7 represent the 5<sup>th</sup> floor or the 7<sup>th</sup> floor, respectively; W and L represent in windward or leeward condition, respectively.)**

Figure 6.15 is the CDF shapes of the selected floors under prevailing wind direction, with open-window condition. It can be seen that the overall CDF shapes are slightly different compared with the results obtained under closed-window condition. When the windows are open, the concentration data are highly intermittent, and the intermittency factors in windward cases are up to 0.6. For each individual point, the CDF shows a gentler slope (higher intensity), with the peak-to-mean ratio also larger than that is shown in Figure 6.14. These results further reveal that the concentration fluctuation is more severe under open-window condition.

However, it should be noted that comparable differences also exist under open-window condition. Comparing Figure 6.15 a2 and b2, the CDF shapes are similar in the vertical upper and lower floors. The results in the same floor are close to each other. In the 5<sup>th</sup> floor under leeward condition, the CDF also shows a long gentle slope characteristic of a highly fluctuating region of the flow with comparatively high peak-to-mean ratio, while the intermittency is about 0.8. This suggests that the differences of basic fluctuation features compared between different measurement points are not significantly changed when the windows are opened, at least for the present cases.

Figure 6.16 shows comparisons of CDF in the same measurement point under the other two wind directions ( $\theta = 45^\circ, \theta = 90^\circ$ ), with closed-window. It can be seen that when the incident angle is  $\theta = 45^\circ$ , the fluctuation intensity of the point P1 in the adjacent upper floor is higher than that of  $\theta = 90^\circ$ , but in the adjacent lower floor, it was lower than that of  $\theta = 90^\circ$ . Comparing with these different CDF shapes, the intermittency factor at point P1 in the 7<sup>th</sup> floor under  $\theta = 90^\circ$  is the largest, which indicates that during 40% of the sampling time, the concentration level detected in that point is about zero.



a) CDF shape at point P1 in the 7<sup>th</sup> floor    b) CDF shape at point P1 in the 5<sup>th</sup> floor

**Figure 6.16 CDF shapes under the other two wind directions. ( $\theta = 45^\circ$ ,  $\theta = 90^\circ$ )**

Both the concentration fluctuation intensity and cumulative distribution function presented above illustrated the fundamental characteristics of the concentration fluctuations. Next, from hazard assessment point of view, the following analysis is based on the “instantaneous” concentration values to further investigate the practical impact induced by the fluctuations.

### **6.4.3 90-Percentile**

Usually, for the target building, the windows of kitchens and bathrooms are open towards the re-entrant space, into which the exhaust air from all the floors are discharged, such as cooking odour generated from cooking processes. With the concern of odour annoyance, the 90-percentile (the concentration level exceeded during 10% of the total time) is presented here, calculated using the 2s-averaged (in prototype) data. This parameter can be used to examine the high concentration level and to evaluate whether it can lead to an experience of annoyance. The definition of an odour unit per volume ( $1 \text{ OU m}^{-3}$ ) is associated with the odorant concentration. Such threshold value is the concentration of a substance that can be detected by half of the people present. However, this concentration level varies from person to person depending on the sensibility for odours, and it is also different from various kinds of odorous substances. Thus, the key parameter to evaluate the odour concentration level is actually the dilution factor. In this section, the 90-percentile is presented in

the following two ways: firstly it is normalized by the mean concentration of each point to illustrate the variation degree at each individual point; secondly it is normalized by the source concentration to give direct information about the dilution level and the frequency of exposure.

**Table 6.3 The 90-percentile normalized by mean concentration under prevailing wind direction with closed-window (Source located in the 6<sup>th</sup> floor)**

	Windward Case				Leeward Case			
<b>Floor</b>	<b>P1</b>	<b>P2</b>	<b>P3</b>	<b>P4</b>	<b>P5</b>	<b>P6</b>	<b>P7</b>	<b>P8</b>
<b>3</b>	2.7	2.6	2.9	2.6	1.9	2.2	2.1	2.1
<b>4</b>	2.8	3.0	3.0	3.3	3.9	4.2	3.3	4.3
<b>5</b>	2.6	2.8	2.9	3.2	3.7	4.1	3.8	4.6
<b>6</b>	2.8	2.9	3.1	3.5	2.5	3.6	4.3	3.6
<b>7</b>	2.8	2.7	2.9	3.2	2.5	2.6	2.7	2.7
<b>8</b>	2.7	2.6	2.8	3.1	2.3	2.2	2.2	2.5
<b>9</b>	2.5	2.6	2.7	2.8	2.1	1.9	2.0	2.1

**Table 6.4 The 90-percentile normalized by mean concentration under other wind conditions with closed-window (Source located in the 6<sup>th</sup> floor)**

	$\theta = 45^\circ$				$\theta = 90^\circ$			
<b>Floor</b>	<b>P1</b>	<b>P2</b>	<b>P3</b>	<b>P4</b>	<b>P1</b>	<b>P2</b>	<b>P3</b>	<b>P4</b>
<b>3</b>	2.6	2.5	2.4	2.2	2.3	2.2	2.4	2.2
<b>4</b>	2.5	2.6	2.5	2.4	2.0	1.9	2.2	2.2
<b>5</b>	2.5	2.6	2.7	2.4	2.0	2.0	2.4	2.3
<b>6</b>	2.2	2.3	2.6	2.5	2.6	2.5	3.0	2.4
<b>7</b>	2.3	2.3	2.3	2.1	3.1	3.3	3.5	4.4
<b>8</b>	2.3	2.2	2.2	1.9	3.6	3.1	2.9	2.2
<b>9</b>	1.9	2.2	2.1	1.8	1.9	1.7	2.1	2.3

The 90-percentile non-dimensioned by the mean concentration is presented in Tables 6.3 and 6.4, under prevailing wind direction and other wind directions, respectively, when the source is located in the 6<sup>th</sup> floor and windows are closed. This can be used to further evaluate the high-concentration effect and the degree of its deviation from the local mean. As shown from the results, this ratio does not show large variation in the focused region, and generally it is ranging from 2 to 5 in the presented cases. In the wind tunnel experiment conducted by Aubrun and Leitl (2004), it was found that the factors between this 90-percentile and the mean concentration were less than 4 in most of the positions located in the vicinity of a pig barn. It can be observed that the ratio fluctuates around 2.8 under windward condition, while it fluctuates around 2.3 when the incident angle  $\theta = 45^\circ$ . This suggests that the levels of turbulence in later case are slightly lower than that of under windward condition. This is expected in view of the fluctuation intensities presented earlier, as shown in Figure 6.13. It should be noted that the ratio is nearly constant in both two cases mentioned above, while it varies in a wider range in the other two cases, in which the studied re-entrant spaces didn't face into the wind and can be treated as "transposed canyon", to some extent. Pavageau and Schatzmann (1999) showed a variable value ranging from 1.5~6 for the ratio 99-percentile over mean concentration, from their wind tunnel studies aimed at the dispersion in a street canyon, while corresponding simulation results also showed similar results (from 1.5 to 5, by Dixon and Tomlin, 2007).

Moreover, when assessing the impact of odours, it is important to study both the concentration of odours and their frequency of occurrence. The examination of the spatial distribution of this 90<sup>th</sup> percentile is also useful to estimate the concentration level at each location affected by the source. Table 6.5 and 6.6 are the 90-percentile

normalized by source concentration under prevailing wind direction and other wind directions, respectively. When the odour concentration at source location was known, the values and positions of short duration peaks could therefore be estimated to check for exceedance of critical thresholds. It can be observed from the results, even in several floors away from the source, the calculated factor can remain larger than 1% in both vertical directions. In some particular positions such as the points that are opposite to the index unit, the 90-percentile concentration can reach one order of magnitude lower than the source concentration. These results directly illustrate the impact from the source. For example, when the exhaust air is released from one household during the cooking processes, at the concentration equal to  $1000 \text{ OU m}^{-3}$ , the 90-percentile concentration obtained in several adjacent households could be several odour units per cubic meter under presented condition. Thus, the possibility of causing odour annoyance can be estimated based on the concentration level, frequency and duration of exposure.

**Table 6.5 The 90-percentile normalized by source concentration under prevailing wind direction with closed-window (Source located in the 6<sup>th</sup> floor)**

	Windward Case (in %)				Leeward Case (in %)			
<b>Floor</b>	<b>P1</b>	<b>P2</b>	<b>P3</b>	<b>P4</b>	<b>P5</b>	<b>P6</b>	<b>P7</b>	<b>P8</b>
<b>3</b>	1.0	0.9	1.0	1.0	0.0	0.0	0.0	0.0
<b>4</b>	1.2	1.2	1.3	1.4	0.9	1.2	1.3	1.6
<b>5</b>	1.6	2.0	2.5	2.9	0.7	0.8	2.0	3.8
<b>6</b>	3.6	4.2	5.6	5.2	6.1	1.6	7.1	10.3
<b>7</b>	1.7	2.4	2.7	2.7	1.6	2.7	4.6	6.8
<b>8</b>	1.1	1.3	1.2	1.3	1.7	2.0	2.2	3.8
<b>9</b>	0.6	1.0	0.8	0.8	1.6	1.6	1.8	2.4

**Table 6.6 The 90-percentile normalized by source concentration under other wind conditions with closed-window (Source located in the 6<sup>th</sup> floor)**

	$\theta = 45^\circ$ (in %)				$\theta = 90^\circ$ (in %)			
<b>Floor</b>	<b>P1</b>	<b>P2</b>	<b>P3</b>	<b>P4</b>	<b>P1</b>	<b>P2</b>	<b>P3</b>	<b>P4</b>
<b>3</b>	1.0	0.8	0.6	0.6	1.5	1.3	1.5	1.5
<b>4</b>	1.4	1.1	1.0	0.9	1.6	1.6	2.3	2.4
<b>5</b>	1.8	1.8	1.7	1.3	2.4	2.7	5.2	6.1
<b>6</b>	4.5	4.3	3.8	3.7	2.9	2.9	7.0	11.9
<b>7</b>	2.1	1.9	1.5	1.2	1.6	1.8	2.9	4.2
<b>8</b>	1.1	0.8	0.6	0.6	0.8	0.6	0.6	0.5
<b>9</b>	0.9	0.6	0.4	0.4	0.2	0.1	0.2	0.2

#### **6.4.4 Infection Risk Assessment**

With regard to the airborne transmission risk of highly infectious diseases, one quantitative infection risk assessment model, i.e., the Wells-Riley model (Riley et al., 1978), is employed to evaluate the risk of these diseases to the neighbors. The assessment is conducted based on both instantaneous peak and mean concentration values. The results are compared to estimate the potential risk induced by instantaneous peak concentration presented during one inhalation period of humans. All the instantaneous concentration values are calculated using the 2s-averaged (in prototype) data.

Based on the concept of “quantum of infection” (a quantum is defined as the number of infectious airborne particles required to infect the person and may consist of one or more airborne particles), the Wells-Riley equation is presented for the purpose of estimating the probability of airborne transmission of an infectious disease (Riley et al., 1978):

$$P = \frac{C}{S} = 1 - \exp\left(-\frac{Iqpt}{Q}\right) \quad (6.2)$$

where  $P$  is the probability of infection,  $C$  is the number of infection cases,  $S$  is the number of susceptibles,  $I$  is the number of infectors,  $p$  is the pulmonary ventilation rate of a person,  $q$  is the quanta generation rate,  $t$  is the exposure time interval, and  $Q$  is the room ventilation rate. Exposure to one quantum of infection gives an average probability of 63% ( $1 - e^{-1}$ ) of becoming infected. The Wells–Riley equation is set up on the assumptions of a well-mixed and steady-state condition. However, the equation can also incorporate spatially distributed infection risk by conducting tracer gas measurements, which do not require the assumptions (Sze To and Chao, 2010). In such measurements, tracer gas is released from the locations of the infectors and the concentrations of the tracer gas at the locations of each susceptible person are then measured, allowing the derivation of spatial distribution of infection risk. Some risk assessment studies have also used these approaches to estimate the infection risk, by employing numerical simulation method (Gao et al., 2008; Tung and Hu, 2008). Here using the experimental results, the infection risk of highly infectious diseases such as measles can be evaluated.

ASHRAE (ASHRAE, 2007) recommends that the outdoor air requirements are 0.03 L/s m<sup>2</sup> in residential buildings over three stories, which is assumed as the constant room ventilation rate during the following studies. Supposing a hypothetical measles outbreak with a high values for quantum generation rate at the source location,  $q = 570/h$  (Rudnick and Milton, 2003), pulmonary ventilation rate at 0.6 m<sup>3</sup>/h (Gao et al., 2008), the calculated infection probabilities are listed in Table 6.7 to Table 6.10, using both mean and instantaneous peak concentration values. The corresponding exposure time is 1h and 2s, respectively. The following results are calculated by the data obtained under closed-window condition due to its relatively high cross-contamination risk.

**Table 6.7 The infection risk calculated by mean and instantaneous peak concentration values (Source located in the 6<sup>th</sup> floor, windward condition)**

Floor	Infection Risk (by Mean values) (in %)				Infection Risk (by Instantaneous Peak values) (in %)			
	P1	P2	P3	P4	P1	P2	P3	P4
3	2.06	1.86	1.87	2.13	0.01	0.01	0.01	0.01
4	2.21	2.18	2.35	2.35	0.01	0.01	0.02	0.01
5	3.11	3.86	4.52	4.80	0.02	0.02	0.03	0.03
6	6.59	7.39	9.14	7.60	0.03	0.03	0.03	0.04
7	3.25	4.63	4.76	4.48	0.02	0.02	0.02	0.03
8	2.16	2.67	2.29	2.26	0.01	0.01	0.01	0.02
9	1.41	1.95	1.58	1.48	0.01	0.01	0.01	0.01

**Table 6.8 The infection risk calculated by mean and instantaneous peak concentration values (Source located in the 6<sup>th</sup> floor, leeward condition)**

	Infection Risk (by Mean values) (in %)				Infection Risk (by Instantaneous Peak values) (in %)			
<b>Floor</b>	<b>P5</b>	<b>P6</b>	<b>P7</b>	<b>P8</b>	<b>P5</b>	<b>P6</b>	<b>P7</b>	<b>P8</b>
<b>3</b>	0.37	0.23	0.40	0.30	0.01	0.00	0.01	0.01
<b>4</b>	1.21	1.51	2.12	2.05	0.01	0.01	0.02	0.02
<b>5</b>	1.04	1.11	2.84	4.35	0.01	0.02	0.03	0.03
<b>6</b>	12.09	2.39	8.42	14.24	0.05	0.03	0.03	0.03
<b>7</b>	3.37	5.47	8.54	12.77	0.01	0.02	0.03	0.03
<b>8</b>	3.77	4.79	5.35	7.87	0.01	0.01	0.02	0.02
<b>9</b>	3.98	4.36	4.77	6.09	0.02	0.01	0.01	0.01

**Table 6.9 The infection risk calculated by mean and instantaneous peak concentration values (Source located in the 6<sup>th</sup> floor,  $\theta = 45^\circ$ )**

	Infection Risk (by Mean values) (in %)				Infection Risk (by Instantaneous Peak values) (in %)			
<b>Floor</b>	<b>P1</b>	<b>P2</b>	<b>P3</b>	<b>P4</b>	<b>P1</b>	<b>P2</b>	<b>P3</b>	<b>P4</b>
<b>3</b>	1.98	1.65	1.44	1.49	0.01	0.01	0.01	0.01
<b>4</b>	2.83	2.31	2.10	2.01	0.01	0.01	0.01	0.01
<b>5</b>	3.71	3.58	3.28	2.75	0.02	0.02	0.02	0.02
<b>6</b>	10.47	9.35	7.55	7.54	0.04	0.03	0.03	0.03
<b>7</b>	4.87	4.33	3.44	2.94	0.02	0.02	0.02	0.02
<b>8</b>	2.63	2.01	1.56	1.54	0.01	0.01	0.01	0.01
<b>9</b>	2.41	1.44	1.12	1.19	0.01	0.01	0.01	0.01

**Table 6.10 The infection risk calculated by mean and instantaneous peak concentration values (Source located in the 6<sup>th</sup> floor,  $\theta = 90^\circ$ )**

	Infection Risk (by Mean values) (in %)				Infection Risk (by Instantaneous Peak values) (in %)			
<b>Floor</b>	<b>P1</b>	<b>P2</b>	<b>P3</b>	<b>P4</b>	<b>P1</b>	<b>P2</b>	<b>P3</b>	<b>P4</b>
<b>3</b>	3.46	3.17	3.40	3.59	0.01	0.01	0.01	0.01
<b>4</b>	4.27	4.51	5.32	5.68	0.01	0.01	0.02	0.02
<b>5</b>	6.24	7.06	10.70	13.07	0.02	0.02	0.03	0.03
<b>6</b>	5.90	5.99	11.65	23.06	0.03	0.03	0.04	0.06
<b>7</b>	2.79	2.86	4.31	5.05	0.02	0.02	0.03	0.03
<b>8</b>	1.15	0.94	1.01	1.17	0.02	0.01	0.01	0.02
<b>9</b>	0.46	0.28	0.38	0.40	0.01	0.01	0.01	0.01

These results give a rough estimation of the infection risk levels at different positions, in terms of both mean and instantaneous peak concentrations. With regard to the mean values, the probabilities can be greater than 10% in vertical adjacent flats and the opposite flat, as shown in Tables 6.8 and 6.10. These mean infection risk probabilities show that in case of an outbreak of highly infectious disease, both the vertical and horizontal transport of infectious diseases in high-rise residential buildings is worthy of due consideration in infection control. It can be seen that the probability calculated by instantaneous peak concentration values is under 0.05% in all the positions for the presented cases. This suggests that the infection risk caused by a transient peak concentration level that is detected in a short time duration can be neglected, comparing with mean infection risk probabilities. Although the peak concentration value can be clearly higher than the mean value, the risk is still significantly low due to the extremely short exposure time. The spatial distribution of infection risk is still characterized by the mean concentration distribution.

It should be pointed out that gas phase surrogate is used to represent infectious particles during present studies, while aerosol mechanics are ignored in estimating their transport. Using gas phase surrogate in the risk assessment considers all the aerosols to be suspended and inhalable, and also ignores the deposition of particles. Thus, the infection risk values calculated here can be expected to overestimate the risk level, compared with that of using respiratory infectious particles.

## **6.5 Summary**

In this chapter, the characteristics of air pollutant dispersion around the typical HRR building design in Hong Kong were thoroughly investigated in a wind tunnel study, using a larger model scale that allowed higher spatial resolution of concentration data. Both mean concentration distributions and its fluctuation characteristics were analyzed and discussed. It was found that the transmission path can be complicated due to the strong interaction between the approaching wind and the complex building shape. With regard to the mean concentration profiles, the results illustrated that the pollutant can spread in both vertical directions, not only in the upward direction as was found under buoyancy effect, but also in the downward direction. Furthermore, dispersion can also occur in the horizontal direction, indicating a potential risk of cross-contamination between the horizontal adjacent flats. By analyzing the pressure differences and possible airflow directions both along a façade and the envelopes of each unit, designers may locate the window openings and exhaust outlets more properly to reduce cross contamination possibilities.

With regard to the pollutant dispersion characteristics under open window condition, it should be addressed that the overall dispersion route is similar with that of closed-window condition. Based on the results presented in this chapter, it can be concluded that under such window-to-floor area ratio, the basic dispersion features don't change significantly between open and closed-window configurations. The airflow pattern and air pollutant dispersion is still dominated by the approaching wind and the block effect of the building walls. However, the mean concentration values obtained under open-window condition were generally within one order of magnitude less than those under closed-window condition.

It should be noticed that the dispersion route illustrated by this study is quite sensitive to both the source location and the wind direction. It can be expected that the approaching incident angle strongly affects the airflow pattern around the building, consequently influences the air pollutant dispersion characteristics. Generally, the upper floors at the leeward have a relatively higher risk of cross-contamination than that of the lower floors. Comparing different source locations, a higher risk was found when the source was located in the middle height of the building.

As to the concentration fluctuations, the discussions were from two points of view. The unsteady characteristics were analyzed based on the fluctuation intensity and the CDF. From practical point of view, the analysis was focused on the cases under closed-window condition with relatively higher risk. The 90-percentile values give a

clearer indication of where the high peak values occur than the intensity does. It is therefore of relevance to the study of peak exposures with regard to odour dispersion process. Finally, the infection risk probability was calculated and analyzed, in terms of mean and instantaneous peak concentrations. This can be helpful in understanding the characteristics of contaminant dispersion in typical building environment, and also help to employ more effective intervention strategies for infection control.

In the long run, the prediction of the pollutant concentration field near buildings is very important for building engineers to design proper air intake and exhaust locations to avoid unwanted consequences. It is our intention that the high precision wind test data illustrated in this chapter could also be used to validate the CFD models in the future work, so that the airflows can be examined in more detail via computational methods.

## **Chapter 7**

### **Concluding Remarks and Recommendations**

The environmental and toxicological impact arising from the dispersion of contaminants around building has become an increasingly important problem, especially in high densely populated areas with crowd living conditions. In this research, the mechanisms of cross-contamination around two typical kinds of high-rise residential building were thoroughly studied under different weather conditions. The presented study is mainly focused on the pollutant originating from the building itself and its dispersion characteristics around building under natural ventilation condition. It is known that the air exchange process during natural ventilation could probably transport the outdoor pollutant into indoor environment. Under crowd living conditions, this lead to the pollutant exhausted from one household could probably re-enter neighboring households and bring a bad results to the resident's health. Designers of high-rise residential apartment buildings may have long overlooked an issue that would not exist for low-rise residential buildings, which is the cross-contamination of the ventilation air. This study provides an insight into such pollutant dispersion process around HRR building under different dominated forces. The exact transmission path revealed in this study can lead to developing more targeted and more effective intervention to prevent this undesirable cross-contamination in high residential blocks.

Two complementary methods, wind tunnel modelling method and simulation method using CFD techniques were applied aiming at different features of pollutant

dispersion process. Firstly, motivated by the possible infectious disease transmission path that was suggested during the SARS outbreak, CFD simulation method was used to study the buoyancy-dominated cross-contamination within a simple-shaped HRR building, and the main purpose for this stage of work is concentrated to the pollutant transportation and its re-entering process. Next, the study was extended to more complicated circumstances. The pollutant dispersion process was investigated from a whole building point of view with approaching atmospheric boundary layer flow. After evaluating the performance of numerical method, wind tunnel method was employed to further illustrate the detailed features of wind-induced cross-contamination around a complex-shaped building. A series of experimental cases were designed and conducted for this purpose. Pressure coefficient distributions, both mean concentration and concentration fluctuation characteristics were analyzed and discussed. It is therefore possible to draw a conclusion on the cross-contamination under different environmental conditions.

## **7.1 Conclusions**

### **Buoyancy-induced Cross-contamination around Slab-shaped Building**

The prevalence of low wind weather conditions in the springtime in Hong Kong may have lead to poor dispersion of the exhaust air, and buoyancy-induced cross-contamination can probably occur with open-window ventilation practices. The CFD simulation results revealed both qualitatively and quantitatively the vertical upward re-entry possibilities of the exhaust air in high rise residential buildings. The main findings can be summarized as follows:

- It is further identified that the exhaust air from one flat can be re-entrained into the adjacent upper room in a windless day. Under buoyancy effect caused by the temperature differences between indoor and outdoor environment, the flats of HRR building with open-windows on the same facade become single-sided ventilated, and the windows function as both inlet and outlet of ventilated air. As a consequence, one kind of inter-flat air flow occurs between vertical adjacent flats, and the exhausted contaminated air can travel with the ambient upward flow and re-enter the vertical adjacent flats.
- Dominated by buoyancy effect, the pollutant transportation route is limited in one direction, i.e. upward in the vertical direction. Moreover, the concentration level is generally two orders of magnitude lower in the upper room than in the adjacent lower room.
- The concentrations of the upper room did not linearly change with the temperature difference. When the indoor/outdoor temperature increased, the increased ventilation rate played dual roles on the change of concentration--a positive role in dilution effect induced by the ventilation, and a negative role in carrying more contaminated exhaust air into the upper room.
- Possible optimizations to prevent this kind of cross-contamination can be introduced based on the dispersion characteristics revealed in this study. The improvement was shown from the simulation results through the comparisons between with or without optimization designs. With regard to architectural design, external ledges above the windows can help to block the ascending airflow, and consequently reduce the re-entry ratio of exhaust air. Alternatively, with regard to ventilation control, using individual mechanical

exhaust in each flat is an obvious option, and the cross-contamination through the open windows could also be avoided or much reduced.

### **Wind-induced Cross-contamination around Cross-shaped Building**

Both physical modelling approach and numerical method were employed to study more complicated interaction between plume dispersion and approaching wind profile. A series of preliminary experiments were first carried out to get general knowledge of wind-induced cross-contamination, and the data were compared with the predicting results to evaluate the numerical methods. After the examination of the predicting performance, wind tunnel method was selected for the detailed investigation. Another series of wind tunnel tests were designed and performed to further study such phenomena. The second stage wind tunnel experimental results offer extensive information about the dispersion field around cross-shaped building under wind effect. The key findings are summarized as follows:

- The performance of CFD models is examined for flow and concentration fields around the complex-shaped building. From the comparisons between simulated pressure coefficient distributions and the preliminary experimental results, it is shown that the predictions are generally acceptable. It is therefore reasonable to check the detailed flow-field from the simulation results, in order to improve the understanding of the complicated interactions between building and airflow. With regard to the dispersion studies, the basic characteristics of wind-induced cross-contamination can be revealed by CFD simulations. However, the comparisons of simulated results with experimental data are not satisfactory enough, and large discrepancies can be

found in some particular regions, especially under oblique wind direction. It can be concluded that, with the presented numerical techniques using the three kinds of  $k-\varepsilon$  models, CFD method is a useful tool for qualitative study. With regard to quantitative studies, in view of the unsatisfactory performance illustrated by the cross comparisons, the presented CFD methods are not recommended for extensive and detailed studies on wind-induced cross-contamination.

- Air pollutant dispersion around HRR building under wind effect is much more complicated than that of under buoyancy effect. The experimental results indicate that the flow pattern around the HRR building has the potential to transport gaseous pollutant within the re-entrance space under wind effect. It is observed that the air pollutant can spread in both vertical directions, not only in the upward direction that was found under buoyancy effect, but also in the downward direction. Furthermore, dispersion can also occur in the horizontal direction.
- The pollutant dispersion characteristics are quite sensitive to both the approaching wind direction and the source location. Generally, when the approaching wind incident angle is  $90^\circ$ , the air-curtain effect that formed in the entrance of the re-entrant space can lead to the worst scenario of cross-contamination. Comparing with different source locations, when the index floor is located in the middle part of the tall building, the cross-contamination risk is generally higher than others. In some particular cases, the pollutant released into the re-entrant space is not easily exhausted and the concentration can remain in the same magnitude along the entire building height within that area.

- Comparing between open-window and closed-window condition, the mean concentration distributions under both configurations are found to be similar. It is suggested that such window-to-floor area ratio (7.4%) is not sufficient large to influence the basic features of airflow and dispersion around the building. The obvious differences of mean concentration profiles only exist in the concentration magnitudes, the overall concentration level is reduced under open-window condition, especially when the approaching wind incident angle are 45° and 90°.
- With regard to the unsteady characteristics of the dispersion process, it is found that for most of the points, the values of the concentration fluctuation intensity are greater than one, suggesting the fluctuations in instantaneous concentration are at least of the same values as the actual mean concentrations. It is therefore necessary to estimate not only the mean concentration but also the concentration fluctuation. From practical point of view, it is found that the instantaneous peak concentration level could probably lead to an experience of odour annoyance. However, with regard to risk assessment of infectious respiratory diseases, a transient peak concentration level that is detected in a short time duration can be neglected, comparing with mean infection risk probabilities. The spatial distribution of infection risk is still characterized by the mean concentration distribution.

From the results shown in this thesis, for the cross-shaped building design, on one hand, it satisfied the building regulations and provided enough lighting area through the open window and share more outdoor spaces. However, on the other hand, cross-

contamination can not be overlooked and effective optimization is needed to prevent such circumstances.

It is the hope of the author that the new problem about HRR building environment introduced in this thesis will prove a useful basis for future HRR building environment research, shedding light on more effective and practice method for the prevention of cross-contamination, and leading to improvements in the wider context of urban air quality modelling and assessment.

## **7.2 Recommendations for the Further Works**

The present work should be further extended to better understanding of the flow and dispersion around HRR building under more complex conditions and provide more effective strategies on the control of HRR building environment. The following recommendations can be given.

Buoyancy may play dominant roles at low wind conditions, as revealed in Chapter 4. While in Chapter 5&6, the study is focused on the situations under wind effect. Eventually, the overall flow and dispersion should be investigated at mixed airflow conditions. The impacts of building facades and ground heating on the wind flow and pollutant transport should also be taken into considerations.

It is recommended to employ more accuracy and more reliable simulation methods in predicting the pollutant dispersion near to the building. With rapid development in

computer hardware and numerical algorithms, the performance of using CFD method can be improved in simulating this physical process, such as using LES turbulence model with higher order numerical schemes to simulate the concentration fluctuation characteristics.

The present study is focused on isolated building, and the influence introduced by neighboring HRR building is ignored. It should be the further step to consider the situation based on the whole estate with group of buildings. The evaluation of cross-contamination can be extended to building arrays. Also, the pollutant originating from one household can be assumed from neighboring buildings.

Understanding these pollutant transmission paths is useful in improving the ventilation design for high-rise residential blocks. Currently, with regard to ventilation design for high-rise residential buildings, open window combined with kitchen and bathroom exhaust fan is the dominant mode, and few high-rise residential buildings are provided with a central stack. Central exhaust stacks may be one of the essential ventilation components for high-rise residential buildings, but this has not been explicitly promulgated in the current ventilation standard and its performance is worthy of further investigation.

## References

- Anonymous. 1984. Building (Planning) Regulations. Laws of Hong Kong. HK: The Hong Kong SAR Government, [Chapter 123].
- Anonymous. 1997. Building (Planning) Regulations. Laws of Hong Kong. HK: The Hong Kong SAR Government, [Chapter 123F].
- Allard, F. 1998. Natural ventilation in buildings: a design handbook. London: James & James.
- Allocca, C., Chen, Q., & Glicksman, L.R. 2003. Design analysis of single-sided natural ventilation. *Energy and Buildings*, 35, 785–795.
- American Society of Heating, Refrigerating and Air-conditioning Engineers. 2005. ASHRAE Handbook - Fundamentals (SI).
- American Society of Heating, Refrigerating and Air-conditioning Engineers. 2007. ASHRAE Handbook- HVAC Applications (SI).
- American Society of Heating, Refrigerating and Air-conditioning Engineers. 2007. ASHRAE Standard 62-2007, Ventilation for Acceptable Indoor Air Quality.
- Asfour, O. S., Gadi, M.B. 2007. A comparison between CFD and Network models for predicting wind-driven ventilation in buildings, *Building and Environment*, 42(12), Pages 4079-4085.
- Aubrun, S. Leitl, B. 2004. Unsteady characteristics of the dispersion process in the vicinity of a pig barn. Wind tunnel experiments and comparison with field data. *Atmospheric Environment*, 38(1), 81-93.,
- Australian Standard, 1989. Minimum Design Loads on Structures. AS1170.2-1989
- Awbi, H.B. 1996. Air movement in naturally-ventilated buildings. Proceedings of the 4th World Renewable Energy Congress (WREC '96), I, 241-247, Denver, USA.
- Ayad, S.S. 1999. Computational study of natural ventilation, *Journal of Wind Engineering and Industrial Aerodynamics*. 82, 49-68.
- Barlow, J.B., Rae W.H. and Pope. A. *Low-speed Wind Tunnel Testing*. (Third Edition), Wiley, New York. 1999.
- Blocken, B., Stathopoulos, T., Saathoff, P., Wang, X. 2008. Numerical evaluation of pollutant dispersion in the built environment: Comparisons between models and experiments. *Journal of Wind Engineering and Industrial Aerodynamics*.

- 96, 4th International Symposium on Computational Wind Engineering (CWE2006), 1817-1831.
- Bojic, M., F. Yik, M. Lee, Influence of plates on flow inside a recessed space generated by rejected heat, *Building and Environment*. 38 (4), , April 2003, Pages 593-604.
- Building Department, 2005. Practice Note for Authorized Persons and Registered Structural Engineers. PNAP, 278.
- Burnett, J. 2005. Indoor Air Quality Certification Scheme for Hong Kong Buildings. *Indoor and Built Environment*, 14, 201-208.
- Burnett, J., Bojic, M., Yik, F. 2005. Wind-induced pressure at external surfaces of a high-rise residential building in Hong Kong. *Building and Environment*. 40, 765-777.
- Cermak J.E. 1975. Applications of fluid mechanics to wind engineering-A freeman scholar lecture. *Transactions of the ASME, J. of Fluids Engineering*, 97, 9-38.
- Cermak, J.E. 1978. Dispersion of Pollutants in the Urban Environment. ASCE Spring Convention and Exhibition Pittsburgh, Pa. Preprint 3269. pp. 29.
- Chan, Andy T. Chung, Michael W. 2003. Indoor-outdoor air quality relationships in vehicle: effect of driving environment and ventilation modes, *Atmospheric Environment*, 37 (27), 3795-3808.
- Chang, C.H., Meroney, R.N. 2003. Concentration and flow distributions in urban street canyons: wind tunnel and computational data, *Journal of Wind Engineering and Industrial Aerodynamics*. 91, 1141-1154.
- Chao, C.Y.H., & Tung, T.C. 2001. An empirical model for outdoor contaminant transmission into residential buildings and experimental verification. *Atmospheric Environment*, 35, 1585-1596.
- Chen, Q. 1995. Comparison of different  $k-\varepsilon$  models for indoor airflow computations. *Numerical Heat Transfer*, 28, 353-369.
- Chen, Qingyan. 2009. Ventilation performance prediction for buildings: A method overview and recent applications. *Building and Environment*, 44(4), 848-858.
- Chen, Q., & Srebric, J. 2002. A procedure for verification, validation, and reporting of indoor environment CFD analyses. *HVAC&R Research*, 8, 201-216.
- Charles C.K. Cheng, K.M. Lam, Richard K.K. Yuen, S.M. Lo, J. Liang, 2007. A study of natural ventilation in a refuge floor, *Building and Environment*, 42(9), 3322-3332.

- Chow, W. K. 2001. Numerical studies of airflows induced by mechanical ventilation and air-conditioning (MVAC) systems. *Applied Energy*. 68, 135-159.
- Cook, N.J., 1985, *The designer's guide to wind loading of building structures. Part2: static structures*, Butterworths Press, London.
- Courant R., Friedrichs K.O., & Lewy H. 1928. On the partial difference equations of mathematical Physics, *Mathematische Annalen*, 100, 32-74.
- Csiba, L., Martinuzzi. R. J. Investigation of bluff body asymmetry on the properties of vortex shedding, *Journal of Wind Engineering and Industrial Aerodynamics*, 2008; 96: (6-7), 1152-1163
- Davidson, M. J., Mylne, K. R., Jones, C. D., Phillips, J. C., Perkins, R. J., Fung, J. C. H., Hunt, J. C. R. 1995. Plume dispersion through large groups of obstacles--A field investigation, *Atmospheric Environment*. 29, 3245-3256.
- Davidson, M. J., Snyder, W. H., Lawson Jr R. E., Hunt, J. C. R. 1996. Wind tunnel simulations of plume dispersion through groups of obstacles, *Atmospheric Environment*. 30, Issue 3715-3731.
- Department of Health, Hong Kong. 2003. Investigation of a cluster of SARS cases in Hing Tung Hse, Tung Tau Estate, from [http://www.info.gov.hk/info/sars/pdf/e\\_hingtung.pdf](http://www.info.gov.hk/info/sars/pdf/e_hingtung.pdf).
- Dick, E. C., L. C. Jennings, K. A. Mink, C. D. Wartgow, and S. L. Inhorn. 1987. Aerosol transmission of rhinovirus colds. *The Journal of Infectious Diseases*. 156: 442-448.
- Dixon, N.S. Tomlin, A.S. 2007. A Lagrangian stochastic model for predicting concentration fluctuations in urban areas. *Atmospheric Environment*, 41(37), 8114-8127.
- Eftekhari, M.M., Marjanovic, L.D., & Pinnock, D.J. 2003. Air flow distribution in and around a single-sided naturally ventilated room. *Building and Environment*, 38, 389 – 397.
- Etheridge, D., & Sandberg, M. 1996. *Building Ventilation: Theory and Measurement*. Chichester: John Wiley & Sons.
- Favarolo, P.A., & Manz, H. 2005. Temperature-driven single-sided ventilation through a large rectangular opening. *Building and Environment*, 40, 689-699.
- Fisk, W., and A. H. Rosenfeld. 1997. Estimates of improved productivity and health from better indoor environments. *Indoor Air* 7: 158-172.
- Fluent. 2005. *Fluent 6.2 User's guide*. Fluent Inc., Lebanon, NH.

- Fracastoro, G.V., Mutani, G., & Perino, M. 2002. Experimental and theoretical analysis of natural ventilation by windows opening. *Energy and Buildings*, 34, 817-827.
- Gan, G. 2000. Effective depth of fresh air distribution in rooms with single sided natural ventilation. *Energy and Buildings*, 31, 65-73.
- Gao, N.P., Niu, J.L., Perino, M., Heiselberg, P. The airborne transmission of infection between flats in high-rise residential buildings: Tracer gas simulation. *Building and Environment*. 2008. 43(11), 1805-1817.
- Gao, N.P., Niu, J.L., Perino, M., Heiselberg, P. The airborne transmission of infection between flats in high-rise residential buildings: Particle simulation, *Building and Environment*, 2009. 44(2), 402-410.
- GB50352-2005. 2005. Code for design of civil buildings. National standard. Complied by Ministry of Construction, PRC.
- GB50368-2005. 2005. Residential building code. National standard. Complied by Ministry of Construction, PRC.
- Goliger, A. M., Milford, R. V. 1988. Sensitivity of the CAARC standard building model to geometric scale and turbulence. *Journal of Wind Engineering and Industrial Aerodynamics*. 31, 105-123.
- Hall, R.C., 1997. Dispersion of releases of hazardous materials in the vicinity of buildings: Phase II—CFD modelling. Contract Research Report 127/1997, HSE Books. Printed and published by The Health and Safety Executive.
- Health, Welfare & Food Bureau, Government of the HKSAR. 2003. Health, Welfare & Food Bureau SARS Bulletin, 28 May 2003, from <http://www.info.gov.hk/info/sars/bulletin/bulletin0528e.pdf>.
- Heinsohn, R.J., & Cimbala, J.M. 2003. *Indoor Air Quality Engineering: Environmental Health and Control of Indoor Pollutants*. New York: Marcel Dekker Inc.
- Heiselburg, P., Jepsen, L.B., Hyldgaard, A., Li, Z.G., Nielson, P.V., & Perino, M. 2003. Short-time airing by single sided natural ventilation – Part 1: Measurements of transient air flow rates. Proceedings of the 4th international symposium on heating, ventilating and air-conditioning 1, 117-124, Beijing, China.

- Higson, H. L., Griffiths, R. F., Jones, C. D., Hall, D. J. Flow and dispersion around an isolated building, *Atmospheric Environment*. 1996; 30(16): 2859-2870.
- Hong Kong Observatory. 2005 Summary of Meteorological Observations in Hong Kong – 2004, Hong Kong, Hong Kong Observatory.
- HKSAR Buildings Department. 2004. Code of Practice on Wind Effects in Hong Kong 2004, Hong Kong Special Administration Region (HKSAR) Buildings Department.
- HKSAR Planning Department. 2005. Feasibility Study for Establishment of Air Ventilation Assessment System (Final Report). Hong Kong Special Administration Region (HKSAR) Planning Department.
- HKSAR Planning Department. 2008. Technical Guide for Air Ventilation Assessment for Developments in Hong Kong. Technique report. Hong Kong Special Administration Region (HKSAR) Planning Department, 28 May 2008,
- Hong Kong Observatory. 2008. Monthly Prevailing Wind Direction and Mean Wind Speed Recorded at the Observatory and Waglan Island between 1971-2000 , 28 May 2008, from  
[http://www.weather.gov.hk/cis/normal/1971\\_2000/normals\\_e.htm](http://www.weather.gov.hk/cis/normal/1971_2000/normals_e.htm)
- Huang, S.H., Li, Q.S., Xu,S.L. 2007. Numerical evaluation of wind effects on a tall steel building by CFD. *Journal of Constructional Steel Research*. 63, 612-627.
- Hunt, G. R., Linden, P. P. 1999. The fluid mechanics of natural ventilation-- displacement ventilation by buoyancy-driven flows assisted by wind, *Building and Environment*, 34(6), 707-720.
- Huang, J.M., Chen, Q., & Ribot, B. 2004. Modelling contaminant exposure in a single-family house. *Indoor and Built Environmen*, 13, 5-19.
- Ji, Y., Cook, M.J., & Hanby, V. 2007. CFD modeling of natural displacement ventilation in an enclosure connected to an atrium. *Building and Environment*, 42, 1158-1172.
- Jiang, Y., Chen Q. 2003. Buoyancy-driven single-sided natural ventilation in buildings with large openings. *International Journal of Heat and Mass Transfer* 46, 973–988.
- Jiang,Y., Chen,Q. 2001. Study of natural ventilation in buildings by large eddy simulation. *Journal of Wind Engineering and Industrial Aerodynamics*. 89, 1155-1178.

- Jones, A.P. 1999. Indoor air quality and health. *Atmospheric Environment* 33, 4535-4564.
- Kastner-Klein, P., Plate, E. J. 1999. Wind-tunnel study of concentration fields in street canyons. *Atmospheric Environment*. 33, 3973-3979.
- Kastner-Klein, P., Leidl, B., Pascheke, F., Schatzmann, M. 2004: Wind-tunnel simulation of the JOINT Urban 2003 tracer experiment. Proceedings of the AMS Symposium on Planning, Nowcasting, and Forecasting in the Urban Zone, January 11-15, Seattle, Washington, USA.
- Katayama, T., Tsutsumi J., Ishii, 1992. A. Full-scale measurements and wind tunnel tests on cross-ventilation. *Journal of Wind Engineering and Industrial Aerodynamics*. 41(44), 2553–2562.
- Khan, Naghman, Su, Yuehong, Riffat, Saffa B. 2008. A review on wind driven ventilation techniques, *Energy and Buildings*, 40(8), 1586-1604.
- Lakehal, D., Rodi, W. 1997. Calculation of the flow past a surface-mounted cube with two-layer turbulence models, *Journal of Wind Engineering and Industrial Aerodynamics*, 67-68, 65-78.
- Liu,C.H., Leung, D.Y.C., Barth, M.C. 2005. On the prediction of air and pollutant exchange rates in street canyons of different aspect ratios using large-eddy simulation, *Atmospheric Environment*. 39, 1567-1574.
- Li, X.X., Liu,C.H., Leung,D.Y.C., Lam, K.M. 2006. Recent progress in CFD modelling of wind field and pollutant transport in street canyons, *Atmospheric Environment*. 40, 5640-5658.
- Li, Yuguo, Delsante, Angelo, Chen, Zhengdong, Sandberg, Mats, Andersen, Bjerre, Alice Marianne; Heiselberg, Per. 2001. Some examples of solution multiplicity in natural ventilation, *Building and Environment*. 36(7), 851-858.
- Li, Y., Duan, S., Yu, I.T.S., & Wong, T.W. 2004a. Multi-zone modeling of probable SARS virus transmission by airflow between flats in Block E, Amoy Gardens. *Indoor Air*, 15, 96-111.
- Li, Y., Huang, X., Yu, I.T.S., Wong, T.W., & Qian, H. 2004b. Role of air distribution in SARS transmission during the largest nosocomial outbreak in Hong Kong. *Indoor Air*, 15, 83-95.
- Li, Y., Leung, G.M., Tang, J.W., Yang, X., Chao, C., & Lin, J.Z., et al. 2006. Role of ventilation in airborne transmission of infectious agents in the build environment – a multidisciplinary systematic review. *Indoor Air*, 17, 2-18.

- Li, Y., Stathopoulos, T. 1997. Numerical evaluation of wind-induced dispersion of pollutants around a building, *Journal of Wind Engineering and Industrial Aerodynamics*, 67-68, 757-766.
- Lin, Zhongping, Deng, Shiming. 2006. A questionnaire survey on sleeping thermal environment and bedroom air conditioning in high-rise residences in Hong Kong. *Energy and Buildings*, 38(11), 1302-1307.
- Linden, P.F. 1999. The fluid mechanics of natural ventilation. *Annual Review of Fluid Mechanics*, 31, 201-238.
- Liu, Xiaoping, Niu, Jianlei, Perino, Marco & Heiselberg, Per. 2008. Numerical simulation of inter-flat air cross-contamination under the condition of single-sided natural ventilation. *Journal of Building Performance Simulation*, 1 (2), 133-147.
- Lubcke, H., Schmidt, St., Rung, T., Thiele, F. 2001. Comparison of LES and RANS in bluff-body flows, *Journal of Wind Engineering and Industrial Aerodynamics*. 89, 1471-1485.
- Macdonald, R.W., Griffiths, R.F., Cheah, S.C., 1997. Field experiments of dispersion through regular arrays of cubic structures. *Atmospheric Environment* 31 (6), 783-795.
- Macdonald, R.W., Griffiths, R.F., Hall, D.J., 1998. A comparison of results from scaled field and wind tunnel modelling of dispersion in arrays of obstacles. *Atmospheric Environment* 32 (22), 3845-3862.
- Mavroidis, I., Griffiths, R. F. 2001. Local characteristics of atmospheric dispersion within building arrays. *Atmospheric Environment*. 35, 2941-2954.
- Mavroidis, I., Griffiths, R. F., Hall, D. J. 2003. Field and wind tunnel investigations of plume dispersion around single surface obstacles, *Atmospheric Environment*. 37, 2903-2918.
- Mavroidis, I., Andronopoulos, S., Bartzis, J.G., Griffiths, R.F. 2007. Atmospheric dispersion in the presence of a three-dimensional cubical obstacle: Modelling of mean concentration and concentration fluctuations, *Atmospheric Environment*. 41, 2740-2756.
- Melbourne, W.H. 1980. Comparison of measurements on the CAARC standard tall building model in simulated model wind flows. *Journal of Wind Engineering and Industrial Aerodynamics*, 6, 73-88.

- Meroney, R.N. 2004. Wind tunnel and numerical simulation of pollution dispersion: a hybrid approach. Invited Lecture. Croucher Advanced Study Institute on Wind Tunnel Modeling, Hong Kong University of Science and Technology, 6–10 December, 2004.
- Meroney, R.N., Leidl, B.M., Rafailidis, S., Schatzmann, M., 1999. Wind tunnel and numerical modelling of flow and dispersion about several building shapes. *Journal of Wind Engineering and Industrial Aerodynamics*. 81, 333–345.
- Mfula, A.M., Kukadia, V., Griffiths, R.F., Hall, D.J. Wind tunnel modelling of urban building exposure to outdoor pollution, *Atmospheric Environment*, 2003. 39(15), 2737-2745.
- Murakami, S. Overview of turbulence models applied in CWE-1997. 1998. *Journal of Wind Engineering and Industrial Aerodynamics*. 74-76, 1-24.
- Nahor, H.B., Hoang, M.L., Verboven, P., Baelmans, M., & Nicolaï, B.M. 2005. CFD model of the airflow, heat and mass transfer in cool stores. *International Journal of Refrigeration*, 28, 368-380.
- Niu, J.L. 2004. Some significant environmental issues in high-rise residential building design in urban area. *Energy and Buildings*, 36, 1259-1263.
- Niu, J.L., & Tung, T.C.W. 2008. On-site quantification of re-entry ratio of ventilation exhausts in multi-family residential buildings and implications. *Indoor Air*, 18, 12-26.
- Ohba, M., Irie, K., Kurabuchi, T. 2001. Study on airflow characteristics inside and outside a cross-ventilation model, and ventilation flow rates using wind tunnel experiments. *Journal of Wind Engineering and Industrial Aerodynamics*. 89,1513-1524.
- Pasquill, F., Smith, F.B., 1983. *Atmospheric Diffusion*, 3rd edition. Ellis Horwood Ltd., Chichester, England.
- Pavageau, M., Schatzmann, M. Wind tunnel measurements of concentration fluctuations in an urban street canyon, *Atmospheric Environment*, 1999. 33(24-25), 3961-3971.
- Perino M, & Heiselberg P. 2003. Short-time airing by single sided natural ventilation – Part2: Comparison of Experimental Results and Model Predictions. *Proceedings of the 4th international symposium on heating, ventilating and air-conditioning 1*, 117-124, Beijing, China.

- Qin, Y., Kot, S.C. 1993. Dispersion of vehicular emission in street canyons, Guangzhou City, South China (P.R.C.). *Atmospheric Environment. Part B. Urban Atmosphere.* 27, 283-291.
- E.C. Riley, G. Murphy, R.L. Riley. Airborne spread of measles in a suburban elementary school. *American Journal of Epidemiology.* 107(1978), pp. 421–432.
- Rudnick, S.N. Milton, D.K. 2003. Risk of indoor airborne infection transmission estimated from carbon dioxide concentration. *Indoor Air.* 13(3):237-245.
- Saathof, P. J., Stathopoulos, T., Dobrescu, M. 1995. Effects of model scale in estimating pollutant dispersion near buildings, *Journal of Wind Engineering and Industrial Aerodynamics.* 54-55, 549-559.
- Sada, K., Sato, A. 2002. Numerical calculation of flow and stack-gas concentration fluctuation around a cubical building, *Atmospheric Environment,* 36(35), 5527-5534.
- Santamouris, M., Wouters, P. 2006. *Building Ventilation: The state of the art, Earthscan.*
- Santos Jane Meri, Jr. Reis Neyval Costa, Goulart Elisa Valentim, Mavroidis Ilias. 2009. Numerical simulation of flow and dispersion around an isolated cubical building: The effect of the atmospheric stratification, *Atmospheric Environment,* 43(34), 5484-5492.
- Schaelin A, J van der Maas, Moser A. Simulation of airflow through large openings in buildings. *ASHRAE Trans.* 1992;98(2):319-328.
- Senthooran,S., Lee, D. D., Parameswaran ,S. 2004. A computational model to calculate the flowinduced pressure fluctuations on buildings. *Journal of Wind Engineering and Industrial Aerodynamics.* 92, 1131 - 1145.
- Seppänen O, Fisk W. 2002. Association of Ventilation Type with SBS symptoms in Office Workers. *Indoor Air.* Vol 12, no 2, 98-112.
- Shi, R.F., Cui, G.X., Wang, Z.S., Xu, C.X., Zhang, Z.S. Large eddy simulation of wind field and plume dispersion in building array, *Atmospheric Environment,* 2008. 42(6), 1083-1097.

- Shih, T.-H., Liou, W. W. Shabbir, A. , Yang, Z. and J. Zhu. 1995. A New  $k-\varepsilon$  Eddy-Viscosity Model for High Reynolds Number Turbulent Flows - Model Development and Validation. *Computers Fluids*, 24(3):227-238.
- Snyder, W.H. 1979. Guideline for fluid modeling of atmospheric diffusion. Environmental Protection Agency, Research Triangle Park, NC 27711, USA. Technical Report, EPA-450/4-79-016(Draft).
- Stathopoulos, Theodore. 1997. Computational wind engineering: Past achievements and future challenges, *Journal of Wind Engineering and Industrial Aerodynamics*, Volumes 67-68, 509-532.
- Stathopoulos, T. 2002. The Numerical Wind Tunnel for Industrial Aerodynamics: Real or. Virtual in the New Millenium? *Wind and Structures*, 5, 193-208.
- Stathopoulos, T., Baskaran, B. A. 1996. Computer simulation of wind environmental conditions around buildings, *Engineering Structures*, 18-11, 876-885.
- Stathopoulos, T., Lazure, L., Saathoff, P., Wei, X., 2002. Dilution of exhaust from a rooftop stack on a cubical building in an urban environment. *Atmospheric Environment*. 36, 4577–4591.
- Sze To, G. N., Chao, C. Y. H. 2010. Review and comparison between the Wells-Riley and dose-response approaches to risk assessment of infectious respiratory diseases. *Indoor Air*, 20(1):2-16.
- Tamura, T., Nozawa, K., and Kondo, K. 2008. AIJ guide for numerical prediction of wind loads on buildings *Journal of Wind Engineering and Industrial Aerodynamics*. 96, 1974 - 1984.
- Tanaka, H., Lawen, N. 1986. Test on the CAARC standard tall building model with a length scale of 1 : 1000. *Journal of Wind Engineering and Industrial Aerodynamics*. 25 15-29.
- Tominaga, Y., Mochida, A., Murakami, S., Sawaki, S. 2008a. Comparison of various revised  $k-\varepsilon$  models and LES applied to flow around a high-rise building model with 1:1:2 shape placed within the surface boundary layer. *Journal of Wind Engineering and Industrial Aerodynamics*. 96, 389-411.
- Tominaga, Y., Mochida, A., Yoshie, R., Kataokad, H., Nozu, T., Masaru, Yoshikawa, M., Shirasawa, T. 2008b. AIJ guidelines for practical applications of CFD to pedestrian wind environment around buildings. *Journal of Wind Engineering and Industrial Aerodynamics*, 96, 1749 - 1761.

- Tominaga, Yoshihide, Stathopoulos, Ted. 2009. Numerical simulation of dispersion around an isolated cubic building: Comparison of various types of  $k-\varepsilon$  models, *Atmospheric Environment*, Volume 43, Issue 20, 3200-3210.
- Van Doormaal, J.P., Raithby, G.D. 1984, "Enhancements of the SIMPLE method for predicting incompressible fluid flows", *Numerical Heat Transfer*, Vol. 7, 147–163.
- Vardoulakis, S., Fisher, B.E.A., Pericleous, K., Gonzalez-Flesca, N. 2003. Modelling air quality in street canyons: a review. *Atmospheric Environment*, 37, 2, 155-182.
- Versteeg, H.K., & Malalasekera, W. 2007. *An introduction to computational fluid dynamics—the finite volume method (Second Edition)*. Harlow, England : Pearson Education Ltd..
- Wargocki P, Sundell J, Bischof W et al. 2002 Ventilation and health in non-industrial indoor environments: report from a European multidisciplinary scientific consensus meeting (EUROVEN). *Indoor Air*;12:113–28.
- Watkins, S., Milbank, J., Loxton, B.J. & Melbourne, W.H. 2006. Atmospheric winds and their implications for microair vehicles', *AIAA Journal*, 44 (11): 2591-2600.
- Wright, N.G., Easom, G.J. 2003. Non-linear  $k-\varepsilon$  turbulence model results for flow over a building at full-scale. *Applied Mathematical Modelling*, 27(12), 1013-1033.
- Yang, J., Yik, F, Zhang, X, Bojic, M. 2005. Designing Estates for Good Cross-Ventilation in High-Rise Residential Buildings in Hong Kong. *HVAC&R Research Journal*. 11, 621-635
- Yu, I.T.S., Li, Y., Wong, T.W., Tam, W., Chan, A.T., & Lee, J.H.W., et al. 2004. Evidence of airborne transmission of the severe acute respiratory syndrome virus. *The New England Journal of Medicine*, 350, 1731-1739.
- Zhang, A., Gu, M. 2008. Wind tunnel tests and numerical simulations of wind pressures on buildings in staggered arrangement. *Journal of Wind Engineering and Industrial Aerodynamics*, 96(10-11),2067-2079
- Zhu, Yifang, Hinds, William C., Krudysz Margaret, Kuhn Thomas , Froines John, Sioutas, Constantinos. 2005. Penetration of freeway ultrafine particles into indoor environments, *Journal of Aerosol Science*. 36(3), 303-322.